3.3.5 Stearic acid effects on Cav1.2 protein

Our investigations on atrial cell electrophysiology show that the major effect of SA was on $I_{Ca\text{-}L}$ density. We therefore used a combination of biochemical and optical techniques to examine SA-induced changes on Cav1.2 protein, the molecular correlate of the underlying channel. Labeling of Cav1.2 and α-actinin Figure 3.3.5 (A-C) shows that SA did not alter Cav1.2 protein localization, i.e., relative to the sarcomeric α-actinin pattern, and was distribution of the Cav1.2 protein was similar to what has been previously described.[304,305] Cav1.2 remains in close proximity to the Z-lines, and the spacing of the Cav1.2 intensity peaks (and of α-actinin) were similar and unchanged by SA treatment (Figure 5C; n = 12, 12). Furthermore, atrial cell Cav1.2 protein levels were not significantly affected by incubation in SA (Figure 3.3.5D; N= 3). These data suggest that alterations in cellular Cav1.2 protein levels is not the mechanism driving the SA-induced changes in $I_{Ca\text{-}L}$. Channel phosphorylation or nitrosylation are well described post-translational mechanisms for $I_{Ca\text{-}L}$ regulation.[306,307] In another set of experiments (see Online Supplement), we investigated the potential roles of these mechanisms. Immunocytochemistry and western blot were carried out using Cav1.2-phospho antibody (Supplemental Figure 3), or Cav1.2-S-nitrocysteine antibody (Supplemental Figure 4). Results from these experiments showed no differences between control and SA treated cells.

3.3.6 Fatty acid effects on t-tubular structure

The membranes of transverse (t)-tubules are well-recognized microdomains for the cellular localization of L-type calcium channels, and their disruptions have been reported to result in a reduction of $I_{Ca\text{-}L}$.[84,263,308] We hypothesized that free fatty acid induced changes in t-tubular architecture or structural integrity could provide an explanation for the reduction in $I_{Ca\text{-}L}$. To examine this possibility, atrial cells were treated with vehicle control media or were incubated in free fatty acids (PA or SA) for 24 hrs, stained with Di-8-ANEPPS and then visualized under confocal microscopy. Control experiments showed that t-tubule structure in atrial cells was not significantly affected by 24 hr cell culture. Additional control experiments (Supplemental Figure 5) established our imaging technique could resolve the previously reported differences between atrial and ventricular t-tubular architectures.[82] In Figure 3.3.6A, images were taken soon after cell isolation (*t* = 0; panels a & b) and 24 hrs in control media (CTL; panels c & d). Insets at the top of Figure 3.3.6A are schematics representing the planes of view for the left (a, c, e, & g) and right (b, d, f, & h) panels. T-tubule pixel intensity was quantified, summed and normalized to total cellular intensity (see method details in methods section) and plotted in Figure 3.3.6B. The imaging results show that cells incubated in PA had a slight but insignificant reduction of t-tubular staining with Di-8-ANEPPS (Figure 3.3.6A; e & f, Figure 3.3.6B). In contrast, SA caused a dramatic reduction in the t-tubule network (Figure 3.3.6A; g & h, Figure 3.3.6B). Compared to control cells, SA caused a ~4-fold decrease in the intensity of t-tubular staining (0.58 ± 0.04 versus 0.16 ± 0.02; ***$p<0.0001$). It is generally acknowledged that t-tubule membranes account for 15-50% of the capacitance of

cardiac ventricular myocytes.[82-84] Consistent with this reduction of t-tubular staining in SA treated cells, we had observed a >15% decrease in whole cell capacitance (see Table 1, Figure 3.3.6C). Importantly, note that our image analysis of 2D cell surface area shows no SA-induced changes in the surface area of atrial cells (Figure 3.3.6D). These data show that the reduction in t-tubular membranes is a possible mechanism for the reduction of $I_{Ca\text{-}L}$ observed with incubation of cells in SA.

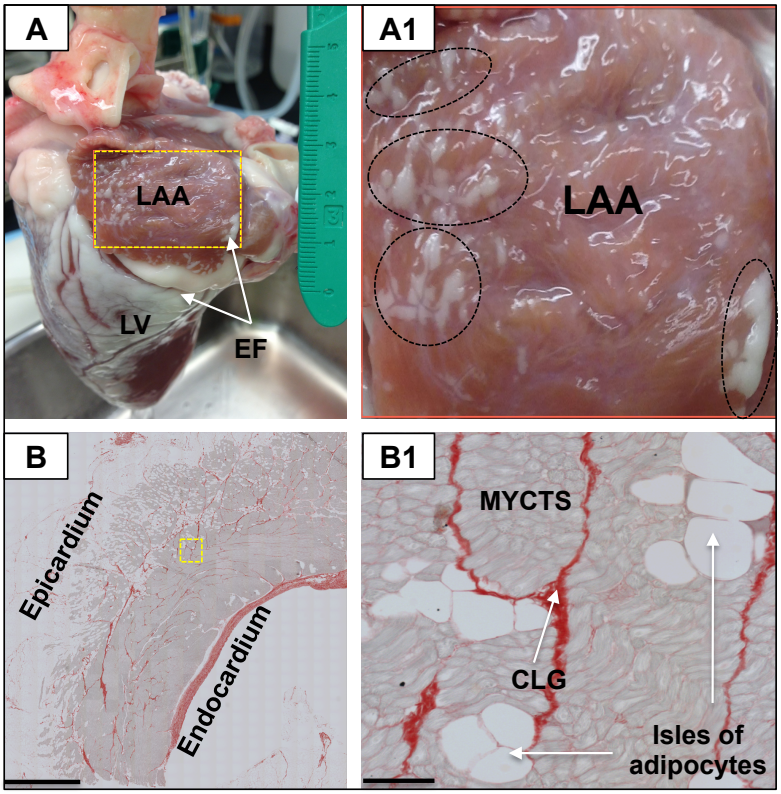

Figure 3.3.1: Epicardial fat tissue distribution on the ovine heart: Panel A: Normal adult sheep heart (Langendorff retrograde perfusion), showing epicardial (atrial and ventricular) fat deposits. (LAA; left atrial appendage LV; left ventricle EF; epicardial fat on atrial and ventricular surfaces). Green scale (in cm) is shown close to the posterior wall, adjacent to the openings of the pulmonary veins. Yellow box is 2 x 3 cm. Panel A1: (inset from Panel A) oval and rounded rectangles represent regions of dense atrial epicardial fat depots. Panel B: LAA tissue section: Note significant epicardial fat layer with extensive adipocyte infiltration of the left atrium. Scale bar: 1mm. Panel B1: Tissue section from yellow inset in panel B showing myocytes (MYCTS), isles of adipocytes, and collagen (CLG) stained with Picoserius. Scale bar: 50 µm.

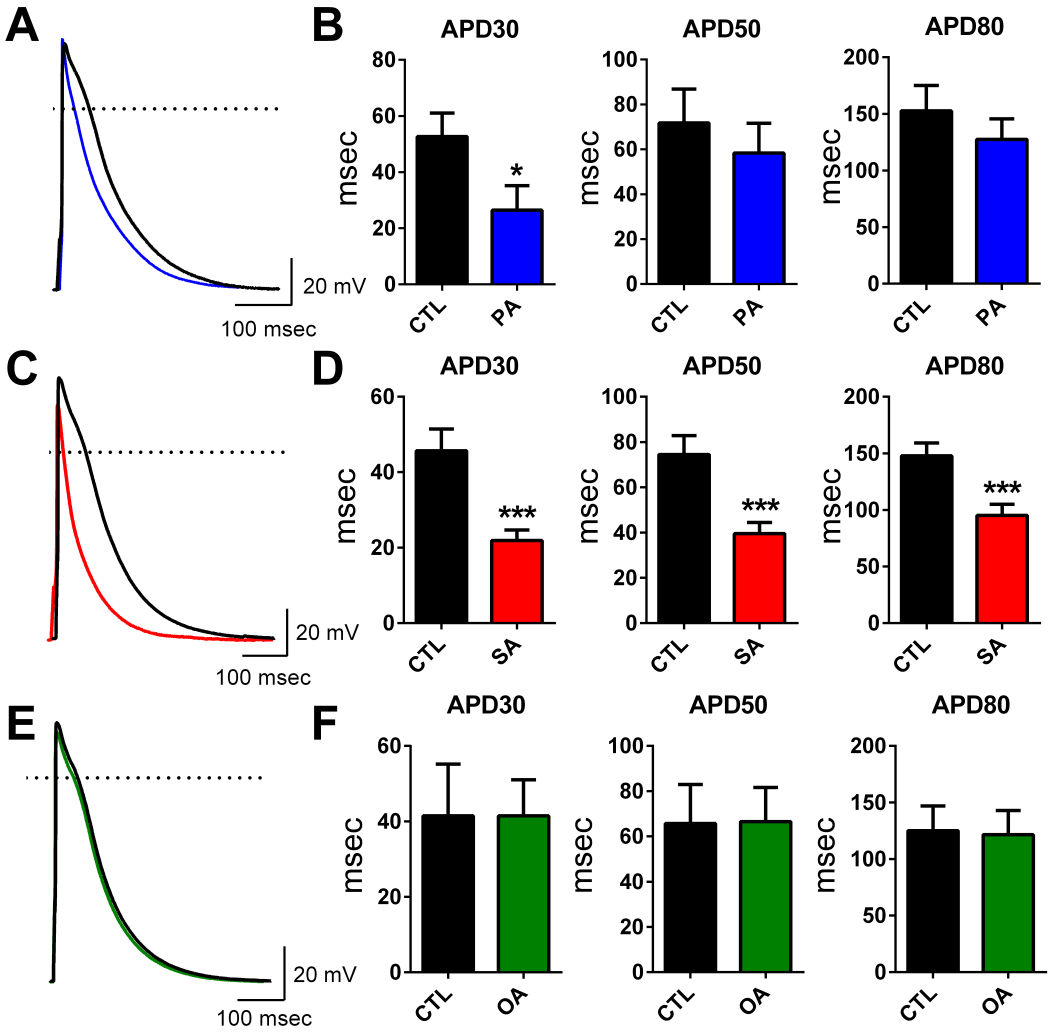

Figure 3.3.2: Saturated free fatty acids, but not a mono-unsaturated fatty acid, shorten action potential duration in atrial cells: Panels A, C, E; Atrial myocyte action potential recordings in control solution (black) and following incubation in solution containing 10 μm palmitic acid (PA, blue), stearic acid (SA, red) or oleic acid (OA, green). Average APD30, 50, & 80 measurements in control (CTL) and following incubation in PA (Panel B, n = 9, 12; *p<0.05), SA (Panel D, n = 22, 24; ***p<0.001) and OA (Panel F, n = 6, 5). Scale bars: 100 msec and 20 mV.

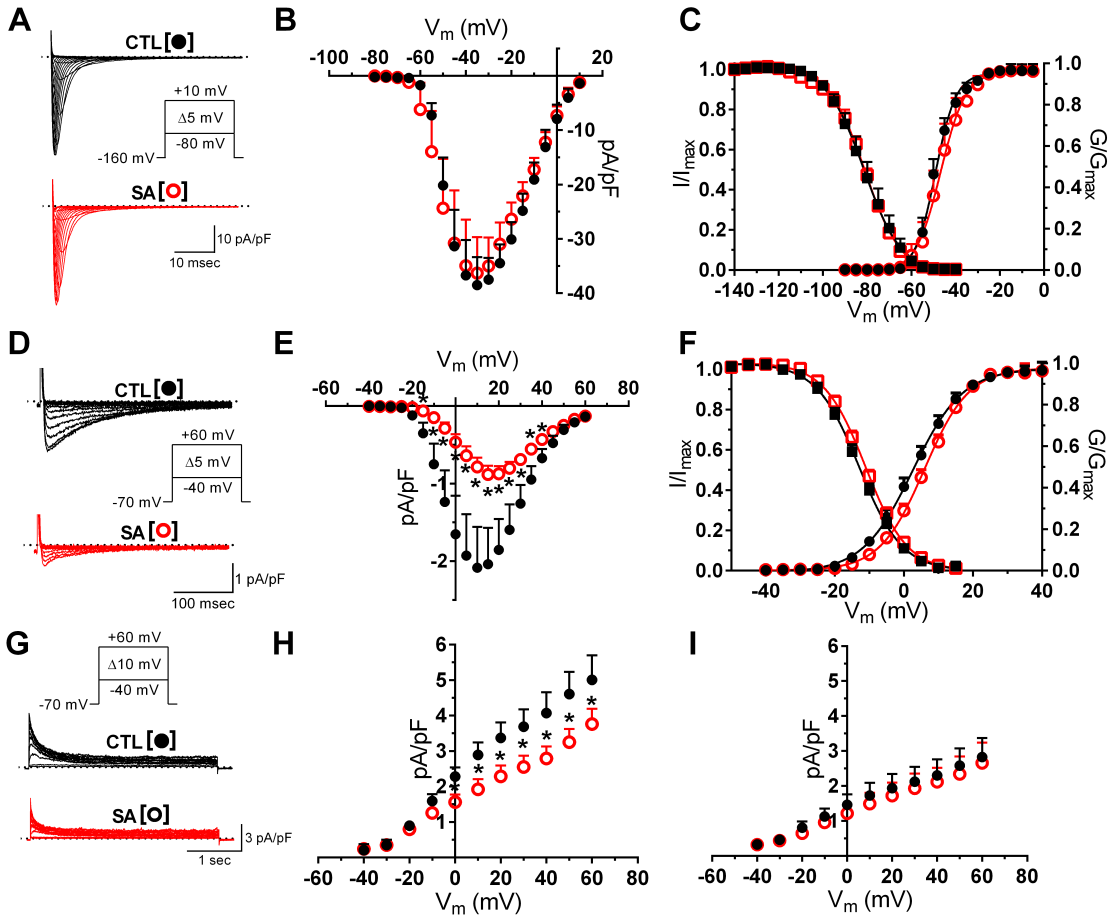

Figure 3.3.3: Voltage-gated ionic currents are differentially affected by stearic acid. Panel A: Representative traces of sodium currents (I_{Na}) in control (CTL, black) and in SA (10 μm; red) treated cells. Inset: voltage-clamp protocol for current activation. Plots of current density (Panel B), and of voltage-dependence of current activation (squares) and inactivation (circles) (Panel C), n = 5, 7). Panel D: Representative traces (selected) of calcium current ($I_{Ca,\,L}$) in CTL and in SA (10 μm; red) treated cells. Inset: voltage-clamp protocol for current activation. Plots of current density (Panel E), and of voltage-dependence of current activation (squares) and inactivation (circles) (Panel F). Incubation of myocytes in SA caused a significant reduction of $I_{Ca,\,L}$ density (n = 24, 22; *p<0.05). Panel G: Transient outward potassium currents (I_{TO}) in CTL and in SA treated cells. Inset: voltage-clamp protocol. Panel H: Current-density measurements showing effects of SA on peak I_{TO}, but not on the steady state current (I_{SS}) (Panel I) (n = 8, 8; *p<0.05).

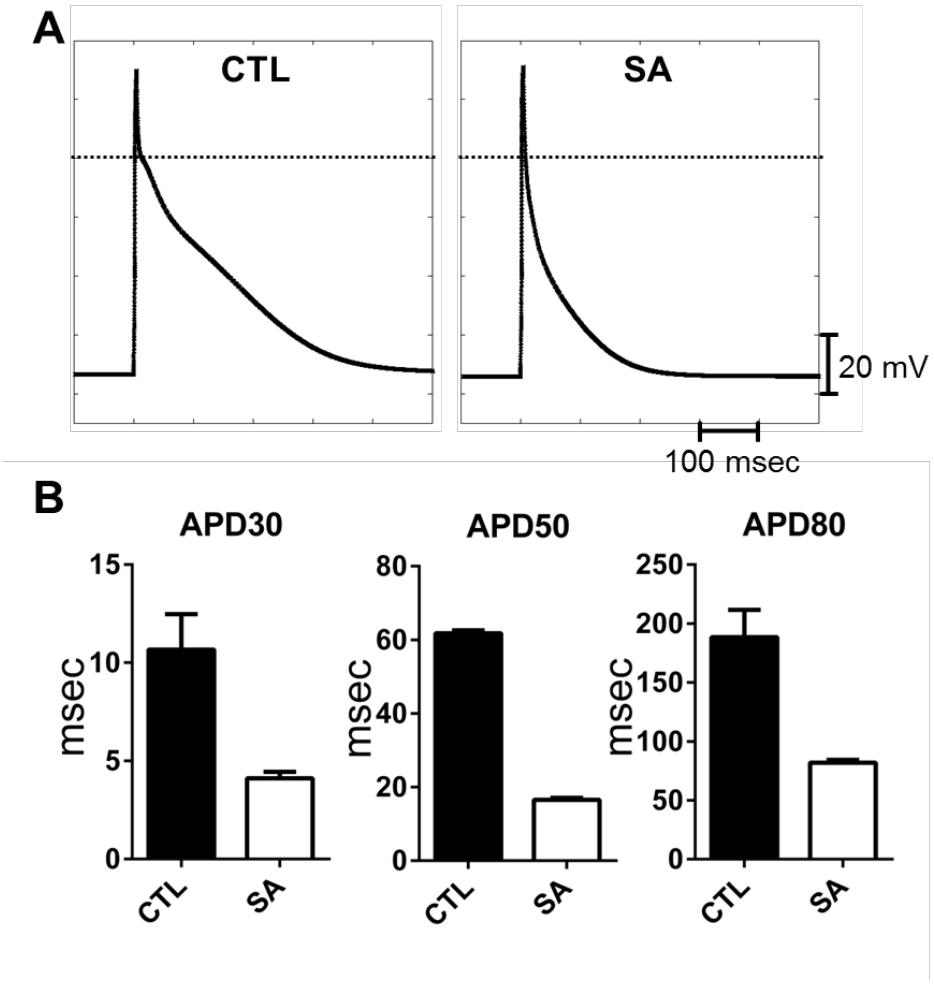

Figure 3.3.4: Human atrial action potential model simulation of stearic acid effects on ionic currents in isolated atrial cells. Panel A: Model generated action potential under control conditions (left) and following SA-induced changes in ionic currents (see text for details) (right). Panel B: Measurements of APD30, 50 & 80 from ten consecutive action potential simulations under control (CTL, black) and with SA treatment (white).

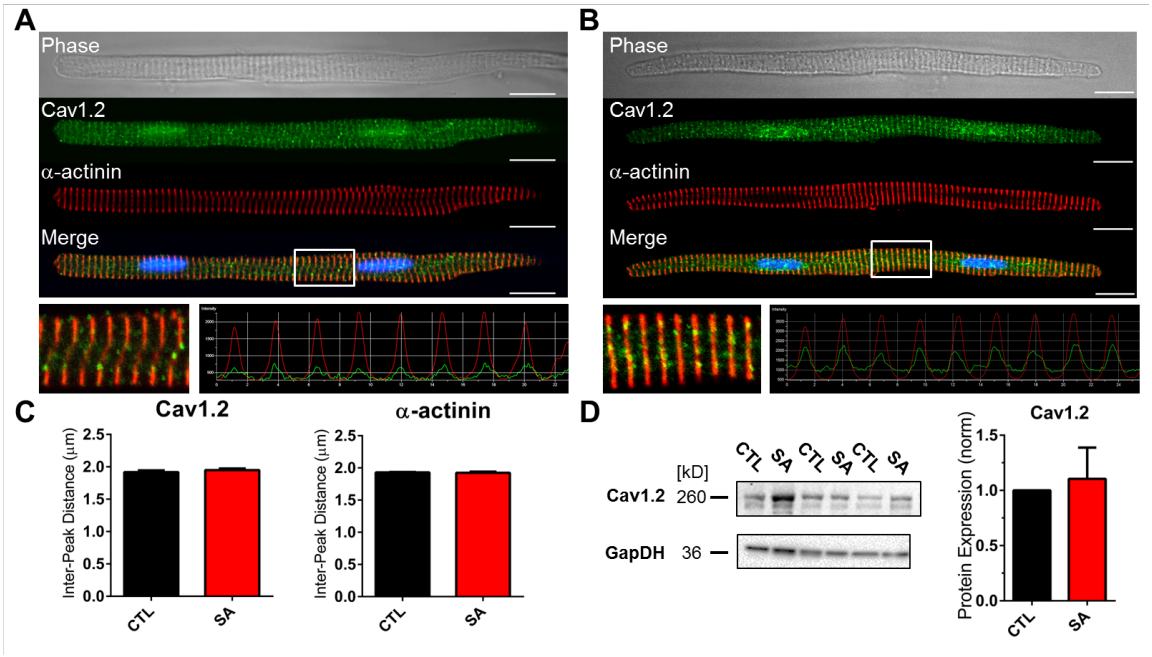

Figure 3.3.5: Cav1.2 Localization and whole cell protein content is not affected by stearic acid. Transmitted light image of an atrial myocyte (top), Cav1.2 protein staining (green), α-actinin staining (red) and a merged image of Cav1.2, α-actinin and DAPI staining (bottom) under control (CTL; Panel A) and following incubation in stearic acid (SA; Panel B). Inset: 20 μm section of the merged image and corresponding intensity profile of Cav1.2 and α-actinin. Scale bars 20 μm. Panel C: Quantification of the intensity profiles shows SA did not alter the mean distance between intensity peaks for Cav1.2 (left) or α-actinin (right; n = 12, 12). Mean distance between Cav1.2 and α-actinin peaks were similar in both groups and unchanged from CTL to SA. Panel D: (left) Western blot for Cav1.2, with GAPDH as a control. Pane D: (right) normalized densitometry plot of Cav1.2 protein levels in CTL and SA treated cell lysates (n = 3).

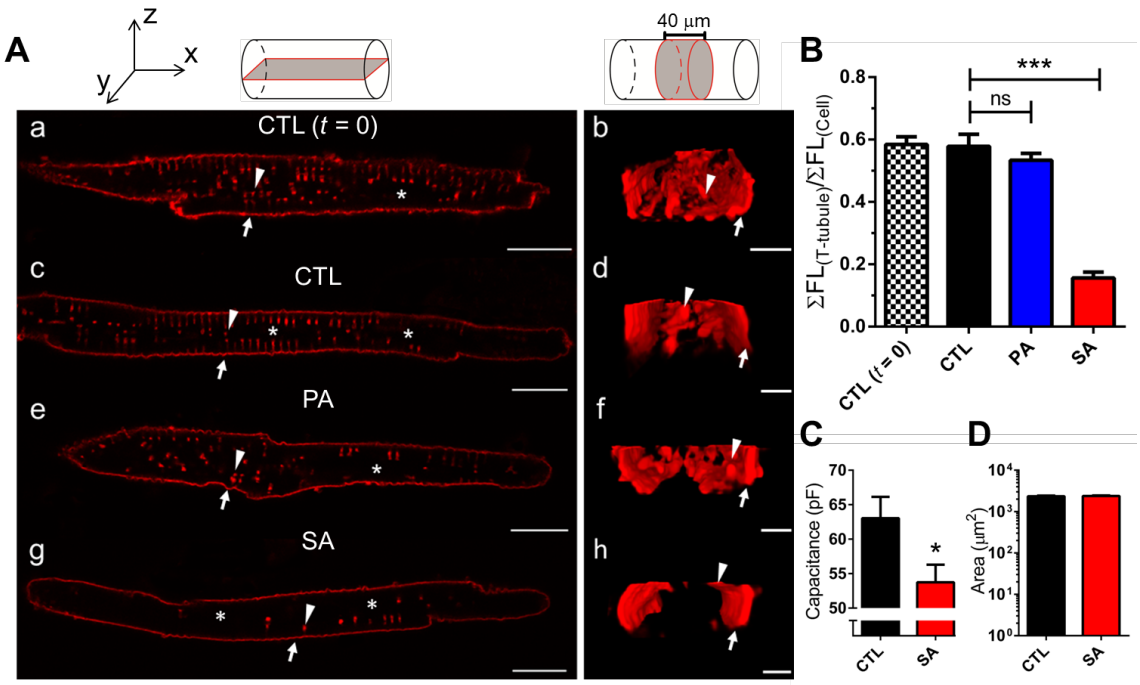

Figure 3.3.6: Stearic Acid disrupts t-tubules in atrial myocytes. Panel A (top): Coordinate axes for reference and schematic diagrams illustrating the fields of view. Panel A: subpanels (a, c, e & g) are XY planar views and (b, d, f & h) are 40 µm ZY cross-sectional views of the same cell. (a & b) Di-8-ANEPPS staining of t-tubules in freshly dissociated (*t* = 0) atrial myocytes (n = 19). After 24 hrs in culture, Control (CTL) cells shown in (c) and (d) retain t-tubule structures (n = 20). (e) and (f) T-tubular structure after chronic incubation of myocytes in PA (n = 19). (g) and (h) reduction in t-tubules after 24 hr incubation of myocytes in SA (n = 25). Arrows indicate the lateral membrane and arrowheads highlight an individual t-tubule in both views. (*) identifies the nuclear region. Scale bars: 20 µm (XY) and 5 µm (ZY). Panel B: Quantification of t-tubules in using the ratio of the t-tubule region and total cell fluorescence. SA reduced the presence of t-tubule structures in LA myocytes (CTL vs. SA; ***p<0.0001 (n = 25), CTL vs. PA; p=ns (n = 19)). Panel C: SA reduced the capacitance of atrial myocytes following incubation in SA (Panel C (n = 83 *p<0.05), but did not alter 2D surface area of myocytes (n = 68).

	RMP (mV)	AP Amplitude (mV)	AP Overshoot (mV)	dv/dt_{max} (mV/msec)	Cell Cap (pF)
CTL n = 9 N = 3	-78.7 ± 0.90	106.5 ± 3.63	28.0 ± 3.44	227.9 ± 12.6	59.2 ± 2.94
PA n = 12 N = 3	-79.5 ± 0.81	118.8 ± 4.20	36.3 ± 3.26	231.8 ± 19.4	63.7 ± 5.15
CTL n = 22 N = 5	-79.2 ± 0.6	126.6 ± 2.52	44.0 ± 2.04	223.9 ± 13.1	63.1 ± 3.08
SA n = 24 N = 5	-80.3 ± 0.7	119.0 ± 2.92	34.3 ± 2.54**	210.0 ± 13.8	53.8 ± 2.55*
CTL n = 6 N = 2	-77.8 ± 0.74	119.0 ± 2.68	37.3 ± 1.92	192.5 ± 18.3	71.1 ± 5.98
OA n = 5 N = 2	-79.5 ± 1.21	123.2 ± 4.02	38.0 ± 2.92	199.7 ± 12.0	64.9 ± 2.79

Table 3.3.1: Electrophysiological properties of atrial myocytes incubated in palmitic (PA), stearic (SA) and oleic (OA) acids. Acquisition of Resting Membrane Potential (RMP), Action Potential (AP) Amplitude, Action Potential Overshoot, dv/dt_{max}, and Cell Capacitance by patch clamp is presented with animal matched controls (CTL). (*$p<0.05$; **$p<0.01$).

3.4 Discussion

In this study, we have investigated the changes in electrical and structural properties of sheep atrial myocytes following incubation of the cells in each of the three epicardial free fatty acids; palmitic, stearic and oleic acids. Whereas the monounsaturated fatty acid, oleic acid, had no measurable effects, the fully saturated acids caused significant changes in myocyte electrophysiological and structural properties, with stearic acid effects being more detrimental than palmitic acid effects. Furthermore, the remodeling effects required chronic application of the fatty acids. The results from our study are important in understanding changes in atrial electrophysiology linked to an overload of these epicardial metabolic biofactors, in the setting of obesity.

Adiposity of atrial myocardium

It is generally known that the pulmonary vein regions have extensive adiposity. It has been suggested that the fat deposits may contribute, by mechanisms yet to be defined, to the aberrant electrical impulses emanating from this region[232,234,238,248,261,309]. Our histological analysis in this study (Figure 1) shows extensive fatty infiltration of the left atrial appendage. As has been suggested, obesity associated increases in atrial epicardial adiposity[237,238,240,249,261,298,310] and any associated increases in the release of biofactors potentially could modify myocardial function by direct or paracrine, and/or by 'vasocrine' mechanisms.[235] The results of our study in the ovine

suggest a potential role of elevated atrial adipocyte biofactors in the structural and electrical remodeling of the atrial myocyte.

Remodeling of membrane ionic currents

Stearic acid is the major saturated free fatty acid in ovine as well as human epicardial adipose tissue, and studies have shown increases in the circulating levels with obesity.[246,257,258,260] However, to date few studies have investigated the consequences of elevated levels of saturated free fatty acids (palmitic and stearic acids) on atrial myocytes isolated from a large mammal. In one comprehensive study, the effects of palmitate on murine ventricular myocyte excitability properties were investigated under acute exposure of the fatty acid.[256] It was reported that palmitate shortened APD, an abbreviation that was the result of an ~20% increase in the voltage-gated potassium currents, consisting of $I_{to,f}$, $I_{K,slow}$ and I_{ss}.[256] The investigators reported that no effects on the inward rectifier current or the voltage-gated calcium current were observed. It was noted that further experiments would require chronic application of the fatty acid challenge on myocytes isolated from a large animal model. Here, we report that chronic application of saturated free fatty acids on ovine atrial cells significantly abbreviated APD. The results show that compared to palmitic acid (30% reduction of APD30), there was a more profound effect on APD abbreviation with stearic acid (60%), an effect that was observed at all phases of the repolarization process. In contrast to these saturated free fatty acids, the mono-unsaturated oleic acid had no effect on APD under similar conditions.

Furthermore, we report that the fatty acids had no effects on the resting membrane potential (and presumably, would have no significant effects on the inward rectifier current), and did not alter properties of the fast voltage-gated sodium currents. Consistent with this, incubation of the cells in stearic acid did not significantly alter upstroke velocity. However, there was a significant reduction in $I_{Ca,L}$ and I_{TO}. The fatty acid effects we report here are different from those previously described [256], presumably reflecting differences in animal models (murine versus ovine), cell types (ventricular versus atrial), and nature of the fatty acid challenge (acute versus chronic).

The cell electrophysiology results, in combination with the simulations using the human atrial cell model, suggest that the selective effects of stearic acid on membrane currents are responsible for the observed changes in atrial cell action potential properties. Thus, the ionic mechanisms underlying APD abbreviation are mediated by fatty acid induced remodeling of the channels underlying $I_{Ca,L}$ and I_{TO}, with a predominant effect on the former. It is interesting that qualitatively similar parallel reductions in the two currents have been reported in AF induced remodeling.[5] The peak I_{TO} density, which is primarily composed of $I_{TO,\,fast}$ and $I_{TO,\,slow}$ was affected by the fatty acid challenge, however we did not observe a change in steady state current (I_{SS}), suggestive of differential stearic acid effects on these voltage-gated potassium channels in this animal model. In theory, a number of different molecular mechanisms can be responsible for the stearic acid induced changes on $I_{Ca,L}$ and I_{TO}, including ion channels remodeling resulting from changes in channel protein expression, post

translational modifications i.e., including channel phosphorylation or nitrosylation.[5] However, results of the biochemical analysis involving confocal microscopy and western blot showed no alterations by such mechanisms with steric acid challenge on Cav1.2. Furthermore, there were no changes in Cav1.2 protein levels in cell lysates following stearic acid treatment. However, presently, we cannot completely rule out such regulatory effects of saturated free fatty acids on these or other channels.

Remodeling of t-tubular architecture

Overall, the biochemical analysis in this study shows that with fatty acid incubation, the amount of Cav1.2 protein remains intact, and is predominantly localized to the t-tubules. It is generally accepted that atrial t-tubular network is fairly prominent in large mammals, and has profound effects on spatio-temporal properties of systolic Ca^{2+} transients.[89,262] Importantly, t-tubules have been implicated in a number of pathological conditions affecting the heart,[205,308,311] probably the result of high susceptibility to remodeling. Given predominant localization of calcium channels in the network, it was suggested that reduced coupling between influx of Ca^{2+} and the release of sarcoplasmic reticulum (SR) Ca^{2+} played a role in the arrhythmogenesis in the ovine AF model.[308] In our experiments, the Di-8-ANEPPS staining with incubation in saturated fatty acids showed a significant reduction of the atrial t-tubule network,[308] with stearic acid>palmitic acid effects. Furthermore, there was a significant reduction in capacitance of myocytes incubated with stearic acid without changes in cellular

morphometry. Confocal microscopic analysis also showed no apparent changes in Cav1.2 localization or α-actinin periodicity. Taken together, these data suggest fatty acid induced modification to the t-tubule invaginations near the lateral membrane, such as by 'pinching off' or physically occluding the pore, thereby preventing access of Di-8-ANEPPS to the network of tubules. Such alterations of the t-tubule structure may also be expected to compromise calcium handling mechanisms. The differential fatty acid effects on ion channels may be attributed to mechanisms associated with channel sub-cellular localization, and/or to fatty acid induced effects on channel molecular properties. Moreover, the effects of the different fatty acids may be dependent on their physio-chemical properties, including chain lengths (16; palmitic versus 18; stearic), as well as on their degree of saturation; fully saturated (stearic; 18: 0) versus the mono-unsaturated (oleic; 18: 1) nature of the fatty acids. In the latter case, elaidic acid, which is the trans isomer of oleic acid, could be used to test such a hypothesis.

Limitations

In the present study, we have focused our experiments in evaluating one group of biofactors, the saturated free fatty acids present in the epicardial adipose tissue of the ovine atrial myocardium. The major limitation of this study is the *in vitro* nature of our experiments. *In vivo*, biofactors produced by adipocytes therein may regulate the atrial myocardium by mechanisms involving additive effects of these (and other) fatty acids. It has been shown that specific combinations of fatty acids found in blood serum under normal conditions can

have physiologically beneficial effects to cardiac structure and function[312]. Nevertheless, this first set of experiments was conducted to begin a systematic evaluation of the individual saturated fatty acids present in obese sheep. The combinatory effects of these fatty acids do warrant investigation in the future. Also, it is expected that the response of cardiac myocytes to the incubation in the fatty acids may be different if the contractile machinery were fully activated during cardiac muscle contraction. These limitations notwithstanding, our results show for the first time, that elevated levels of a main metabolic biofactor of epicardial adiposity (saturated free fatty acids) remodels the T-tubular architecture of atrial cells in this large animal model, plays a key role in ion channel remodeling, and in arrhythmogenicity associated with obesity.

Conclusions

Chronic application of saturated free fatty acids leads to the remodeling of the normal architecture of t-tubules and the properties of membrane ionic currents in atrial cells. Chronic application of stearic acid modifies the t-tubular network, primarily affecting functional properties of I_{CaL}, with potential implications in abnormal atrial electrical excitation.

3.5 Methods

The University Committee on the Use and Care of Animals (UCUCA) at the University of Michigan (protocol 10552-2) approved all experiments. Briefly, atrial cell were isolated using the standard Langendorff retrograde perfusion

methods[293]. Current- and voltage-clamp experiments, including solutions for all experiments, biochemical and optical techniques have been previously published[1,304],

Isolation of Adult Ovine Myocytes:

Sheep atrial myocytes were isolated using the Langendorff retrograde perfusion method as previously described[1,293,304]. The protocol followed conforms of the Guide for Care and Use of Laboratory Animals published by the United States National Institutes of Health (NIH) Publication No. 85-23, revised 1996. Briefly, male sheep (25-30 kg) were anesthetized with sodium pentobarbital (30 mg/kg I.V.). Following thoracotomy, the heart was immediately removed, transported from the necropsy room in ice-cold cardioplegic solution containing (in mmol/L): Glucose 280, KCl 13.44, $NaHCO_3$ 12.6, Mannitol 34. The aorta was cannulated and retrogradely perfused (180 mL/min) with Tyrode's solution containing (in mmol/L): NaCl 148, KCl 5.4, $MgCl_2$ 1.0, $CaCl_2$ 1.8, NaH_2PO_4 0.4, Glucose 5.5, HEPES 15; pH 7.4 (NaOH) at 37^oC until the effluent was clear of blood. Subsequently, a Ca^{2+} free solution containing (in mmol/L): NaCl 148, KCl 5.4, $MgCl_2$ 1.0, NaH_2PO_4 0.4, Glucose 5.5, HEPES 15; pH 7.4 (NaOH) was perfused for at least 10 minutes or until all contractions ceased. Collagenase (160 units/mL; Worthington Type II) was added to the Ca^{2+} free solution and perfused for 40 minutes. After cells were properly digested, a 1.5 cm x 1.5 cm region of the free wall bordering the posterior section of the left atrial chamber was collected for dissociation. Sectioned tissue was then placed in KB solution containing (in

mmol/mL): KCl 80, $MgSO_4$ 5, KH_2PO_4 30, Glucose 20, EGTA 0.25, Creatine 5, β-Hydroxybutyric acid 5, Taurine 20, Pyruvic acid 5, ATP 5; pH 7.4 (KOH). Left atrial cells were isolated by gentle teasing and mechanical agitation. The isolated cells were kept at room temperature in KB solution for another 30 minutes before Ca^{2+} reintroduction[293]. Cells were centrifuged and resuspended in a normal Tyrode solution at room temperature until use in acute (t = 0) experiments. In all other experiments, cells were centrifuged, plated and cultured in M199 medium with 3% penicillin/streptomycin, as previously described[273].

Preparation of Free Fatty Acids Solutions:

All solutions were prepared fresh for each experiment similar to previously described[313]. We dissolved palmitic (Sigma), stearic (Sigma) or oleic acid (Sigma) in 1 mL dimethyl sulfoxide (DMSO). Separately, we dissolved "fatty acid free" bovine serum albumin (Sigma) in 19 mL of DiH_2O. The FFA/DMSO solution was added stepwise (to prevent precipitation) to 19 mL of DiH_2O/BSA to create a 3 mM FA stock at 37^{o}C. This stock was added directly to either M199+ culture media (chronic experiments) or to normal Tyrode's (acute experiments) to create a 10 μM working solution. We chose a 10 μM concentration based oon the findings of Padmanabhan et al and Veiga-Lopez et al [258,314] in measuring the serum free fatty acid concentrations of lean and obese sheep. Discrepancies in exact fatty acid concentration vary from study to study based on analysis methodology but the percentage increase in lean vs. obese is quantitatively similar [315]. In order to directly compare the effects of each FA, our experiments

tested each FA at one concentration. Our experimental concentration (10 μM) is the physiologically observed concentration in obese sheep serum for stearic acid alone. Palmitic acid and oleic acid are significantly less abundant in lean and obese sheep serum[258].

Single Cell Preparation for Experiments:

All experiments, unless otherwise stated, were conducted at 24 hours. Due to the high experimental variability in the outbred ovine model system, we have presented all experimental data with animal matched controls similar to Musa et al[304]. Furthermore, the analysis was conducted in this manner due to the inability to acquire all data sets within the experimental time frame.

Single Cell Electrophysiology

The external solution, pipette filling solution, and protocols used for recording individual currents are described below in detail.

Action Potential Recordings:

Borosilicate glass electrodes were pulled using a Brown-Flaming puller (model P-97), yielding a tip resistance of 3-5 mΩ when filled with pipette solution. Action potentials were recorded on a 700B Multiclamp amplifier at 37^{o}C (Molecular Probes) in normal HEPES Tyrode solution as previously described [1]. Briefly, cells were stimulated using a DS8000 Stimulator (World Precision Instruments) with 3-5 msec current pulses. Pulse trains of 20 stimuli were elicited at 1 Hz. Action

potential duration values (APD30, 50, 80) were determined as the repolarization percent from the peak to baseline using custom software. All statistics (two tailed Student t tests) were carried out using Prism 6 (GraphPad).

External solution (mmol/L): NaCl 148, NaH_2PO_4 0.4, $MgCl_2$ 1, Glucose 5.5, KCl 5.4, $CaCl_2$ 1.0, HEPES 15; pH 7.4 (NaOH).

Pipette filling solution (mmol/L): KCl 148, $MgCl_2$ 1, EGTA 0, HEPES 5, Creatine 2, K_2-ATP 5, Phosphocreatine 5; pH 7.2 (KOH).

Voltage Clamp Experiments:

Whole-cell recordings from isolated sheep atrial myocytes were done using standard methods[293]. All recordings were conducted at room temperature, and were performed using an Axopatch-200B Amplifier and/or 700B Multiclamp amplifier (Molecular Devices Sunnyvale, CA) and data acquisition and analysis were performed utilizing pClamp10.2 software (Molecular Devices Sunnyvale, CA). Pipette resistances ranged from 2-3 MΩ. Access resistance was compensated to 1-2 MΩ. Input resistance was 500 MΩ to 1 GΩ.

Sodium Current

External Solutions (mmol/L): NaCl 5, $MgCl_2$ 1, $CaCl_2$ 1.0, $CdCl_2$ 0.1, HEPES 20, Glucose 11, CsCl 132.5 (pH = 7.35 with CsOH).

Pipette filling solution (mmol/L): NaCl 5, CsF 135, EGTA 10, MgATP 5, HEPES 5 (pH = 7.2 with CsOH).

Protocol: In order to record sodium currents cells were held at -160 mV followed by depolarizing steps from -80 to +10 mV in 5 mV increments. The duration of

the voltage steps were 300 msec with a 5 second interval between successive voltage steps. Voltage-dependence of inactivation was assessed by holding at −160 to −40 mV followed by a 30-ms test pulse to −40 mV to elicit I_{Na}.

Analysis: Voltage-dependent activation of I_{Na} was assessed by generating conductance voltage relationships (m-infinity curves) and fitting the data with a standard Boltzman function (Origin 8.1).

L Type Calcium currents

External solutions (mmol/L): NaCl 137, CsCl 5.4, $MgCl_2$ 1, $CaCl_2$ 1.2, HEPES 10, Glucose 10, 4-Aminopyridine (4-AP) 2, (pH 7.35 with NaOH)[294].

Pipette filling solution (mmol/L): CsCl 120, TEA-Cl 20, $MgCl_2$1, MgATP 5, Na_2GTP 0.2, HEPES 10, and EGTA 10 (pH 7.2 with CsOH)[294].

Voltage dependence of peak $I_{Ca,L}$ was measured by holding at -70mV; 300-msec voltage steps were applied from -50 to +60 mV in 5 mV increments. The interval between voltage steps was 3 sec. Voltage-dependence of inactivation was assessed by holding at -70 to +10 mV followed by a 30 msec test pulse to +10mV to elicit I_{Ca} (Origin 8.1).

Depolarization-activated potassium currents

External solutions (mmol/L): NaCl 148, NaH_2PO_4 0.4, $MgCl_2$ 1, Glucose 5.5, KCl 5.4, $CaCl_2$ 1.0, HEPES 15 (pH 7.4 with NaOH). To block sodium channels and calcium channels 30 µmol/L TTX (Tetrodotoxin) and 5 µmol/L Nifedipine was added to the external solution.

Pipette filling solutuion (mmol/L): KCl 138, EGTA 10, HEPES 10, $MgCl_2$ 1, glucose 5 (pH 7.4 with KOH).

Protocol: Potassium currents were recorded using 5-second depolarizing pulses to potentials between -40 mV and +60 mV from a holding of -70 mV. Voltage steps were in steps of 10 mV at 15 sec intervals[43].

Antibodies:

Primary antibodies used were: Rabbit polyclonal anti-Cav1.2 (Alomone Labs), Phospho Serine-1928 (Badrilla) and Rabbit polyclonal anti-S-nitrocysteine (Abcam), Mouse monoclonal sarcomeric α-actinin (Sigma). Secondary antibodies used were: Donkey anti-mouse Dylight 549, Donkey anti-rabbit Dylight 488 (Jackson ImmunoResearch), rabbit GAPDH antibody (Sigma-Aldrich).

Immunofluorescence:

Immunofluorescence analysis was carried out on myocytes plated on 22 mm glass coverslips. Cells were fixed with 3% paraformaldehyde in PBS, and then blocked with 10% Normal Donkey Serum in 0.1% Triton-X100 in PBS (NDS) for 1 h at room temperature. Incubation with primary antibodies was done in 5% NDS, overnight at 4°C. The next day coverslips were washed with 0.1% Triton-X100 in PBS (PBS-T, 3 x 10 min) and incubated for 90 minutes at room temperature with secondary antibodies diluted in 5% NDS. Coverslips were then washed with PBS-T (3 x 10 min) and PBS (1 x 10 min). Samples were treated with with 4',6-Diamidino-2-Phenylindole, Dihydrochloride (DAPI), a nucleus marker, (Molecular Probes) and then mounted onto slides using FluoromountG (SouthernBiothech).

Immunostained preparations were analyzed by confocal microscopy (Nikon A1R) to determine protein localization in relation to cell morphology. Line scanning analysis of 20 μm sections was conducted similar to Musa et al[304].

SDS-PAGE and Immunoblotting:

Control and treated cardiac myocytes were washed in cold PBS, lysed directly in the modified loading buffer (Tris•HCl, 25 mmol/l; NaCl, 150 mmol/l; EDTA, 1 mmol/l; NaF, 4 mmol/l; Sodium ortho-vanadate, 2 mmol/l; 1% Triton X-100, protease inhibitor, 5% glycerol, 1%SDS, 0.05%bromophenol blue, 5% β mercaptoethanol) and sonicated. Lysates (20 μL) were separated by gel electrophoresis in one-dimensional 4-20% sodium dodecyl sulfate polyacrylamide gel (Invitrogen) in Tris-Glycine buffer (Fisher). Separated proteins were transferred to nitrocellulose (Bio-Rad, 0.45 μm pore size) in a Hoeffer transfer apparatus. Nonspecific binding sites were blocked by incubation with 5% nonfat dry milk (NFM) in PBS with 0.05% Tween-20 (PBS-T). Membranes were then incubated with specific primary antibodies (0.5-1 ug/ml) diluted in 5% NFM overnight at 4^{o}C. Following four ~5 minute washes in PBS-T, membranes were incubated with horseradish peroxidase (HRP)-conjugated secondary antibodies (Jackson Immunorersearch) for roughly one hour. Antigen complexes were visualized using enhanced chemiluminescence (Pierce). Protein bands (top bands, were doublets are present) were quantified by digital densitometry with a BioRad Fluor-S imager and Quantity One software (Bio-Rad). Precision Plus

Protein All Blue Standards (Bio-Rad) was used to determine molecular weight of all blots. GAPDH was used as a control in all experiments.

Transverse Tubule Imaging:

Protocol: 1 mg of voltage-sensitive dye di-8-ANEPPS (Life Technologies, Carlsbad, CA) was dissolved in 1 mL of DMSO and used as a stock (stored at 4^{o}C). Working solution was prepared as a 50:50 v/v mix of di-8-ANEPPS stock and 20% pluronic acid as previously described[82]. 15 uL of stock solution was used per 1 mL 300 μM Ca^{2+} Tyrode solution. Myocytes were allowed to incubate for 10 min before imaging.

Imaging: Imaging of t-tubules was done on a confocal microscope (Nikon A1R) using a 60x oil immersion objective. Three-dimensional rendering of atrial and ventricular myocytes was constructed by stacking 15-25 XY planar images. Images were acquired with 0.5 μm spacing. Confocal images were visualized and analyzed with the NIS-Elements program (Nikon).

Analysis: To determine the extent of t-tubular network within a given cell, we manually created a region of interest (R1) inside the periphery of the cell (excluding the lateral membrane and intercalated disk). A second region of interest was created just outside the border of the lateral membrane and the intercalated disk and encapsulated the entire cell (R2). These regions were quantified by pixel intensity summation in NIS-Elements (Nikon, Japan). A third region of interest was created in either the nuclear region or a region lacking t-tubules (R3). The area of R3 was extrapolated to the surface areas of R1 and R2 and was used to correct the data for background fluorescence. After correction, we took the ratio of R1/R2 as a measure of t-tubular content in a given cell. This analysis was repeated individually for each cell and a mean ratio ± SEM was calculated for each group.

External solution (mmol/L): NaCl 148, NaH_2PO_4 0.4, $MgCl_2$ 1, Glucose 5.5, KCl 5.4, $CaCl_2$ 0.3, HEPES 15; pH 7.4 (NaOH).

Preparation of Adipocyte-Conditioned Media

Epicardial adipose tissue was removed from regions detailed in Figure 1. Cells were isolated as previously described.[316] Minced adipocyte factions were digested using Type I Collagenase (Worthington Labs) for 45-60 min @ 37^{o}C with continuous shaking. Cells were spun at 500g for 5 min to separate adipocytes from stromovascular cells. Purified adipocytes were sterile filtered (100 µm filter). 100 µL of digested and filtered adipocytes was cultured for 24 hrs prior to application to left atrial myocytes. At 24 hours, adipocytes were removed from the culture media (adipocyte conditioned media) and applied to myocytes for an additional 24 hrs. We used media from myocytes incubated for 24 hrs as a control. Experiments were conducted at a total of 48 hours in culture (24 hrs in control media or ACM).

Statistical Analyses:

Data are presented as the mean ± SEM. $Ca_V1.2$ and alpha actinin periodicity was determined by linear regression fits o f the data. APD analyses, voltage clamp experiments and calcium transient data and alpha smooth muscle actin western data used a two tailed unpaired Student t-tests and were carried out using Prism 5 (GraphPad) or Excel (Microsoft). Significance was defined by p-values ≤0.05

Chapter 4

Thesis Discussion and Future Directions

4.1 Major Interpretations

Repolarization, the major determinant of action potential duration (APD), refers to the return of transmembrane voltage after peak depolarization, towards hyperpolarized (resting) potentials. In the heart, a variety of ion channels and transporters work in a voltage- and time-dependent synchrony to initiate and terminate contraction during systole and diastole. The studies presented in this dissertation serve to further our understanding, through comprehensive electrophysiological and biochemical techniques, the major ionic mechanisms associated with the heterogeneous morphology of the cardiac action potential. Furthermore, the individual studies highlight the well-established diversity of ionic currents and action potential morphology across multiple regions of the heart and the species dependent differences therein. Investigations of the mechanisms determining APD are crucial to our understanding of the causes of reentrant activity: the major driver of arrhythmogenicity in the heart. The focus of this dissertation on Purkinje and atrial cells share a unique commonality in that they are designed to favor electrical conduction over mechanical force generation. However, it was the finding of this dissertation that I_{Ca}, the essential current in

excitation-contraction coupling, plays a major role in shaping AP morphology. Specifically, the studies presented here detail the instrumental role of I_{Ca} in determining differential repolarization of APs obtained from septal, apical, Purkinje and atrial myocytes. Both studies demonstrate the important contributions of each form of I_{Ca} (I_{CaT} and I_{CaL}) in generating the unique morphology found in mouse Purkinje cells and ovine atrial myocytes. Furthermore, these studies highlight the functional role of myocyte structure and ion channel microdomains in determining electrophysiological behavior. In its entirety, the results presented in this dissertation focuses on the diverse expression, localization and density of ion channels and the currents they produce, in the myocardium under physiological and pathophysiological conditions.

The initial study of this dissertation demonstrates for the first time, the electrophysiological characterization of wildtype mouse Purkinje cells, it developed a novel numerical simulation to further understand cytosolic calcium diffusion and the role of I_{CaT} in generating a prolonged APD. During our isolation process we successfully identified the unique morphological characteristics of mouse Purkinje cells compared to ventricular myocytes. Serendipitously, we also characterized a “transitional” myocyte that contains morphological properties similar to that of ventricular myocytes while maintaining electrophysiological properties that closely resemble Purkinje cells.

The second study of this dissertation focused on the electrophysiological and structural properties of isolated atrial cells of the ovine model exposed to

FAs. Increased adiposity has been suggested to be an active site for secretion of biofactors. FAs secreted from adipocytes have been suggested as potential mediators of altering cardiac myocyte function. Specifically, those FAs released from neighboring epicardial adipose tissue may act a paracrine regulator of myocyte function. We chose to investigate the electrophysiological consequences of acute, short-term (4-6 hrs) and chronic (24 hrs) incubation of the three major FAs found in ovine epicardial adipose tissue with atrial myocytes. Our data suggests that stearic and palmitic acid, which are saturated FAs, have the potential to affect the electrophysiological properties of atrial myocytes. Atrial myocyte APD was significantly reduced with reductions to both I_{CaL} and I_{TO}. These ionic currents play active roles in determining the APD of atrial cells. We utilized a previously published model of the human atrial AP and modified I_{CaL} and I_{TO} according to our experimental data. These ionic modifications recapitulated our observed APD truncation in ovine atrial cells. Interestingly, we observed a significant decrease in cell capacitance without a change in cell dimensions. Using confocal microscopy we determined that the t-tubule network in stearic acid treated cells was severely diminished compared to controls. Given the dependence of Cav1.2 function of the delivery of calcium ions to the distal t-tubule adjacent to the junctional SR, any blockage or disruption of the t-tutuble system would compromise I_{CaL} by effectively reducing the local concentration of calcium available for transport through the channel and potentially block the propagation of the electrical impulse to activate these channels. The exact mechanism by which stearic acid alters t-tubule membranes remains unknown

but our data suggests a remodeling at the sarcolemmal membrane. This is due, in part to the preserved striated pattern of Cav1.2 in stearic acid treated cells.

4.2 Heterogeneity in Ion Channel Expression Causes Regional Specialization

Proper function of the myocardium is dependent on the appropriate timing of contraction across all regions of the heart, which is controlled by time-dependent depolarization and repolarization of cardiac myocytes. PCs are specialized to deliver rapid conduction of the electrical impulse from the atria to the ventricles and aid in the synchronous activation of the ventricular myocardium. Interestingly, a loss of synchrony in the His-Purkinje system may initiate fatal ventricular arrhythmias[15-17,148,317]. Our investigations into PCs support previous evidence that PCs are characterized by a specialized expression of ionic currents compared to ventricular myocytes. In order to provide rapid conduction from the atria to the ventricles, PCs have been characterized by large amplitude I_{Na} and a higher dv/dt_{max} as compared to the surrounding ventricular myocytes[318,319]. Furthermore, It was previously shown that PCs have pacemaker activity allowing for ventricular contractions in the absence of atrial stimulation[318,319]. Our data confirm unique I_{Na} density and pacemaker activity in contributing to the role of the His-Purkinje system in the murine heart. These data support species dependent similarities in the functional role of the conduction system.

Most importantly, our data demonstrate a striking difference between the AP morphology of PCs and neighboring ventricular myocytes. This was due

primarily, from the presence of I_{CaT} in PCs and reduced I_{TO} density compared to ventricular myocytes. These differences are markedly different from the comparative studies of AP morphology in PCs in the ovine, where PC APD is similar to that of ventricular myocytes[280]. However, multiple studies[278,320-322] in the canine and rabbit have reported similar observations to those observed here. In the murine, the role of a prolonged repolarization phase may function to limit the potential for reentrant arrhythmias. Specifically, the prolonged plateau phase of murine PCs may act as a safe guard to triggered activity under normal physiological conditions of the working myocardium. However, given the high heart rate (>600 bpm) of the mouse and that PCs are characterized across species by higher upstroke velocity, intercellular coupling, longer APD and spontaneous pacemaker activity, the role of PCs in generating reentrant activity remains controversial[56,148,323-325]. The PC/ventricular myocyte junction has been suggested to play a crucial role in the initiation and maintenance of ventricular arrhythmias. To date, the exact mechanism by which this occurs remains unknown but has been suggested to be the result of triggered activity (e.g. EADs & DADs) originating from PCs. The contribution of triggered activity has been suggested to arise from the altered state of calcium handling in these cells compared to ventricular myocytes[268]. These differences may be due to increased I_{Na}, lack of t-tubules and differing modes of calcium activation (in PC versus ventricular myocyte) [326-328]. Therefore, it has become increasingly clear that PC contributions in generating reentrant activity may be a consequence of specialization of ionic currents and calcium handling in these cells.

4.3 Ion Channel Microdomains as Targets for Remodeling

Our observations of the specialized conduction system elicit specific details regarding the membrane ionic mechanisms governing action potential morphology. During the maturation of the second study of this dissertation, it became evident that simple membrane expression of ion channels was insufficient to explain the remodeling we observed by FAs. This added level of complexity revealed the importance of trafficking and membrane localization in physiological and pathophysiological remodeling of myocytes. Localization of Cav1.2 into t-tubular microdomains is a well-studied phenomenon and its importance in the maintenance and regulation of EC coupling cannot be understated[7,54,77]. Our data suggest that stearic acid (SA) preferentially remodels I_{CaL} due to the high concentration of Cav1.2 in t-tubular microdomains. We supported this hypothesis from multiple perspectives during the progression of this study. First we investigated I_{Na}, which remains unaffected by SA treatment. It has been shown previously[329,330] that Nav1.5, the major isoform underlying I_{Na} is highly concentrated at the intercalated disc with a minimal presence in the t-tubular network. The separate populations of Cav1.2 and Nav1.5 allows for specificity in AP remodeling due to disparate ion channel microdomains in the atrial myocyte (e.g. intercalated disc vs. t-tubules). Furthermore, our imaging of the t-tubular membranes demonstrates significant structural remodeling through a currently unknown mechanism. Given our immunocytochemistry and western data, we believe Cav1.2 channel localization to t-tubular microdomains is not

disrupted. However, the apparent structural remodeling, potentially at the Z-groove of the t-tubule invagination, causes I_{CaL} to be preferentially affected during SA treatment. Remodeling of the t-tubular membrane, which as been demonstrated in multiple pathophysiological animal models (see Louch et al[263] for detailed review) suggests a precedent for the novel remodeling we observe with I_{CaL} during SA treatment.

4.4 Progression from the Murine to the Ovine Model

The ovine model was used in the second study due to the epicardial fat distribution with concentrated depots near the posterior left atrium (LA) and left atrial appendage similar to the epicardial adipose depot in humans. Two saturated FAs (SFAs), palmitic acid (PA) and stearic acid (SA) and one mono-unsaturated FA, oleic acid (OA) are the three major FAs in epicardial adipose of the ovine model, and comprise approximately 85% (25%, 35% & 25.5% respectively) of all free FAs found in blood serum[257,258]. Furthermore, compared to controls, changes in SFA levels in obese humans and in sheep are quantitatively similar[258-261]. The presence of increased epicardial adipose tissue has been suggested to elevate local FA concentrations in the atrial myocardium. In addition, fatty infiltration (*adiposis cardiaca*) from the epicardial surface has been suggested to increase arrhythmogenicity and usually increases with obesity and certain disease conditions of the heart, which is not present in the rodent model[234,238,248].

Our transition to the ovine model in place of the murine was also supported by significant differences in activated metabolic pathways from the lean to obese state. Recently, a study by Li et al[331] performed a rigorous functional genomics screen of lean and diet-induced obese rodents. Their gene-expression profiles were compared to lean and obese human profiles from previously published studies. They concluded rodents to be an “adequate” model for studying adipogenesis but highlighted major differences in the metabolic responses to lipid metabolism, such as fatty acid oxidation. These discrepancies, coupled with the lack of measureable epicardial adipose tissue in the rodent model, suggests the presence and metabolic pathways associated with lipids in rodents differs significantly from large mammals. Analogous to epicardial adipose tissue, humans and other large mammals (e.g. dogs and sheep) share complex atrial t-tubule structure that is absent in rodent atrial myocytes[84,262]. Recently, it has been shown that the t-tubule network in the atria is remodeled during certain pathological conditions[263]. Use of the rodent model would have limited our ability to observe structure-function relationships of t-tubules in the atrial myocardium. In addition, the electrophysiological differences between the rodent and human further supports our use of a large animal model. The human and sheep heart beat at roughly 1-2 Hz with the rodent heart beating at a frequency closer to 10 Hz. Due to these fundamental physiological differences, the underlying ionic composition of myocytes in rodents generates action potentials of vastly different morphology compared to those in humans. In order to avoid further complicating our electrophysiological interpretations after incubating myocytes with FAs, we

have chosen to use a model that better serves as a surrogate for human cardiac physiology.

4.5 Future Directions: Study 1

1. Elucidate gating mechanisms, unitary events and molecular identification of the major PC ion channels: Chapter 2 provides the first ionic profile of wildtype murine PCs. However, the biophysical characterization of ionic currents that underlie the PC AP is incomplete. To better profile the properties of these ion channels, generating activation and inactivation curves (fit to Boltzmann functions) are appropriate for the major ion channels studied here. These experiments would be identical in type, with minor technical differences (e.g. voltage-clamp parameters) to those presented in Chapter 3. These experiments would provide crucial information of the gating properties of each ion channel, which could be integrated into our model and potentially demonstrate further differences between PCs and ventricular myocytes. In the majority of ionic currents investigated in this study, we observed marked differences in whole cell current density. Whole cell current density is represented by the expression $I = NiP_o$. Experimentally, differences in one or more of these parameters are defined as a: (1) change in unitary conductance properties (γ) (2) alteration in the open probability of the unitary conductance (P_o) and (3) a change in the number of functional channels in the membrane (N). To date, we have not investigated the underlying mechanisms responsible for these differences in PCs compared to

VMs. To address these limitations we would probe protein content using western blot analysis of a membrane preparation. This technique allows for probing of protein content of an enriched plasma membrane fraction. The major pitfall of these experiments is the quantity of sample needed to probe on an SDS-Page gel. Purkinje fibers of the murine heart are especially low in number and are considerably frailer than their ventricular myocyte counterparts. Furthermore, efficient separation of PCs from ventricular myocytes may prove problematic and contaminate of our PC sample. Therefore, it may prove beneficial to probe membrane proteins via extracellular-loop specific antibodies and visualize with high-resolution confocal microscopy. The benefits of these experiments are two-fold: (1) analysis of membrane proteins, while qualitative, provides useful information regarding the relative abundance of these ion channels across cell types and (2) visualization via confocal microscopy provides the molecular localization of these proteins (e.g. intercalated disc, sarcolemma, etc.) which has not yet been defined in the murine PC. Analysis of unitary conductance (Y) and open-probability (P_o) would be achieved through rigorous single channel analysis similar to previously described[273]. Generation events conductance, open and closed time histograms of unitary events may provide useful information in determining differences between PC and VM ion channel current density. The molecular correlates that underlie the ionic currents in PCs have not been investigated in this dissertation. The use of single cell real-time PCR for comparative analysis between PCs and ventricular myocytes offers gene expression patterns on a variety of electrophysiological targets not limited to ion

channels (e.g. scaffolding proteins, signal transduction pathways etc.). As an example, the data from these experiments would provide useful information in characterizing the pacemaker current (I_f) in PCs, which to date has no known molecular correlate.

2. Investigations into "transitional" cells: For over 40 years, the scientific community has been aware of a unique cardiac cell type existing at the junction of Purkinje fibers and the ventricular myocardium[332]. These junctions, integral in Purkinje-myocyte coupling, have been implicated in the initiation and maintenance of ventricular arrhythmias[333]. Observations of this cell type in the $Cx40^{GFP/+}$ mice demonstrate their presence in the murine model. To date, there is no information regarding the electrophysiological characteristics of this cell type in the murine model. Continuing, similar to the study presented in Chapter 2, with transitional cells and determining the underlying mechanisms of excitation are crucial in fully understanding Purkinje-myocyte coupling and the role transitional cells play in ventricular arrhythmias. The major limitations to investigating transitional cells are the limited quantity and near impossibility in differentiating these cells from normal ventricular myocytes in the wildtype murine heart. The use of the $Cx40^{GFP/+}$ is a viable alternative. However, the role of expressing GFP and Cx40 may have unintended homeostatic consequences, which is the underlying reason this model was not used in our study. Despite this limitation, use of this mouse would eliminate a major technical difficulty associated with successful identification of transitional cells.

3. Integration of transgenic Cx40$^{GFP/+}$ mouse: Successful isolation and distinction of cardiac PCs proved to be the major limiting factor in our experiments. In future projects, the integration of the transgenic Cx40$^{GFP/+}$ mouse, shown in our study, would eliminate the difficulty in distinguishing PCs from neighboring VMs. Furthermore, the mating of the Cx40$^{GFP/+}$ mouse with mouse models of cardiac disease would allow investigators to study the contribution of PCs and "transitional" myocytes to various inherited arrhythmias. Furthermore, successful characterization of "transitional" myocyte ionic currents could be integrated into the VM numerical model in this dissertation.

4.6 Future Directions: Study 2

Future Directions

Throughout this dissertation, my doctoral studies have demonstrated the underlying mechanisms responsible for myocyte AP morphology and in this particular study, the ionic currents responsible for electrophysiological remodeling of atrial APD. Unlike the initial study in Purkinje cells, the mechanisms governing differing APDs in this study are the result of structural remodeling, which directly contributes to the functional ionic composition of our cells incubated with SA. There are a number of experiments in which to pursue these mechanisms, along with supportive experiments to gain additional insight into the role SA has on atrial myocyte electro-mechanical function.

Major Directions

1. T-tubule remodeling mechanism: It has been suggested that during metabolic stress, t-tubule remodeling may be the consequence of mitochondrial enlargement, which causes the occlusion of the t-tubular lumen[334]. In cardiac myocytes, mitochondria are the site of FA oxidation and diets causing elevated serum FA levels lead to mitochondrial stress and enlargement (MtSE)[335,336]. It has been demonstrated previously that stearic and palmitic acid have differential metabolic pathways in human patients any may underlie the differences in t-tubule remodeling demonstrated in this dissertation[337]. Therefore, it is my hypothesis that treatment with stearic acid causes MtSE, which blocks the t-tubule lumen. To test this hypothesis, use of cyanide as a mitochondrial metabolic stressor, would be employed as previously described[334] to demonstrate enlargement of mitochondria are sufficient to occlude the t-tubule lumen in ovine atrial myocytes. Next, the use of pharmacologic inhibitors of FA transport and oxidation would be used to elucidate the necessary steps involved in MtSE. To rule out SA integration into the membrane, which may alter ion channel function[338] independent of t-tubule remodeling, the use of Arylpiperazines (inhibitors of FATP) during SA treatment is warranted. Arylpiperazine treatment allows for the determination of whether t-tubule remodeling is the sole contributor to the electrophysiological alterations observed in this dissertation or whether FAs have a more direct mechanism of action on ion channel function[339]. Given the lack of acute and short term (4-6 hour)

remodeling by stearic acid it is unlikely that the fatty acid transport protein (FATP), located on the sarcolemmal membrane, is a major contributor to the t-tubule remodeling. However, we cannot rule out that SA accumulation in the sarcolemmal and t-tubular membranes may have a time course greater than 6 hours. Since, we cannot rule out FA entry into myocytes by transport proteins other than FATP we will attempt direct inhibition of mitochondrial FA transport proteins. Perhexiline inhibits transport of FAs by carnitine palmitoyl transferase (CPT-1), which is located on the outer mitochondrial membrane. Experiments involving Perhexiline during SA treatment aid in determining whether mitochondrial uptake and subsequent metabolism of SA are responsible for the remodeling observed in this dissertation. In order to understand whether the accumulation of Fatty Acyl-Carinitine (downstream metabolite of CPT-1) alone causes mitochondrial stress, or if β-oxidation of Fatty Acyl-CoA (downstream metabolite of Fatty Acyl-Carinitine) is responsible for MtSE, treatment with Ranolazine to block β-oxidation will be implemented. Ranolazine is a partial fatty acid oxidation (pFOX) inhibitor, which directly blocks β-oxidation, presumably by decreasing the ratios of NADH/NAD+ and acetyl-CoA/free CoA in the mitochondrial matrix[340,341]. To examine whether any of these pharmacologic treatments alter FA induced MtSE we will use either immunocytochemistry with readily available mitochondrial antibodies (Millipore, Abcam, Sigma-Aldrich etc.) and examine mitochondrial calcium retention capacity as previously described[342] to determine the health of mitochondria in SA treated cells. Separate treatments of atrial myocytes with Cyanide (without SA), Arylpiperazines, Perhexiline and

Ranolazine may offer mechanistic insight into the remodeling observed during SA incubation by defining whether (1) MtSE is sufficient to block t-tubules (2) whether membrane fluidity is altered by SA and whether this alters channel function (3) whether MtSE occurs due to accumulation of metabolites at the inner/outer mitochondrial membrane or (4) whether accumulation of Fatty Acyl-CoA and its β-oxidation in the mitochondrial matrix are causes of MtSE.

To further understand the remodeling of t-tubules, localization of t-tubule specific proteins via high-resolution confocal microscopy could be implemented to elucidate whether an alteration has occurred solely at the Z-groove and/or the structural integrity of t-tubules near the myocyte core are effected. BIN1 has been previously described[92] in the initiation of t-tubule genesis and localizing Cav1.2 to the t-tubule space. Utilizing this protein as a marker for t-tubule integrity at sub-sarcolemma levels would provide insight to whether the t-tubule network remains intact after exposure to SA. Alternative t-tubule markers are described further in Kostin et al[343] (e.g. Junctophilin-2, Caveolin-3, Telethonin (Tcap). We would accompany staining of t-tubule specific proteins with known non-t-tubule proteins (e.g. Nav1.5, Cx40, N-cadherin etc.), which are primarily localized to the intercalated disc, as a negative control.

2. Direct observation of Remodeled t-tubule Structure: My doctoral thesis suggests that SA structurally remodels t-tubules causing a significant reduction of I_{CaL}. Insight into the process by which SA causes these structural abnormalities would provide a direct mechanism of action to the remodeling process. It appears,

through morphometry measurements, that myocytes incubated with SA retain their size but have a reduced capacitance. Given these observations, we hypothesize SA causes a modification at the sarcolemma and fuses the t-tubule pore (invaginations) at the surface or along their length. A direct test of this unresolved question would invoke a scanning ion conductance microscope, which uses a scanning pipette to produce a topographic representation of the surface of a live atrial cell similar to Lyon et al[205]. Direct observation of Z-grooves, the opening of t-tubules, would produce detailed surface topography and provide insight to the structural integrity of t-tubules at the sarcolemma. To date, remodeling associated with t-tubules is poorly understood. Since we have introduced lipids into our test conditions and we hypothesize changes to the membrane at the sarcolemma, observations of the Z-groove will not provide biochemical data of t-tubule remodeling. Therefore, use of electron spin resonance (ESR) or nuclear magnetic resonance spectroscopy (NMR) to determine the membrane composition of atrial myocytes incubated with SA may aid in determining whether membrane fluidity is altered. It has been shown previously[344] that altered membrane composition contributes to detubulation and reductions in I_{CaL} in isolated fetal skeletal muscle cells after modulation of membrane lipids. The results from these experiments may offer a biochemical mechanism in determining the remodeling of the t-tubular network in atrial myocytes treated with SA.

2. Quantify t-tubules in an obese ovine model: The major limitation of this study is the *in vitro* nature of all experiments performed. While there is substantial evidence of t-tubule remodeling *in vivo*, we cannot rule out the observations of t-tubule remodeling in this study is the artifact of myocytes being removed from the intact myocardium. To circumvent this limitation, visualization of the t-tubular networks in lean and obese sheep (age-matched) atrial myocytes similar to those generated in Abed et al[298]. The investigators of this study performed diagnostic observations and demonstrated significant structural (e.g. fibrosis) and electrical remodeling (e.g. conduction velocity), predisposing these animals to AF. However, no studies were conducted to determine the cellular mechanisms predisposing these animals to AF (e.g. EC coupling alterations). In addition, the implication of such results from obese sheep would be limited in their applicability to the study presented in this dissertation, as there are a number of other biofactors present (e.g TGFβ, PDGF, etc.) from the elevated levels of fibrosis in obese hearts. As an alternative, the grafting of obese epicardial adipose pads to the epicardium of lean sheep would provide a novel model to observe direct consequences of increased epicardial adipose tissue mass and secretion of associated biofactors on myocardial function. Intravenous injection of SA, PA and/or OA into a lean sheep may also elucidate the importance of each FA specifically, as outlined in this dissertation, and in combination to those levels found in obese sheep.

Minor Directions

1. Field stimulation experiments: To better model our findings as a surrogate for *in vivo* conditions, the use of IonOptix C-Pace Stimulator would provide continuous (or interval) stimulation of atrial myocytes in culture. We have demonstrated that 24 hr culturing of atrial myocytes does not result in dedifferentiation of the t-tubular architecture, which as been shown to occur during long term culturing. However, we hypothesize that the t-tubular architecture remodeling may be influenced by a two-fold benefit to this system: (1) stimulation of the cell membrane, simulating *in vivo* conditions which continuously utilizes EC coupling machinery which is not present in our current conditions and (2) increased metabolic activity of atrial myocytes in culture which may influence FA uptake and utilization. Furthermore, there is no guarantee that field stimulation will cause a discernible difference in our culturing conditions and the results yielded from these experiments compared to the results presented in this dissertation.

2. Incubate atrial myocytes with FAs in combination: It has been shown previously that the specific content of FAs in both *in vivo* and *in vitro* conditions has profound effects on myocyte function and is required for myocyte remodeling[312]. Our experiments tested the effects of FAs individually and at equal concentrations. Introduction of a FA media containing all major FAs in similar ratios to those observed *in vivo* could provide differing or conflicting results from those obtained here. We hypothesize a culturing media containing two SFAs would have compound effects on atrial myocyte remodeling. However,

we cannot discard the potential (neutral) effects of oleic acid and whether its presence will alter the remodeling observed by PA and SA.

3. Triggered calcium release (EC coupling): Given our t-tubule imaging, we expect calcium induced calcium release to be severely effected by SA. However, we have not directly shown triggered calcium release through RyR2 channels to be detrimentally altered by t-tubule remodeling. Furthermore, use of a ratiometric calcium indicator (Fura-2AM) will provide measurements of basal cytosolic calcium concentrations. Therefore, IonOptix measurements using Fura-2AM and field stimulation could demonstrate potential SA induced effects on RyR2 leak (basal cytosolic concentration), RyR2 calcium release and SERCA2a/NCX reuptake and warrant further investigation.

Appendix

Study 1: The ionic basis of the action potential in isolated mouse cardiac Purkinje cell

Results

Purkinje cell model: The Purkinje single cell model was paced at 1 Hz for 50 sec to attain steady states before using for the computer simulations. Figure S9 shows the action potential (AP) recorded in the experiments (reproduced from Figure 2 in the main manuscript) and the AP obtained by the computer model during 1 Hz pacing. We were able to reproduce the morphological AP features of the Purkinje cell in our model. Table 7 compares detailed AP characteristics from experiments and the model.

Table 1.1. Action potential characteristics of Purkinje cells obtained experimentally and by using the PC model.

Parameter	Experiments	Model
V_{rest}	-82 ± 1 mV	-77.1 mV
dV/dt_{max}	212 ± 15 mV/ms	237.1 mV/ms
APD_{50}	4.7 ± 0.3 ms	9.3 ms

APD_{70}	14.4 ± 1.6 ms	22.4 ms
APD_{90}	68.6 ± 5 ms	67.1 ms

Modified ventricular myocyte model: Similarly, we adjusted the Li et al.[270] VM model parameters to reproduce the experimentally observed AP characteristics in VMs obtained from the apex region. Figure S10 shows sample APs recorded experimentally (left) and obtained by using the modified VM model (right). Table S8 lists the detailed comparison between experimental data and the model based on AP characteristics.

Table 1.2. Action potential characteristics of Apex myocytes obtained experimentally and by using the modified VM model.

Parameter	Experiments	Model
V_{rest}	-79 ± 0.3 mV	-78.95 mV
dV/dt_{max}	114 ± 12.9 mV/ms	170 mV/ms
APD_{50}	3.3 ± 0.6 ms	6.3 ms
APD_{70}	9.3 ± 2.2 ms	11.7 ms
APD_{90}	44.1 ±4.9 ms	30.2 ms

Mathematical Modeling

A morphologically realistic numerical model of a PC was developed starting from a mouse ventricular myocyte model by Li et al.[8] and adapted, based on our experimental data. The PC was assumed to be of cylindrical shape, based on experimental measurements, and consists of a simplistic cytosolic calcium diffusion process to obtain more realistic calcium dynamics. The detailed description of the model and the ionic formulations are provided in the following section. The contribution of I_{CaT} was studied by blocking it in the PC model. The rise time of Ca^{2+} transients was varied by varying the diffusion coefficient (D_{Ca}) in the PC model to study the effects of slow Ca^{2+} transients. In addition, a PC model without cytosolic Ca^{2+} diffusion was implemented in order to study the contribution of the spatiotemporal Ca^{2+} diffusion on the APD characteristics of the PC. The PC model performance was compared with ventricular myocyte (VM) model by Li et al.[270] also modified to fit our experimental data obtained from apex myocytes.

Purkinje cell numerical model

Our model is morphologically distinct than the myocyte model. Unlike ventricular myocytes, Purkinje cells are devoid of t-tubules[326] which leads to a rather distinct calcium activation process in which calcium ions have to diffuse through the cytoplasm to reach the SR before they trigger calcium-induced-calcium-release (CICR).[327] Therefore, we implemented a simplistic cytosolic calcium diffusion process to obtain more realistic calcium dynamics in our model. The Purkinje cell

was assumed to be regular cylindrical in shape with dimensions obtained from our experiments explained in the main manuscript (4 μm radius and 129 μm length) as shown in Appendix Figure 1. The SR was located at the center of the cell spanning the whole length as shown in the figure. The radius from the center of the cell to the surface of SR was set to 2 μm.

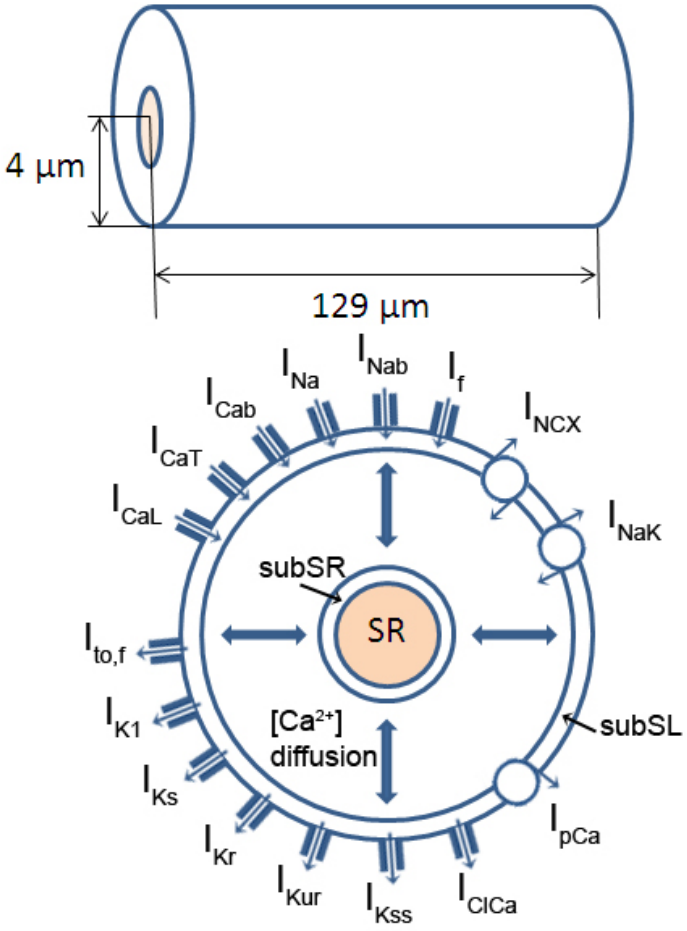

Appendix Figure 1: Schematic diagram of the mouse Purkinje cell model with sarcolemmal currents and calcium fluxes. The model consists of spatiotemporal radial cytosolic diffusion process as depicted by the two-way arrows.

The SR consisted of two compartments, namely, the release compartment, called junctional SR (JSR), and the uptake compartment, called network SR (NSR) (not shown in the figure). Ionic flux to and from the SR is collected in a small compartment around the SR, called subSR compartment. Similarly, sarcolemmal currents are collected in the subSL compartment beneath the cell membrane. Diffusion of the cytosolic Ca^{2+} ions was modeled as a function of a space coordinate between subSL and subSR compartments in addition to a time coordinate (two-sided arrows in Figure 2.5.1).

The following ionic current components were modified in order to reproduce the AP morphology and restitution properties recorded from the experiments performed in our laboratory. Other formulations in the Li model[270] remain unchanged.

Fast Na^+ current (I_{Na})

The formulation for the fast Na^+ current was based on a mammalian ventricular myocyte model (LRd 1999)[345]. The parameters of the following formulation were adapted to fit our experimentally obtained I_{Na} current density data. The experimental data was adjusted for temperature-dependent changes using Q_{10} factor of 1.5[19,12] which resulted in a +5 mV shift towards depolarized potentials in the experimental curves (Figure 2.5.2). Current density at physiological temperature was calculated by the temperature dependence relation[19]:

$I_{(T=t2)} = I_{(T=t1)} . Q^{(t2-t1)/10}$, where $t1$ = 22 °C, $t2$ = 37 °C and $Q = 1.5$. An additional +10 mV shift was introduced to compensate for physiological $[Na]_o$

concentration (134 mM).[346] The maximum conductance of the current (G_{Na}) was adjusted to obtain maximum dV/dt of 230 mV/ms. Thus, the fast Na^+ current was modeled as:

$$I_{Na} = G_{Na} m^3 hj(V - E_{Na})$$

$$\tau_x = \frac{1}{(\alpha_x + \beta_x)}$$

where x in the subscript can be *m*, *h* or *j*. E_{Na} is the reversal potential for sodium.

$$\alpha_m = 0.32 \frac{V + 47.13}{1 - e^{-0.1(V+47.13)}}$$

$$\beta_m = 0.086 e^{-V/11}$$

If $V < -40$ mV,

$$\alpha_h = 0.135 e^{(80+V)/-6.8}$$

$$\beta_h = 3.56 e^{0.079V} + 310000 e^{0.35V}$$

$$\alpha_j = (-127140 e^{0.2444V} - 0.00003474 e^{-0.04391V}) \frac{(V + 37.78)}{(1 + e^{0.311(V+79.23)})}$$

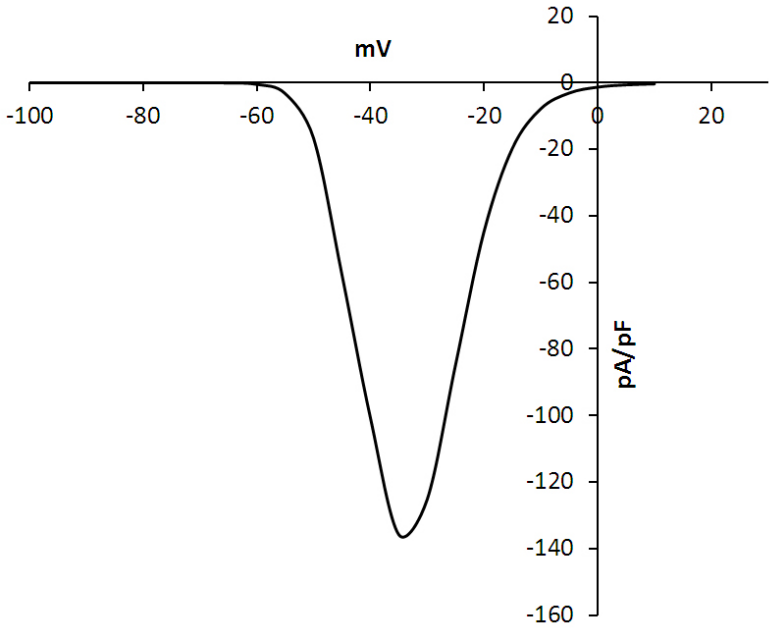

Appendix Figure 2: Fast sodium current density in the computer model ,based on the experimental data adjusted to physiological temperature (37°C) (Q_{10} = 1.5) and $[Na]_o$

$$\beta_j = \frac{0.1212e^{-0.01052V}}{1+e^{-0.1378(V+40.14)}}$$

And if $V \geq -40$ mV,

$$\alpha_h = \alpha_j = 0$$

$$\beta_h = \frac{1}{0.13(1 + e^{(V+10.66)/11.1})}$$

$$\beta_j = \frac{0.3e^{-0.0000002535V}}{(1 + e^{-0.1(V+32)})}$$

L-type calcium current (I_{CaL})

The L-type Ca^{2+} channel (I_{CaL}) Markovian formulation was modified from Li et al.[270] The voltage-dependent inactivation gate (y) in the original model was retained to capture the voltage inactivation kinetics of the channel. The Ca^{2+}-dependent transition from the closed state *C* to the inactivated state *I* was

modified to be a function of Ca^{2+} concentration in the subSL compartment ($[Ca^{2+}]_{subSL}$). Thus, the I_{CaL} was formulated as follows:

$$I_{CaL} = G_{CaL}\delta \times V \times O \times y \frac{[Ca^{2+}]_o e^{-\delta V} - [Ca^{2+}]_{subSL}}{1 - e^{-\delta V}}$$

Where G_{CaL} is the maximum conductance of the channel, O is the channel open probability, and $\delta = zF/RT$, with z being the valence of Ca^{2+}.

T-Type calcium current (I_{CaT})

The T-type Ca^{2+} channel, also called the low-threshold Ca^{2+} channel, activates at potentials ranging from -50 mV to -30 mV and displays fast inactivation. T-type calcium current (I_{CaT}) formulation was based on Puglisi-Bers model[347] modified to fit our experimental data.

$$I_{CaT} = G_{CaT}.b.g.(V - E_{Ca})$$

Where G_{CaT} is the maximum channel conductance and E_{Ca} is the reversal potential for calcium ions. The voltage-dependence of the activation gate (b) and the inactivation gate (g) is modified as follows:

$$b_\infty = \frac{1}{1 + e^{-(V+53)/8.1}}$$

$$b_\tau = 0.1 + \frac{5.4}{1 + e^{(V+100)/3}}$$

$$g_\infty = \frac{1}{1+e^{(V+66)/6.6}}$$

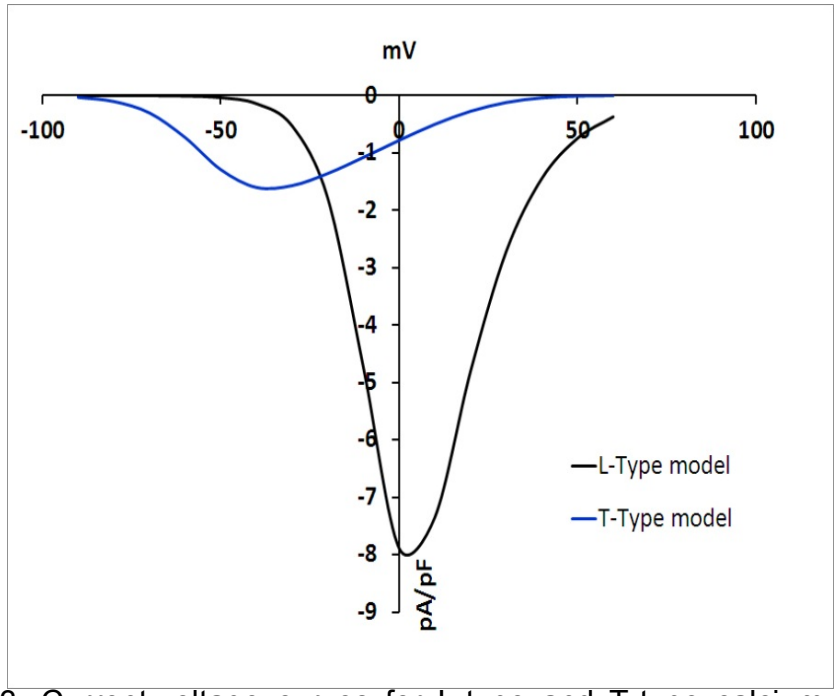

Appendix Figure 3: Current-voltage curves for L-type and T-type calcium currents in the PC model based on the experimental data adjusted to

$$g_\tau = 0.1 + \frac{34}{1 + e^{(V+65)/25}}$$

Appendix Figure 3 shows the current density curves for I_{CaL} and I_{CaT} obtained by fitting our experimental data (adjusted to 37°C using Q10 factor of 1.7).

Time-independent K^+ current (I_{K1})

The formulation for the time-independent K^+ current (I_{K1}) was modified in accordance to our experimental data as follows:

$$I_{K1} = G_{K1} \times \frac{[K^+]_o}{[K^+]_o + 210} \times \frac{(V - E_K)}{1.9149 + e^{0.0998(V-E_K)}} - 0.2142$$

Where, E_K is the reversal potential for K^+ ions, and $[K^+]_o$ is the extracellular K^+ concentration. The model I_{K1} density curve shown in Figure 2.5.4 was obtained by fitting to experimental data adjusted to 37°C using Q_{10} =1.5.

Transient Outward Potassium current (I_{to})

The formulation of I_{to} was based on Li et al.[1] which included the fast ($I_{to,f}$) and slow ($I_{to,s}$) components of the current. We chose to exclude $I_{to,s}$ since it is not

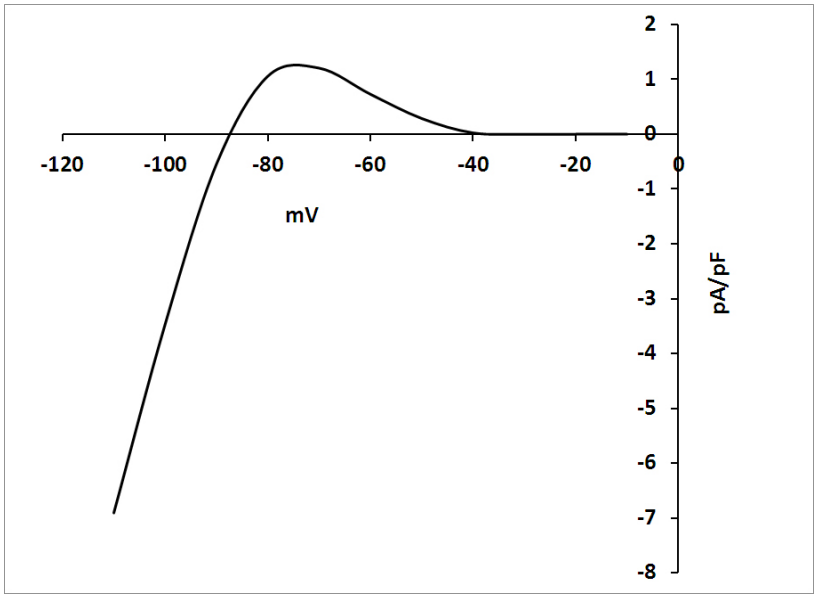

Appendix Figure 4: Current-voltage curve for I_{K1} obtained by the PC model based on experimental data adjusted to 37°C (data not shown).

found in mouse Purkinje cells. The parameters of $I_{to,f}$ formulation were adapted as follows:

$$I_{to,f} = G_{K\_tof} \times a_{tof}^3 \times i_{tof}(V - E_K)$$

The voltage-dependence of the activation gate (a_{tof}) was formulated as,

$$\alpha_a = 0.38 \times e^{0.0332(V+49.6609)}$$

$$\beta_a = 0.3857 \times e^{-0.0089(V+49.6609)}$$

Where, α_a and β_a are the voltage-dependent rate constants for activation.

The inactivation gate i_{tof} was formulated as follows,

$$\frac{d}{dt} i_{tof} = \frac{i_{tof,ss} - i_{tof}}{\tau_{itof}}$$

The inactivation time constant, τ_{itof}, and proportion of inactivated channels at steady state, $i_{tof,ss}$, are given by,

$$\tau_{itof} = 9.6645 + \frac{10.9362}{1 + e^{(V+51.4)/5.0}}$$

$$i_{tof,ss} = \frac{1}{1 + e^{(V+67.2857)/6.1514}}$$

Appendix Figure 5 shows I_{to} current density obtained in the model based on the

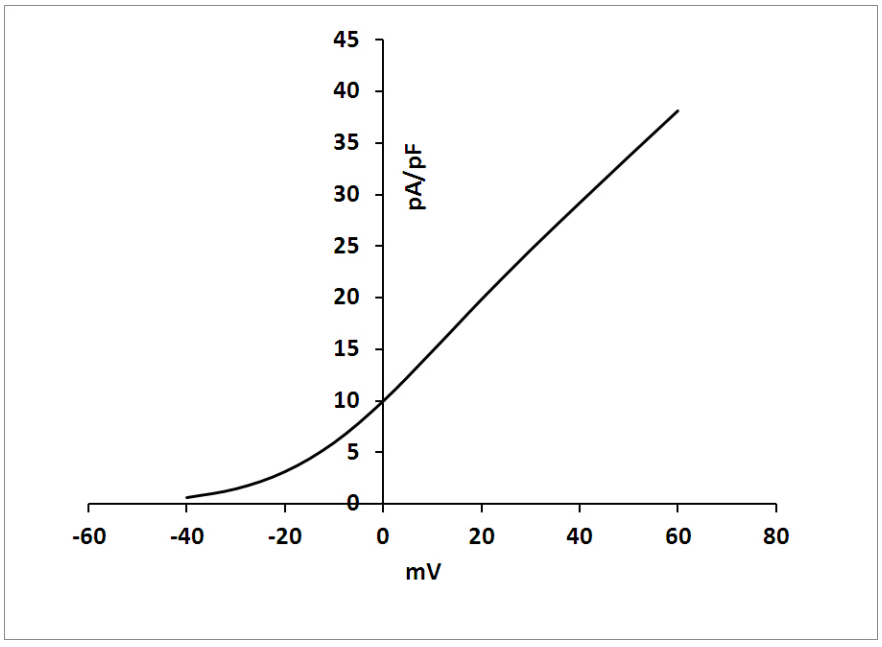

Appendix Figure 5: Current-voltage curve for I_{to} obtained from PC model

experimental data adjusted to physiological temperature (37°C) (data not shown) using Q_{10}=1.5.

Sodium-Calcium Exchanger (I_{NCX})

Current through the NCX (I_{NCX}) was based on formulation used in Li et al.[270] with one modification. The NCX in our model extrudes calcium ions from the subSR compartment and hence depends on $[Ca^{2+}]_{subSR}$, as follows:

$$I_{NCX} = \frac{V_{NCX}^{max}}{1+\left(\frac{K_{mAllo}}{[Ca^{2+}]_{subSR}}\right)^2} \cdot \frac{[Na^+]_i^3.[Ca^{2+}]_o.e^{\eta VF/RT} - +[Na^+]_o^3.[Ca^{2+}]_{subSR}.e^{(\eta-1)VF/RT}}{\left\{\begin{matrix} K_{mCao}.[Na^+]_i^3 + K_{mNao}^3.[Ca^{2+}]_{subSR} + K_{mNai}^3.[Ca^{2+}]_o.\left(1+\frac{[Ca^{2+}]_{subSR}}{K_{mCai}}\right) \\ +K_{mCai}.[Na^+]_o^3.\left[1+\left(\frac{[Na^+]_i}{K_{mNai}}\right)^3\right] + [Na^+]_i^3.[Ca^{2+}]_o + [Na^+]_o^3.[Ca^{2+}]_{subSR} \end{matrix}\right\}.[1+k_{sat}e^{(\eta-1)VF/RT}]}$$

Where V_{NCX}^{max} is the maximum voltage through NCX, K_{mAllo} is the affinity for allosteric $[Ca^{2+}]_{subSR}$, η is the energy barrier position controlling the voltage dependence of INCX; K_{mCao}, K_{mCai}, K_{mNao} and K_{mNai} are the transport affinities for Ca^{2+} and Na^+ outside and inside the cell.

Hyperpolarization-Activated Current (I_f)

Hyperpolarization-activated current, I_f, was based on the formulation used by Stewart et al.[348]

$$I_{fK} = G_{fK}.y.(V - E_K)$$

$$I_{fNa} = G_{fNa}.y.(V - E_{Na})$$

$$I_f = I_{fK} + I_{fNa}$$

Where, y is the channel activation gate. E_K and E_{Na} are the reversal potentials for potassium and sodium ions, respectively, and , G_{fK} and G_{fNa} are maximum current densities produced by potassium ions and sodium ions,. The parameters of voltage-dependence of the activation were adapted as follows:

$$\tau_y = \frac{4000}{(\alpha_y + \beta_y)}$$

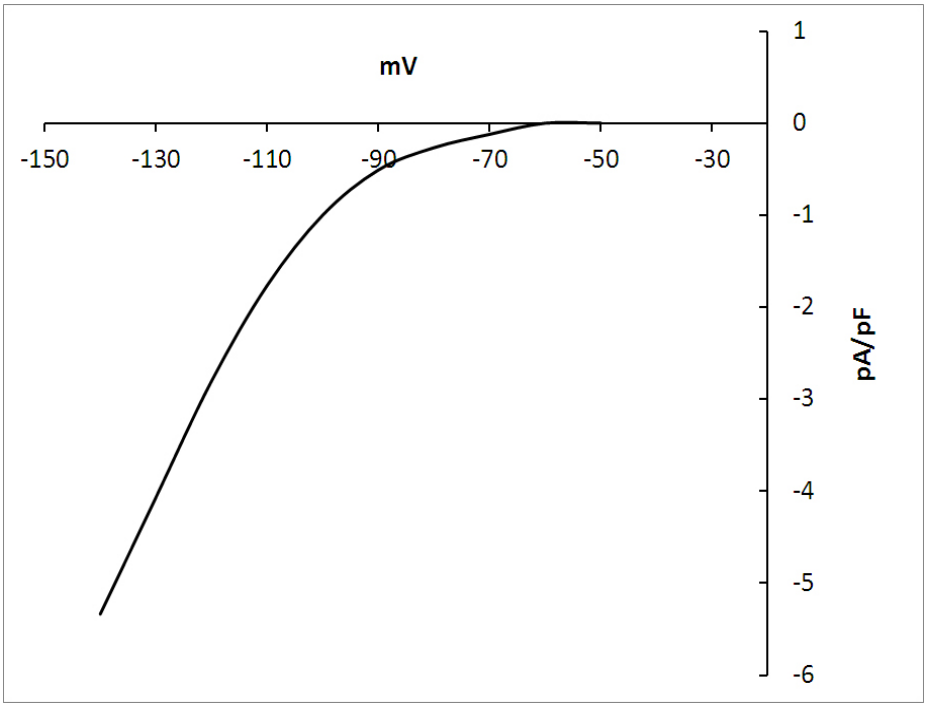

Appendix Figure 6: Current-voltage curve for I_f obtained in the PC model based on experimental data.

$$\alpha_y = e^{-0.5-0.053V}$$

$$\beta_y = e^{3.6+0.11V}$$

$$y_\infty = \frac{1}{1 + e^{(V+90.6)/6.8}}$$

Appendix Figure 6 shows I_f current density obtained in the model which was based on the experimental data.

Ca^{2+}-activated Cl^- current, $I_{Cl,Ca}$

$I_{Cl,Ca}$ was based on Bonderenko et al.[349] formulation in which intracellular calcium concentration was replaced by $[Ca^{2+}]_{subSL}$ as follows:

$$I_{Cl,Ca} = G_{Cl,Ca}.O_{Cl,Ca}\frac{[Ca^{2+}]_{subSL}}{[Ca^{2+}]_{subSL} + K_{m.Cl}}(V - E_{Cl})$$

Where $G_{Cl,Ca}$ is the maximum conductance, $O_{Cl,Ca}$ is the channel open probability, $K_{m.Cl}$ is the half-saturation constant and $E_{Cl}$is the Cl^- reversal potential.

Cytosolic calcium transients

The intracellular calcium formulation was based on the Deo-Hou neonatal rat model.[350] The SR was modeled with two compartments, namely, the release compartment, also called junctional SR (JSR), and the uptake compartment, also called network SR (NSR). The Ca^{2+} is released from JSR compartment via ryanodine receptors (RyRs). The formulation of RyR2 flux was based on the modifications by Korhonen et al.[351] as follows:

$$J_{RyR} = k_{RyR}.P_{open}.([Ca^{2+}]_{JSR} - [Ca^{2+}]_{subSR})$$

$$K_{m,RyR} = \frac{3.51}{1 + e^{([Ca^{2+}]_{JSR} - 530)/200}} + 0.25$$

$$\frac{dP_{open}}{dt} = \frac{P_{closed}k_{open}}{1 + (K_{m.RyR}/[Ca^{2+}]_{subSR})^4} - k_{close}P_{open}$$

$$P_{closed} = 1 - P_{open}$$

The Ca^{2+} flux between the NSR and subSR compartments was described by SR Ca^{2+} ATPase (SERCA). The SERCA equation was modified from Korhonen et al.[351] formulation by adding a constant term, k_{SERCA}, as follows:

$$J_{SERCA} = k_{SERCA} \times \frac{V_{max,f}([Ca^{2+}]_{subSR}/K_{mf})^H - V_{max,r}([Ca^{2+}]_{NSR}/K_{mr})^H}{1 + ([Ca^{2+}]_{subSR}/K_{mf})^H + ([Ca^{2+}]_{NSR}/K_{mr})^H}$$

Where $V_{max,f}$ and K_{mf} are maximum SERCA flux and half-saturation for forward SERCA, respectively. Similarly, $V_{max,r}$ and K_{mr} correspond to the reverse direction SERCA. H is the Hill coefficient for SERCA and was set equal to 2.

The Ca^{2+} accumulated in the subSL compartment is extruded by the NCX and the sarcolemmal Ca^{2+} pump (I_{pCa}). The I_{pCa} was formulated as follows:

$$I_{pCa} = I_{pCa}^{max} \times \frac{([Ca^{2+}]_{subSL})^2}{K_{m,pCa}^2 + ([Ca^{2+}]_{subSL})^2}$$

Where I_{pCa}^{max} is the maximum Ca2+ pump current and $K_{m,pCa}$ is the Ca^{2+} half-saturation constant.

Cytosolic Calcium Diffusion

Ca^{2+} enters the cell via L-type and T-type calcium channels which open into subSL compartment. These ions diffuse through the cytoplasm between subSL and subSR compartments via fire-diffusion-fire-propagation.[352] Similarly, the calcium concentration in the subSR compartment ($[Ca^{2+}]_{subSR}$) triggers the SR Ca^{2+} release through the RyR2 channels through the calcium-induced-calcium-

release (CICR) mechanism. The sudden increase in $[Ca^{2+}]_{subSR}$ may also give rise to diffusion waves in the cytoplasm. The Ca^{2+} diffusion process was implemented based on Korhonen et al.[350] as follows:

$$\frac{\partial c}{\partial t} = \beta_i . (D_{Ca} \nabla^2 c + J_{Ca}),$$

where, $c = [Ca^{2+}]_i$, β_i is the function determining Ca^{2+} buffering, D_{Ca} is the diffusion coefficient, J_{Ca} is the Ca^{2+} flux, and ∇^2 is the Laplacian operator for spatial derivative. The c in the above equation was implemented as a function of time and radial distance from the core (r) as follows:

$$\frac{\partial c(r,t)}{\partial t} = \beta_i (c(r,t)) . \left[D_{Ca} \frac{\partial^2 c(r,t)}{\partial r^2} + \frac{2 D_{Ca}}{r} \frac{\partial c(r,t)}{\partial r} + J_{Ca}(r,t) \right],$$

In order to implement radial diffusion, the above equation was reduced to a system of ODEs by approximating into concentric cores with step size of ∇r = 0.1 μm. Further details can be found in Korhonen et al.[351] The diffusion coefficient, D_{Ca}, was fitted to 7 μm^2/ms to obtain Ca^{2+} diffusion velocity of approximately 0.35 μm/ms as observed in neonatal and atrial cells.[17]

The J_{Ca} in the above equation is the SR Ca^{2+} flux (J_{CaSR}) when $r = r_{SR}$, SL Ca^{2+} flux (J_{CaSL}) when $r = r_{SL}$, and zero with other values. The J_{CaSR} and J_{CaSL} were calculated as follows:

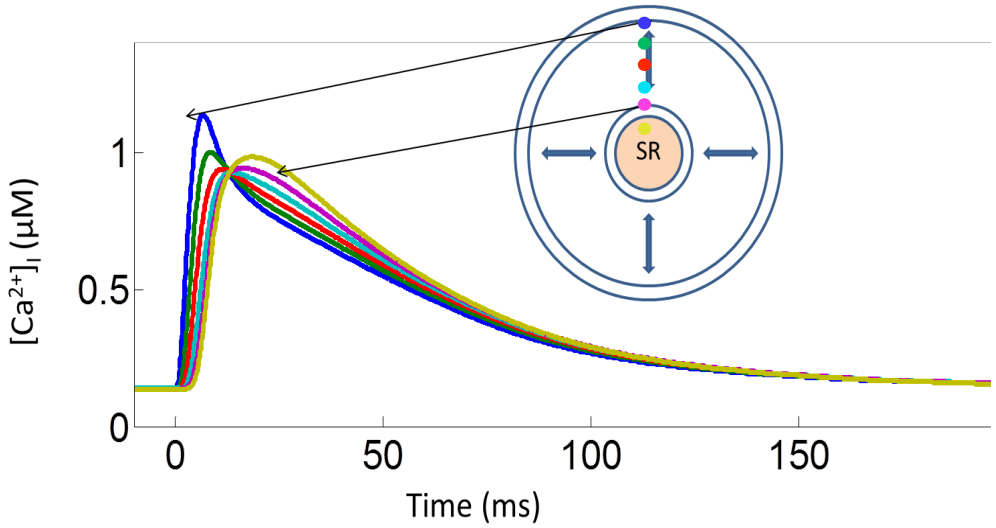

Appendix Figure 7. Cytosolic diffusion of calcium from subSL compartment (blue) to subSR compartment (yellow) during 1 Hz pacing.

$$J_{CaSR} = J_{RyR} - J_{SERCA} + J_{leak}$$

$$J_{CaSL} = (2I_{NCX} - I_{CaL} - I_{CaT} - I_{Cab} - I_{pCa}) \times \frac{A_{cap} C_m}{F \times 10^{-6}}$$

Appendix Figure 7 shows the diffusion of Ca^{2+} ions from subSL to subSR during 1Hz pacing. The cytosolic Ca^{2+} wave was initiated at the subSL due to influx of Ca^{2+} ions through I_{CaL} and I_{CaT} channels and traveled towards subSR. Upon reaching subSR, it elevated the local Ca^{2+} concentration in the subSR compartment which triggered the SR Ca^{2+} release via RyR2 channels. Thus there existed a lag between the Ca^{2+} influx and Ca^{2+} release from the SR.

Calcium transients in the cytosol were averaged and fitted to intracellular calcium parameters measured during calcium imaging experiments on GFP mice Purkinje cells (n=5). The time to peak (T_p) and decay time (T_d) of the average $[Ca]_i$ trace, measured as shown in the top trace in Fig. S8, were adjusted to the

experimentally measured durations (listed in Table 2.5.1). T_p was measured between the onset and the peak of Ca^{2+} transient, whereas, T_d was measured from the peak to its 95% decay. The peak amplitude (PA) of the calcium transients was adjusted to 0.9 μM. Table 2.5.1 lists the calcium transients parameters recorded in the experiments and obtained in the model.

Table 1.3 Intracellular calcium transient parameters obtained in experiments and model.

Parameter	**Experiments**	**Model**
Peak Amplitude (PA)	31.193 ± 0.91 AU	0.9 μM
Time to Peak (T_p)	18.8 ± 13.2 ms	12.5 ms
Decay time (T_d)	261 ± 69.18 ms	240.5 ms

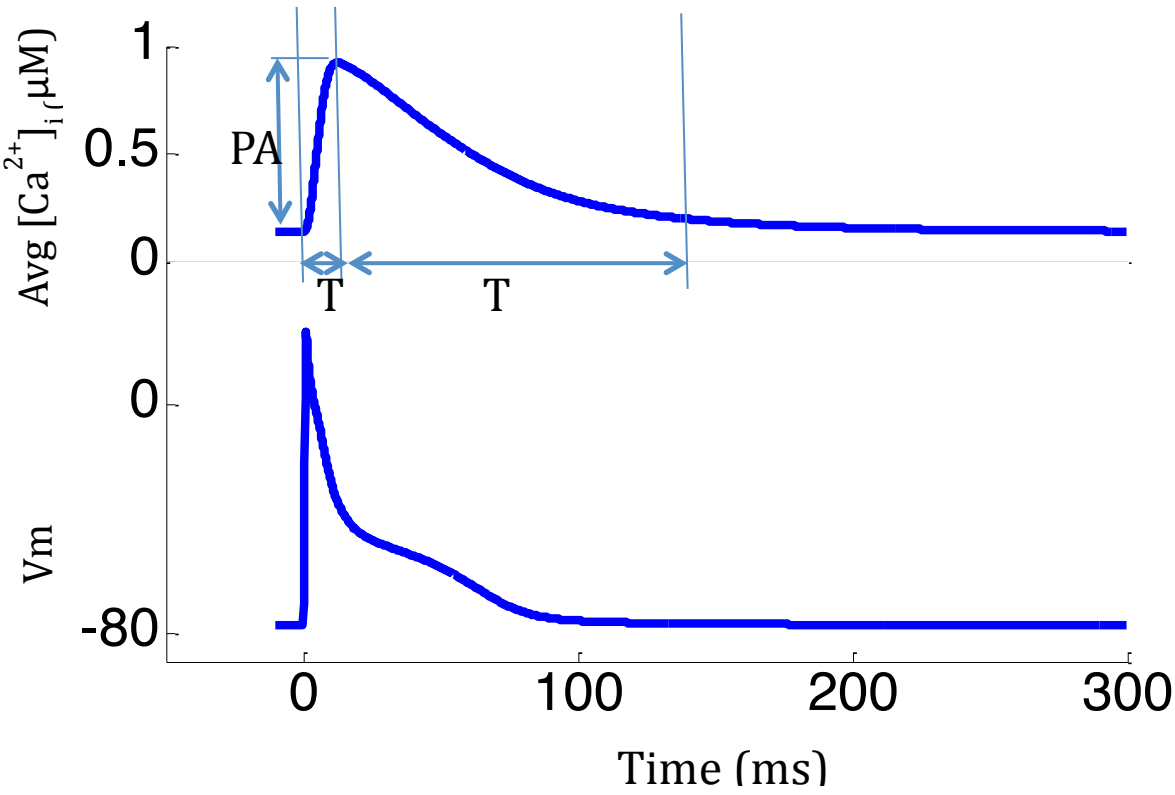

Appendix Figure 1.8. Average cytosolic calcium transient (top) during an action potential (bottom) elicited by 1Hz stimulus in the PC model. PA: Peak Amplitude, T_p: Time to Peak, and T_d: Decay time.

Na^+ Concentration

$$\frac{d[Na^+]_i}{dt} = -(I_{Na} + I_{Nab} + 3I_{NCX} + 3I_{NaK} + I_{fNa}) \times \frac{A_{cap}C_m}{V_{myo}F}$$

K^+ Concentration

$$\frac{d[K^+]_i}{dt} = -(I_{Stim} + I_{to,f} + I_{K1} + I_{Ks} + I_{Kr} + I_{Kss} + I_{Kur} - 2I_{NaK} + I_{fK}) \times \frac{A_{cap}C_m}{V_{myo}F}$$

Table 1.4: lists the dimensions and environmental parameters of our Purkinje model. The modified parameters are given in Table 2.5.3.

Table 1.4. Structural and environmental parameters

Parameter	*Definition*	*Value*
L	*Length of the cell*	129 μm
r	*Radius of the cell*	4 μm
C_m	Specific membrane capacitance	1 μF/cm^2
A_{cap}	Capacitive membrane area	7.99×10^{-5} cm^2
V_{myo}	Myoplasmic volume	3.89×10^{-6} μL
V_{JSR}	Junctional SR volume	0.0078 pL
V_{NSR}	Network SR volume	0.1556 pL
V_{subSR}	Volume of subSR compartment	0.0828 pL
V_{subSL}	Volume of subSL compartment	0.2470 pL
F	Faraday constant	7.878 C/mmol
T	Absolute temperature	0.059 K
R	Ideal gas constant	0.0133 J/mol K
$[Ca^{2+}]_o$	Extracellular Ca^{2+} concentration	1400 μM
$[Na^{+}]_o$	Extracellular Na^{+}	5400 μM

	concentration	
$[K^+]_o$	Extracellular K^+ concentration	134000 μM

Table 1.5: Modified parameters in the Purkinje model

Parameter	*Definition*	*Value*
G_{Na}	Maximum I_{Na} conductance	16 mS/μF
G_{CaL}	Maximum I_{CaL} conductance	0.0775 mS/μF
G_{CaT}	Maximum I_{CaT} conductance	0.02 mS/μF
G_{K1}	Maximum I_{K1} conductance	0.5930 mS/μF
$G_{K\_to,f}$	Maximum $I_{to,f}$ conductance	0.3429 mS/μF
V_{NCX}^{max}	Maximum Na-Ca exchange rate	7.878 pA/pF
I_{NaK}^{max}	Maximum Na-K pump current	2.51086 pA/pF
G_{fK}	Maximum I_{fK} conductance	0.059 mS/μF
G_{fNa}	Maximum I_{fNa} conductance	0.0133 mS/μF
k_{RyR}	Scaling factor for J_{RyR}	0.03 ms^{-1}
G_{Kur}	Maximum I_{Kur} conductance	0.1474 mS/μF
G_{Kss}	Maximum I_{Kss} conductance	0.0482 mS/μF
I_{pCa}^{max}	Maximum Ca^{2+} pump current	0.0955 pA/pF
k_{SERCA}	SERCA constant	0.5

Purkinje cell model without Ca^{2+} diffusion

In order to study the individual contribution of diffusion process to the APD morphology, we also implemented the Purkinje cell model without spatial Ca^{2+} diffusion process. The subSL and subSR compartments in the model were connected through a transfer flux, J_{Xfer} (τ_{Xfer} = 0.63 ms). The resulting intracellular calcium formulation was as follows:

$$J_{Xfer} = ([Ca^{2+}]_{subSL} - [Ca^{2+}]_{subSR})/\tau_{Xfer}$$

$$\frac{d[Ca^{2+}]_{subSR}}{dt} = \beta_i \cdot (J_{leak} + J_{Xfer} - J_{SERCA} + (2I_{NCX} - I_{Cab} - I_{pCa}) \times \frac{A_{cap} C_m}{F \times 10^{-6}})$$

$$\frac{d[Ca^{2+}]_{subSL}}{dt} = \beta_i \cdot (J_{RyR} - J_{Xfer} - (I_{CaL}) \times \frac{A_{cap} C_m}{F \times 10^{-6}})$$

Ventricular Myocyte Model

The ventricular myocyte model by Li et al.[270] was modified in our study as follows: 1) the fast sodium current (INa) formulation in the model was replaced with that from the mammalian ventricular myocyte model (LRd 1999)[345] for easiness in fitting to the experimental data without losing numerical stability. 2) The calcium dynamics in the model requires very small time steps in numerical integration. Therefore we solved the calcium dynamics at smaller time steps (0.1 μs) whereas the rest of the ionic currents were updates every 10 μs. This allowed us to accelerate the computer simulations without significant loss of accuracy. The maximum conductance parameters of several ion currents in the model were modified to fit our experimental data in mice ventricular myocytes in the apical region. Following are the only changes made to the original model by Li.et al.[270]

Time-independent K^+ current

The formulation for the time-independent K^+ current (I_{K1}) was modified in accordance to our experimental data as follows:

$$I_{K1} = G_{K1} \times \frac{[K^+]_o}{[K^+]_o + 210} \times \frac{(V - E_K)}{1.7 + e^{0.0896(V-E_K)}}$$

Where, E_K is the reversal potential for K^+ ions, and $[K^+]_o$ is the extracellular K^+ concentration. The maximum channel conductance, G_{K1}, was set to 0.3150 in order to match experimental I_{K1} density.

Table 1.6 Modified parameters in the ventricular myocyte model

Parameter	*Definition*	*Value*
G_{Na}	Maximum I_{Na} conductance	9.6 mS/μF
P_{CaL}	Maximum I_{CaL} conductance	3.0 mS/μF
G_{K1}	Maximum I_{K1} conductance	0.315 mS/μF
$G_{K\_to,f}$	Maximum $I_{to,f}$ conductance	0.42776 mS/μF
V_{NCX}^{max}	Maximum Na-Ca exchange rate	5.9085 pA/pF
I_{NaK}^{max}	Maximum Na-K pump current	1.51646 pA/pF
G_{Kur}	Maximum I_{Kur} conductance	0.225 mS/μF
G_{Kss}	Maximum I_{Kss} conductance	0.0595 mS/μF

Study 2: Saturated Fatty Acids Disrupt T-Tubules and Shorten Atrial Action Potential Duration

Acute exposure of fatty acids does not affect action potential morphology

Acute perfusion of PA on LA myocytes did not alter action potential morphology as shown in Appendix Figure 1.1A. Quantification of the data revealed no differences at all values measured shown in Appendix Figure 1.1B (APD30: CTL: 44.32 ± 6.909 vs. PA: 42.34 ± 8.847; APD50: CTL: 76.33 ± 11.54 vs. PA: 73.83 ± 10.20; APD80: CTL: 144.5 ± 15.61 vs. PA: 138.3 ± 13.89 msec (CTL: N=3, n=13; PA: N=3, n=15). We also acutely perfused SA and found it did not alter the electrophysiology of LA cells, as shown in Supplemental Figure 1C. Quantification of the data yielded no differences between CTL and acute SA treatment shown in Appendix Figure 1.1D (APD30: CTL: 38.31 ± 6.907 vs. SA: 39.65 ± 5.099; APD50: CTL: 71.23 ± 11.71 vs. SA: 68.93 ± 7.627; APD80: CTL: 140.2 ± 15.77 vs. SA: 132.4 ± 14.05 msec (CTL: N=3, n=13; SA: N=3, n=13). To determine whether SA had short-term effects on LA myocyte action potentials we incubated SA on cells for 4-6 hours. Appendix Figure 1.1E are representative action potential recordings from short-term cultured cells. Quantification of the data showed no differences between CTL and short-term SA incubated cells shown in Appendix Figure 1.1F (APD30: CTL: 40.71 ± 7.236 vs. SA: 43.24 ± 6.892; APD50: CTL: 73.61 ± 10.49 vs. SA: 74.00 ± 9.692; APD80: CTL: 145.8 ± 18.94 vs. SA: 151.9 ± 13.79 msec (CTL: N=2, n=7; SA: N=2, n=9).

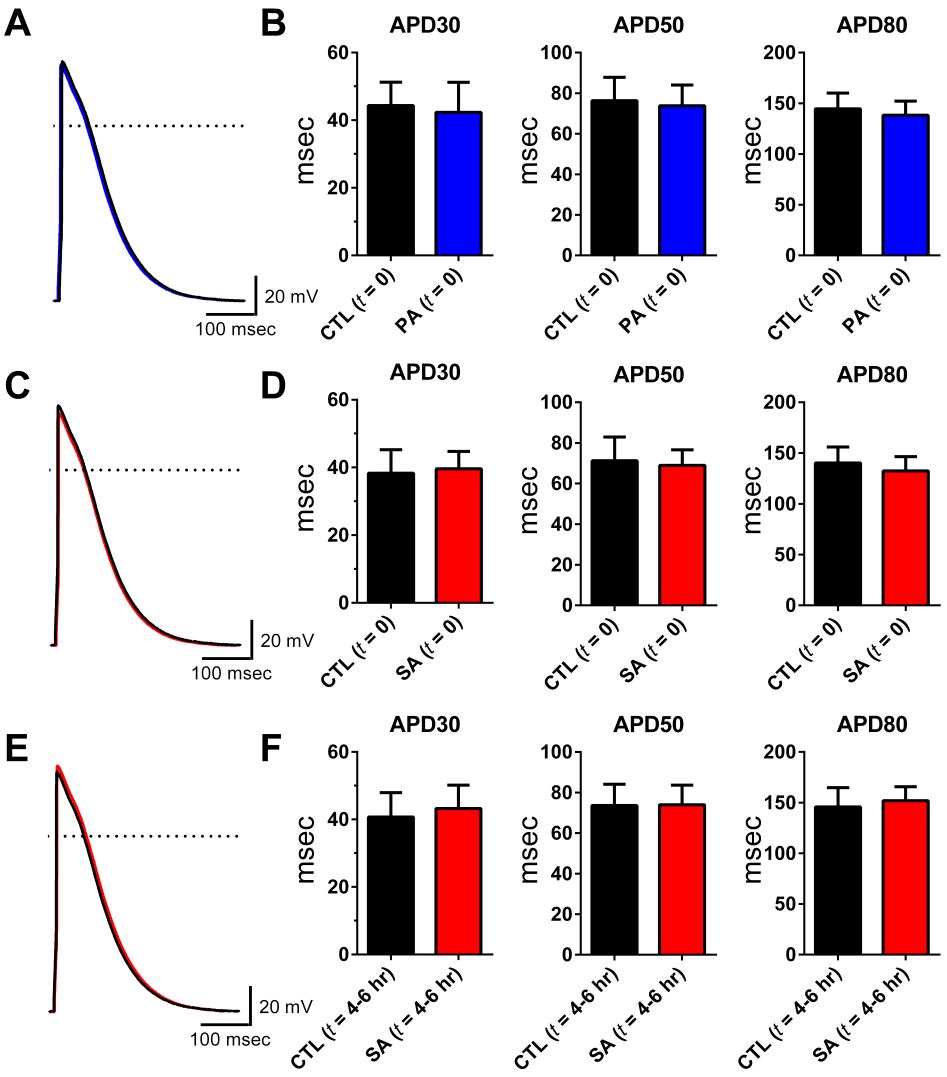

Appendix Figure 2.1: Acute exposure to free fatty acids has no effect on atrial myocytes. Panel A: Representative action potential recordings under acute fatty acid application of control (CTL; black) and of PA (blue) solutions. Panel B: Quantification of APD30, 50 & 80 values (CTL: n = 13, PA: n = 15). Panel C: Representative action potential recordings under acute fatty acid application of control (CTL; black) and of SA (red) solutions. Panel D: Quantification of APD30, 50 & 80 values in CTL and SA treated cells (n = 13, 13). Panel E: Representative traces of cells incubated 4-6 hrs with CTL (black) and SA (red). Quantification of APD30, 50, 80 values showed no difference between both groups (n = 7, 9). Scale bars: 100 msec and 20 mV.

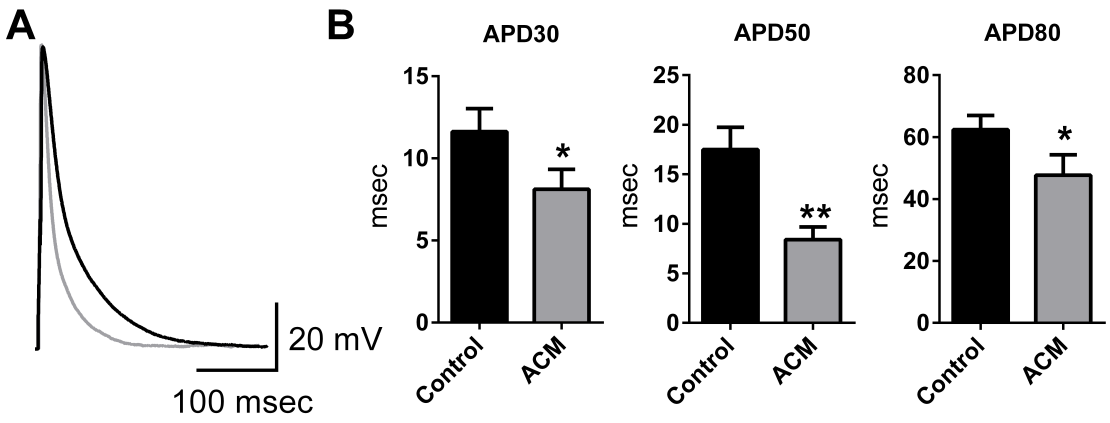

Appendix Figure 2.2: Adipocyte-Conditioned Media (ACM) shortens action potential duration in atrial myocytes. Panel A: Representative current clamp traces of left atria cells treated with myocyte media (Control, black) and ACM (grey). Panel B: ACM reduced APD at all three values measured (*p<0.01, **p<0.001; n = 11, 10).

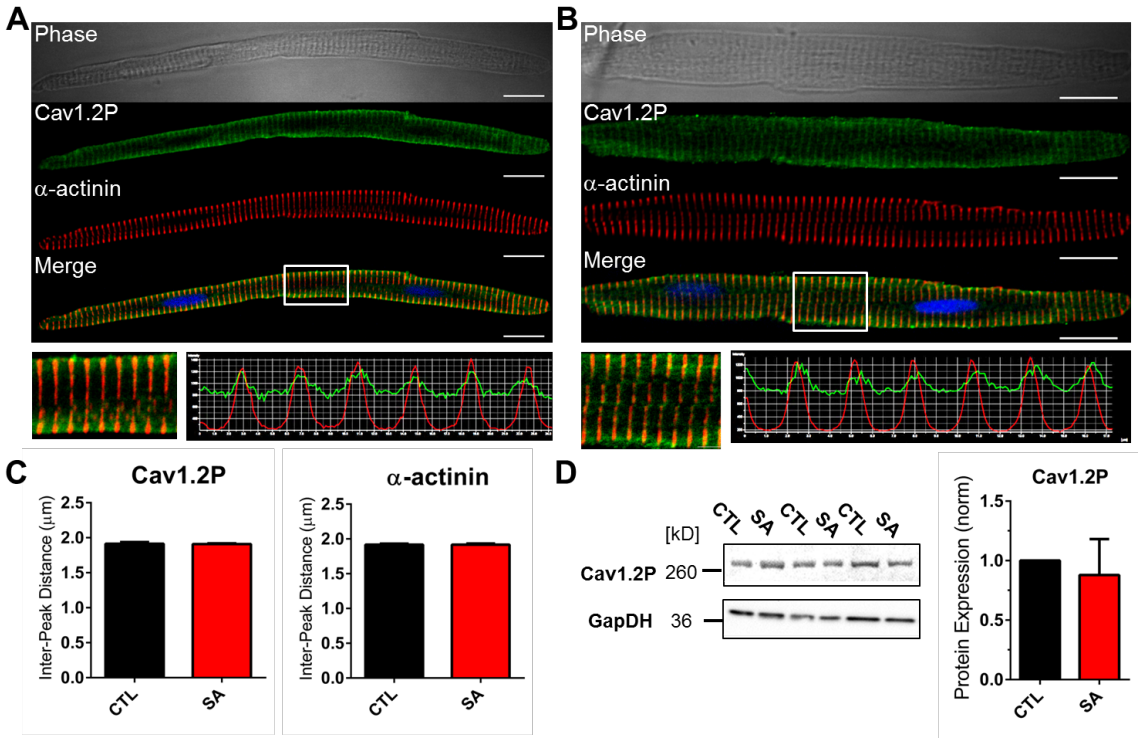

Appendix Figure 2.3: Cav1.2 phosphorylation at serine 1928 is not affected by stearic acid. Panel A/B: Immunofluorescence images of transmitted light, Cav1.2 phosphorylation (Cav1.2P), α-actinin and a merged image under control (CTL) and stearic acid (SA) treatment (n = 24, 22). Scale bars: 20 μm. Panel C: Quantification of the intensity profiles shows SA did not alter the mean distance between intensity peaks for Cav1.2P (left) or α-actinin (right; n =12, 12). Mean distance between Cav1.2P and α-actinin peaks were similar in both groups and unchanged from CTL to SA. Panel D: (left) Western blot for Cav1.2P with GAPDH as a control. Pane D: (right) normalized densitometry plot of Cav1.2P protein levels in CTL and SA treated cell lysates (N = 3).

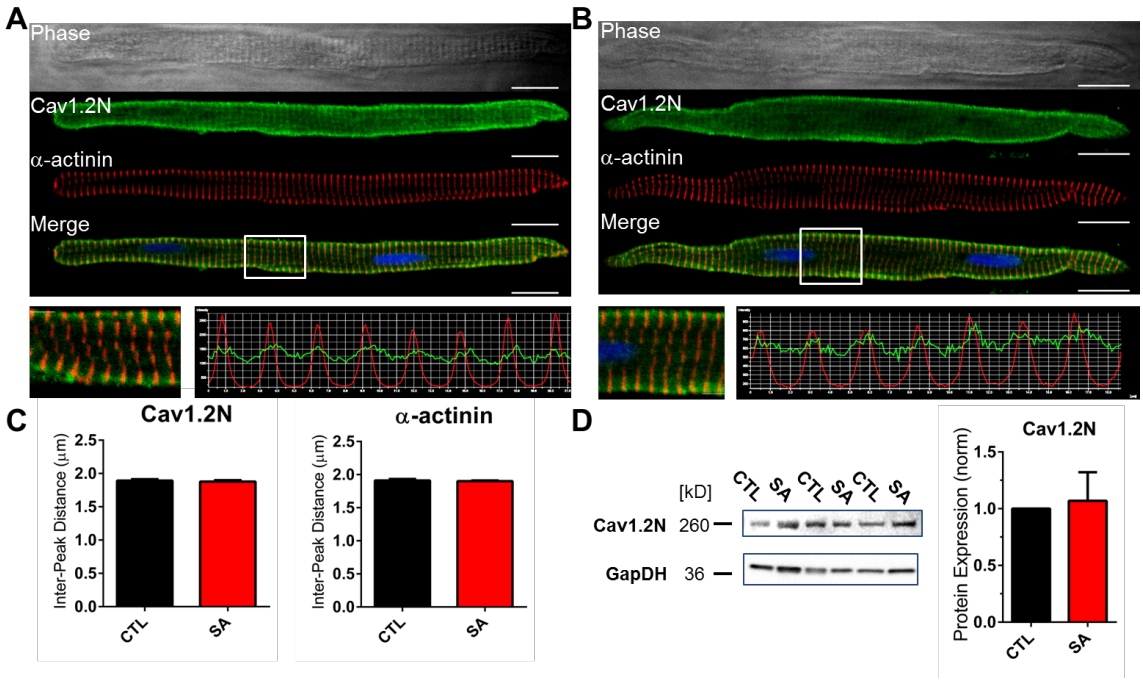

Appendix Figure 2.4: Cav1.2 nitrosylation is not affected by stearic acid. Panel A/B: CTL and SA immunofluorescence images of transmitted light, Cav1.2 nitrosylation (Cav1.2N), α-actinin and a merged image (n = 23, 20) Scale bars: 20 μm. Panel C: Quantification of the intensity profiles shows SA did not alter the mean distance between intensity peaks for Cav1.2N (left) or α-actinin (right; n = 12, 12). Mean distance between Cav1.2N and α-actinin peaks were similar in both groups and unchanged from CTL to SA. Panel D: (left) Western blotting for Cav1.2N with GAPDH as a control. Pane D: (right) normalized densitometry plot of Cav1.2N protein levels in CTL and SA treated cell lysates (N = 3).

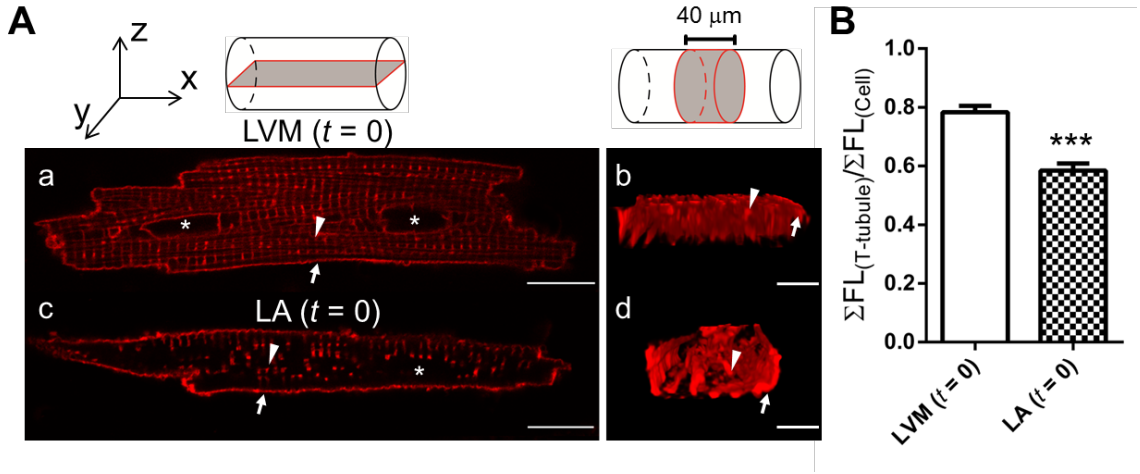

Appendix Figure 2.5: Comparison of t-tubule structure in sheep atrial and ventricular myocytes. Panel A (top): Coordinate axis for reference and schematic diagrams illustrating the fields of view. Panel A: subpanels (a) and (c) are XY planar views and (b) and (d) are 40 µm ZY cross-sectional views of the same cell. (a) and (b) Di-8-ANEPPS stain of t-tubules in a freshly dissociated (t = 0) left ventricular myocyte (LVM) which contains an extensive t-tubule network. For comparisons, (c) and (d) show a freshly dissociated (t = 0) left atrial (LA) cell in control. Panel B: Quantification of t-tubules in LVM (n = 23) and LA myocytes (n = 19) using the ratio of the t-tubule region and total cell fluorescence. LA myocytes have less uniform t-tubule structures compared to LVM (***$p<0.0001$, n = 19).

References

1. Vaidyanathan R, O'Connell RP, Deo M, et al. The ionic bases of the action potential in isolated mouse cardiac Purkinje cell. *Heart rhythm : the official journal of the Heart Rhythm Society.* Jan 2013;10(1):80-87.
2. Wei S, Guo A, Chen B, et al. T-tubule remodeling during transition from hypertrophy to heart failure. *Circulation research.* Aug 20 2010;107(4):520-531.
3. Soeller C, Cannell MB. Examination of the transverse tubular system in living cardiac rat myocytes by 2-photon microscopy and digital image-processing techniques. *Circulation research.* Feb 19 1999;84(3):266-275.
4. Nerbonne JM. Molecular basis of functional voltage-gated K+ channel diversity in the mammalian myocardium. *The Journal of physiology.* Jun 1 2000;525 Pt 2:285-298.
5. Nattel S, Maguy A, Le Bouter S, Yeh Y-H. Arrhythmogenic Ion-Channel Remodeling in the Heart: Heart Failure, Myocardial Infarction, and Atrial Fibrillation. *Physiol. Rev.* April 1, 2007 2007;87(2):425-456.
6. Nattel S, Carlsson L. Innovative approaches to anti-arrhythmic drug therapy. *Nature reviews. Drug discovery.* Dec 2006;5(12):1034-1049.
7. Bers DM. Cardiac excitation-contraction coupling. *Nature.* Jan 10 2002;415(6868):198-205.
8. Hayashi H, Lux RL, Wyatt RF, Burgess MJ, Abildskov JA. Relation of canine atrial activation sequence to anatomic landmarks. *The American journal of physiology.* Mar 1982;242(3):H421-428.
9. Anderson RH, Ho SY. The architecture of the sinus node, the atrioventricular conduction axis, and the internodal atrial myocardium. *Journal of cardiovascular electrophysiology.* Nov 1998;9(11):1233-1248.
10. Grant RP. Notes on the Muscular Architecture of the Left Ventricle. *Circulation.* Aug 1965;32:301-308.
11. Streeter DD, Jr., Spotnitz HM, Patel DP, Ross J, Jr., Sonnenblick EH. Fiber orientation in the canine left ventricle during diastole and systole. *Circulation research.* Mar 1969;24(3):339-347.
12. Fenton TR, Cherry JM, Klassen GA. Transmural myocardial deformation in the canine left ventricular wall. *The American journal of physiology.* Nov 1978;235(5):H523-530.
13. Jay V. The extraordinary career of Dr Purkinje. *Arch Pathol Lab Med.* May 2000;124(5):662-663.
14. Tawara S. Das Reizleitungssytem des saugetierherzens. *Gustav Fischer, Jena.* 1906.
15. Bogun F, Good E, Reich S, et al. Role of Purkinje fibers in post-infarction ventricular tachycardia. *Journal of the American College of Cardiology.* Dec 19 2006;48(12):2500-2507.
16. Lopera G, Stevenson WG, Soejima K, et al. Identification and ablation of three types of ventricular tachycardia involving the his-purkinje system in patients with heart disease. *Journal of cardiovascular electrophysiology.* Jan 2004;15(1):52-58.

17. Weerasooriya R, Hsu LF, Scavee C, et al. Catheter Ablation of Ventricular Fibrillation in Structurally Normal Hearts Targeting the RVOT and Purkinje Ectopy. *Herz.* Nov 2003;28(7):598-606.
18. Di Maio A, Ter Keurs HE, Franzini-Armstrong C. T-tubule profiles in Purkinje fibres of mammalian myocardium. *Journal of muscle research and cell motility.* 2007;28(2-3):115-121.
19. Desplantez T, Dupont E, Severs NJ, Weingart R. Gap junction channels and cardiac impulse propagation. *The Journal of membrane biology.* Aug 2007;218(1-3):13-28.
20. Ono N, Yamaguchi T, Ishikawa H, et al. Morphological varieties of the Purkinje fiber network in mammalian hearts, as revealed by light and electron microscopy. *Archives of histology and cytology.* 2009;72(3):139-149.
21. Shimada T, Nakamura M, Kitahara Y, Sachi M. Surface morphology of chemically-digested Purkinje fibers of the goat heart. *Journal of electron microscopy.* 1983;32(3):187-196.
22. Sugi Y, Hirakow R. Freeze-fracture studies of the sinoatrial and atrioventricular nodes of the caprine heart, with special reference to the nexus. *Cell and tissue research.* 1986;245(2):273-279.
23. Tseng GN, Robinson RB, Hoffman BF. Passive properties and membrane currents of canine ventricular myocytes. *The Journal of general physiology.* Nov 1987;90(5):671-701.
24. Persson F, Andersson B, Duker G, Jacobson I, Carlsson L. Functional effects of the late sodium current inhibition by AZD7009 and lidocaine in rabbit isolated atrial and ventricular tissue and Purkinje fibre. *European journal of pharmacology.* Mar 8 2007;558(1-3):133-143.
25. Light PE, Cordeiro JM, French RJ. Identification and properties of ATP-sensitive potassium channels in myocytes from rabbit Purkinje fibres. *Cardiovascular research.* Nov 1999;44(2):356-369.
26. Zaza A, Malfatto G, Rosen MR. Electrophysiologic effects of ketanserin on canine Purkinje fibers, ventricular myocardium and the intact heart. *The Journal of pharmacology and experimental therapeutics.* Jul 1989;250(1):397-405.
27. Varro A, Balati B, Iost N, et al. The role of the delayed rectifier component IKs in dog ventricular muscle and Purkinje fibre repolarization. *The Journal of physiology.* Feb 15 2000;523 Pt 1:67-81.
28. Robinson RB, Boyden PA, Hoffman BF, Hewett KW. Electrical restitution process in dispersed canine cardiac Purkinje and ventricular cells. *The American journal of physiology.* Nov 1987;253(5 Pt 2):H1018-1025.
29. Balati B, Iost N, Simon J, Varro A, Papp JG. Analysis of the electrophysiological effects of ambasilide, a new antiarrhythmic agent, in canine isolated ventricular muscle and purkinje fibers. *General pharmacology.* Feb 2000;34(2):85-93.
30. Hagiwara N, Irisawa H, Kameyama M. Contribution of two types of calcium currents to the pacemaker potentials of rabbit sino-atrial node cells. *The Journal of physiology.* Jan 1988;395:233-253.

31. Souders CA, Bowers SL, Baudino TA. Cardiac fibroblast: the renaissance cell. *Circulation research.* Dec 4 2009;105(12):1164-1176.
32. Spotnitz HM, Sonnenblick EH, Spiro D. Relation of ultrastructure to function in the intact heart: sarcomere structure relative to pressure volume curves of intact left ventricles of dog and cat. *Circulation research.* Jan 1966;18(1):49-66.
33. Page E. Quantitative ultrastructural analysis in cardiac membrane physiology. *The American journal of physiology.* Nov 1978;235(5):C147-158.
34. Grant AO. Cardiac Ion Channels. *Circulation: Arrhythmia and Electrophysiology.* April 1, 2009 2009;2(2):185-194.
35. Benson DW, Wang DW, Dyment M, et al. Congenital sick sinus syndrome caused by recessive mutations in the cardiac sodium channel gene (SCN5A). *J Clin Invest.* Oct 2003;112(7):1019-1028.
36. Kodama I, Nikmaram MR, Boyett MR, Suzuki R, Honjo H, Owen JM. Regional differences in the role of the Ca2+ and Na+ currents in pacemaker activity in the sinoatrial node. *The American journal of physiology.* Jun 1997;272(6 Pt 2):H2793-2806.
37. Munk AA, Adjemian RA, Zhao J, Ogbaghebriel A, Shrier A. Electrophysiological properties of morphologically distinct cells isolated from the rabbit atrioventricular node. *The Journal of physiology.* Jun 15 1996;493 (Pt 3):801-818.
38. Wehrens XH, Abriel H, Cabo C, Benhorin J, Kass RS. Arrhythmogenic mechanism of an LQT-3 mutation of the human heart Na(+) channel alpha-subunit: A computational analysis. *Circulation.* Aug 1 2000;102(5):584-590.
39. Zhang H, Holden AV, Boyett MR. Sustained inward current and pacemaker activity of mammalian sinoatrial node. *Journal of cardiovascular electrophysiology.* Aug 2002;13(8):809-812.
40. Perez-Reyes E. Molecular physiology of low-voltage-activated t-type calcium channels. *Physiological reviews.* Jan 2003;83(1):117-161.
41. Benitah JP, Gomez AM, Virsolvy A, Richard S. New perspectives on the key role of calcium in the progression of heart disease. *Journal of muscle research and cell motility.* 2003;24(4-6):275-283.
42. Boyett MR, Honjo H, Kodama I. The sinoatrial node, a heterogeneous pacemaker structure. *Cardiovascular research.* Sep 2000;47(4):658-687.
43. Xu H, Guo W, Nerbonne JM. Four kinetically distinct depolarization-activated K+ currents in adult mouse ventricular myocytes. *The Journal of general physiology.* May 1999;113(5):661-678.
44. Nerbonne JM, Kass RS. Molecular physiology of cardiac repolarization. *Physiological reviews.* Oct 2005;85(4):1205-1253.
45. Guo W, Li H, London B, Nerbonne JM. Functional consequences of elimination of i(to,f) and i(to,s): early afterdepolarizations, atrioventricular block, and ventricular arrhythmias in mice lacking Kv1.4 and expressing a dominant-negative Kv4 alpha subunit. *Circulation research.* Jul 7 2000;87(1):73-79.

46. Liu DW, Gintant GA, Antzelevitch C. Ionic bases for electrophysiological distinctions among epicardial, midmyocardial, and endocardial myocytes from the free wall of the canine left ventricle. *Circulation research.* Mar 1993;72(3):671-687.
47. Antzelevitch C, Sicouri S, Litovsky SH, et al. Heterogeneity within the ventricular wall. Electrophysiology and pharmacology of epicardial, endocardial, and M cells. *Circulation research.* Dec 1991;69(6):1427-1449.
48. Guo W, Xu H, London B, Nerbonne JM. Molecular basis of transient outward K+ current diversity in mouse ventricular myocytes. *The Journal of physiology.* Dec 15 1999;521 Pt 3:587-599.
49. Shaw RM, Rudy Y. Ionic mechanisms of propagation in cardiac tissue. Roles of the sodium and L-type calcium currents during reduced excitability and decreased gap junction coupling. *Circulation research.* Nov 1997;81(5):727-741.
50. Isomoto S, Kurachi Y. Function, regulation, pharmacology, and molecular structure of ATP-sensitive K+ channels in the cardiovascular system. *Journal of cardiovascular electrophysiology.* Dec 1997;8(12):1431-1446.
51. Noma A. ATP-regulated K+ channels in cardiac muscle. *Nature.* Sep 8-14 1983;305(5930):147-148.
52. Downey JM. Ischemic preconditioning Nature's own cardioprotective intervention. *Trends in cardiovascular medicine.* Sep-Dec 1992;2(5):170-176.
53. Findlay I. The ATP sensitive potassium channel of cardiac muscle and action potential shortening during metabolic stress. *Cardiovascular research.* Jun 1994;28(6):760-761.
54. Bers DM, Perez-Reyes E. Ca channels in cardiac myocytes: structure and function in Ca influx and intracellular Ca release. *Cardiovascular research.* May 1999;42(2):339-360.
55. Bean BP. Two kinds of calcium channels in canine atrial cells. Differences in kinetics, selectivity, and pharmacology. *The Journal of general physiology.* Jul 1985;86(1):1-30.
56. Cerrone M, Noujaim SF, Tolkacheva EG, et al. Arrhythmogenic mechanisms in a mouse model of catecholaminergic polymorphic ventricular tachycardia. *Circulation research.* Nov 9 2007;101(10):1039-1048.
57. Fabiato A, Fabiato F. Calcium and cardiac excitation-contraction coupling. *Annual review of physiology.* 1979;41:473-484.
58. Fozzard HA. Excitation-contraction coupling in the heart. *Advances in experimental medicine and biology.* 1991;308:135-142.
59. Horie M, Hayashi S, Kawai C. Two types of delayed rectifying K+ channels in atrial cells of guinea pig heart. *The Japanese journal of physiology.* 1990;40(4):479-490.
60. Sanguinetti MC, Jurkiewicz NK. Delayed rectifier outward K+ current is composed of two currents in guinea pig atrial cells. *The American journal of physiology.* Feb 1991;260(2 Pt 2):H393-399.

61. Sanguinetti MC, Jurkiewicz NK. Role of external Ca2+ and K+ in gating of cardiac delayed rectifier K+ currents. *Pflugers Archiv : European journal of physiology.* Feb 1992;420(2):180-186.
62. Guo J, Wang T, Yang T, et al. Interaction between the cardiac rapidly (IKr) and slowly (IKs) activating delayed rectifier potassium channels revealed by low K+-induced hERG endocytic degradation. *The Journal of biological chemistry.* Oct 7 2011;286(40):34664-34674.
63. Lopatin AN, Nichols CG. Inward rectifiers in the heart: an update on I(K1). *Journal of molecular and cellular cardiology.* Apr 2001;33(4):625-638.
64. Nichols CG, Lopatin AN. Inward rectifier potassium channels. *Annual review of physiology.* 1997;59:171-191.
65. Cho HS, Takano M, Noma A. The electrophysiological properties of spontaneously beating pacemaker cells isolated from mouse sinoatrial node. *The Journal of physiology.* Jul 1 2003;550(Pt 1):169-180.
66. Shinagawa Y, Satoh H, Noma A. The sustained inward current and inward rectifier K+ current in pacemaker cells dissociated from rat sinoatrial node. *The Journal of physiology.* Mar 15 2000;523 Pt 3:593-605.
67. Vandenberg CA. Inward rectification of a potassium channel in cardiac ventricular cells depends on internal magnesium ions. *Proceedings of the National Academy of Sciences of the United States of America.* Apr 1987;84(8):2560-2564.
68. Mazzanti M, DiFrancesco D. Intracellular Ca modulates K-inward rectification in cardiac myocytes. *Pflugers Archiv : European journal of physiology.* Jan 1989;413(3):322-324.
69. Ficker E, Taglialatela M, Wible BA, Henley CM, Brown AM. Spermine and spermidine as gating molecules for inward rectifier K+ channels. *Science.* Nov 11 1994;266(5187):1068-1072.
70. Lopatin AN, Makhina EN, Nichols CG. Potassium channel block by cytoplasmic polyamines as the mechanism of intrinsic rectification. *Nature.* Nov 24 1994;372(6504):366-369.
71. Lopatin AN, Makhina EN, Nichols CG. The mechanism of inward rectification of potassium channels: "long-pore plugging" by cytoplasmic polyamines. *The Journal of general physiology.* Nov 1995;106(5):923-955.
72. Anumonwo JM, Lopatin AN. Cardiac strong inward rectifier potassium channels. *Journal of molecular and cellular cardiology.* Jan 2010;48(1):45-54.
73. DiFrancesco D. The role of the funny current in pacemaker activity. *Circulation research.* Feb 19 2010;106(3):434-446.
74. Anumonwo JM, Delmar M, Jalife J. Is the "funny" current funnier than we thought? *Journal of cardiovascular electrophysiology.* Apr 1994;5(4):394-396.

75. Verkerk AO, Wilders R. Pacemaker activity of the human sinoatrial node: effects of HCN4 mutations on the hyperpolarization-activated current. *Europace : European pacing, arrhythmias, and cardiac electrophysiology : journal of the working groups on cardiac pacing, arrhythmias, and cardiac cellular electrophysiology of the European Society of Cardiology.* Mar 2014;16(3):384-395.

76. Zhou Z, Lipsius SL. Na(+)-Ca2+ exchange current in latent pacemaker cells isolated from cat right atrium. *The Journal of physiology.* Jul 1993;466:263-285.

77. Bers DM. *Excitation-Contraction Coupling and Cardiac Contractile Force.* Dordrecht, Netherlands: Kluwer Academic Publishers; 2001.

78. Pogwizd SM, Schlotthauer K, Li L, Yuan W, Bers DM. Arrhythmogenesis and contractile dysfunction in heart failure: Roles of sodium-calcium exchange, inward rectifier potassium current, and residual beta-adrenergic responsiveness. *Circulation research.* Jun 8 2001;88(11):1159-1167.

79. Lindner E. Die submikroskopische Morphologie des Herzmuskels. 1956.

80. Forbes MS, Hawkey LA, Sperelakis N. The transverse-axial tubular system (TATS) of mouse myocardium: its morphology in the developing and adult animal. *Am J Anat.* Jun 1984;170(2):143-162.

81. Bossen EH, Sommer JR, Waugh RA. Comparative stereology of the mouse and finch left ventricle. *Tissue Cell.* 1978;10(4):773-784.

82. Moench I, Meekhof KE, Cheng LF, Lopatin AN. Resolution of hyposmotic stress in isolated mouse ventricular myocytes causes sealing of t-tubules. *Exp Physiol.* Jul 2013;98(7):1164-1177.

83. Christe G. Localization of K(+) channels in the tubules of cardiomyocytes as suggested by the parallel decay of membrane capacitance, IK(1) and IK(ATP) during culture and by delayed IK(1) response to barium. *Journal of molecular and cellular cardiology.* Dec 1999;31(12):2207-2213.

84. Ibrahim M, Gorelik J, Yacoub MH, Terracciano CM. The structure and function of cardiac t-tubules in health and disease. *Proc Biol Sci.* Sep 22 2011;278(1719):2714-2723.

85. He J, Conklin MW, Foell JD, et al. Reduction in density of transverse tubules and L-type Ca(2+) channels in canine tachycardia-induced heart failure. *Cardiovascular research.* Feb 1 2001;49(2):298-307.

86. Haddock PS, Coetzee WA, Cho E, et al. Subcellular [Ca2+]i gradients during excitation-contraction coupling in newborn rabbit ventricular myocytes. *Circulation research.* Sep 3 1999;85(5):415-427.

87. Forbes MS, van Neil EE. Membrane systems of guinea pig myocardium: ultrastructure and morphometric studies. *Anat Rec.* Dec 1988;222(4):362-379.

88. Heinzel FR, Bito V, Volders PG, Antoons G, Mubagwa K, Sipido KR. Spatial and temporal inhomogeneities during Ca2+ release from the sarcoplasmic reticulum in pig ventricular myocytes. *Circulation research.* Nov 29 2002;91(11):1023-1030.

89. Dibb KM, Clarke JD, Horn MA, et al. Characterization of an extensive transverse tubular network in sheep atrial myocytes and its depletion in heart failure. *Circulation. Heart failure.* Sep 2009;2(5):482-489.
90. Bossen EH, Sommer JR. Comparative stereology of the lizard and frog myocardium. *Tissue Cell.* 1984;16(2):173-178.
91. Chen F, Mottino G, Klitzner TS, Philipson KD, Frank JS. Distribution of the Na+/Ca2+ exchange protein in developing rabbit myocytes. *The American journal of physiology.* May 1995;268(5 Pt 1):C1126-1132.
92. Hong TT, Smyth JW, Gao D, et al. BIN1 localizes the L-type calcium channel to cardiac T-tubules. *PLoS Biol.* Feb 2010;8(2):e1000312.
93. Al-Qusairi L, Weiss N, Toussaint A, et al. T-tubule disorganization and defective excitation-contraction coupling in muscle fibers lacking myotubularin lipid phosphatase. *Proceedings of the National Academy of Sciences of the United States of America.* Nov 3 2009;106(44):18763-18768.
94. Mitcheson JS, Hancox JC, Levi AJ. Action potentials, ion channel currents and transverse tubule density in adult rabbit ventricular myocytes maintained for 6 days in cell culture. *Pflugers Archiv : European journal of physiology.* Apr 1996;431(6):814-827.
95. Landstrom AP, Beavers DL, Wehrens XH. The junctophilin family of proteins: from bench to bedside. *Trends in molecular medicine.* Mar 14 2014.
96. Zhang L, Kelley J, Schmeisser G, Kobayashi YM, Jones LR. Complex formation between junctin, triadin, calsequestrin, and the ryanodine receptor. Proteins of the cardiac junctional sarcoplasmic reticulum membrane. *The Journal of biological chemistry.* Sep 12 1997;272(37):23389-23397.
97. Landstrom AP, Kellen CA, Dixit SS, et al. Junctophilin-2 expression silencing causes cardiocyte hypertrophy and abnormal intracellular calcium-handling. *Circulation. Heart failure.* Mar 2011;4(2):214-223.
98. van Oort RJ, Garbino A, Wang W, et al. Disrupted junctional membrane complexes and hyperactive ryanodine receptors after acute junctophilin knockdown in mice. *Circulation.* Mar 8 2011;123(9):979-988.
99. Ibrahim M, Siedlecka U, Buyandelger B, et al. A critical role for Telethonin in regulating t-tubule structure and function in the mammalian heart. *Human molecular genetics.* Jan 15 2013;22(2):372-383.
100. Ringer S. A further Contribution regarding the influence of the different Constituents of the Blood on the Contraction of the Heart. *The Journal of physiology.* Jan 1883;4(1):29-42 23.
101. Rougier O, Vassort G, Garnier D, Gargouil YM, Coraboeuf E. Existence and role of a slow inward current during the frog atrial action potential. *Pflugers Archiv : European journal of physiology.* 1969;308(2):91-110.
102. Nilius B, Hess P, Lansman JB, Tsien RW. A novel type of cardiac calcium channel in ventricular cells. *Nature.* Aug 1-7 1985;316(6027):443-446.

103. Tanabe T, Takeshima H, Mikami A, et al. Primary structure of the receptor for calcium channel blockers from skeletal muscle. *Nature.* Jul 23-29 1987;328(6128):313-318.
104. Ellis SB, Williams ME, Ways NR, et al. Sequence and expression of mRNAs encoding the alpha 1 and alpha 2 subunits of a DHP-sensitive calcium channel. *Science.* Sep 23 1988;241(4873):1661-1664.
105. Ruth P, Rohrkasten A, Biel M, et al. Primary structure of the beta subunit of the DHP-sensitive calcium channel from skeletal muscle. *Science.* Sep 8 1989;245(4922):1115-1118.
106. Jay SD, Sharp AH, Kahl SD, Vedvick TS, Harpold MM, Campbell KP. Structural characterization of the dihydropyridine-sensitive calcium channel alpha 2-subunit and the associated delta peptides. *The Journal of biological chemistry.* Feb 15 1991;266(5):3287-3293.
107. Galizzi JP, Borsotto M, Barhanin J, Fosset M, Lazdunski M. Characterization and photoaffinity labeling of receptor sites for the Ca2+ channel inhibitors d-cis-diltiazem, (+/-)-bepridil, desmethoxyverapamil, and (+)-PN 200-110 in skeletal muscle transverse tubule membranes. *The Journal of biological chemistry.* Jan 25 1986;261(3):1393-1397.
108. Sharp AH, Imagawa T, Leung AT, Campbell KP. Identification and characterization of the dihydropyridine-binding subunit of the skeletal muscle dihydropyridine receptor. *The Journal of biological chemistry.* Sep 5 1987;262(25):12309-12315.
109. Sieber M, Nastainczyk W, Rohrkasten A, Hofmann F. Reconstitution of the purified receptor for calcium channel blockers. *Biomed Biochim Acta.* 1987;46(8-9):S357-362.
110. Vaghy PL, Striessnig J, Miwa K, et al. Identification of a novel 1,4-dihydropyridine- and phenylalkylamine-binding polypeptide in calcium channel preparations. *The Journal of biological chemistry.* Oct 15 1987;262(29):14337-14342.
111. Striessnig J, Scheffauer F, Mitterdorfer J, Schirmer M, Glossmann H. Identification of the benzothiazepine-binding polypeptide of skeletal muscle calcium channels with (+)-cis-azidodiltiazem and anti-ligand antibodies. *The Journal of biological chemistry.* Jan 5 1990;265(1):363-370.
112. Striessnig J, Glossmann H, Catterall WA. Identification of a phenylalkylamine binding region within the alpha 1 subunit of skeletal muscle Ca2+ channels. *Proceedings of the National Academy of Sciences of the United States of America.* Dec 1990;87(23):9108-9112.
113. Curtis BM, Catterall WA. Phosphorylation of the calcium antagonist receptor of the voltage-sensitive calcium channel by cAMP-dependent protein kinase. *Proceedings of the National Academy of Sciences of the United States of America.* Apr 1985;82(8):2528-2532.

114. Hosey MM, Borsotto M, Lazdunski M. Phosphorylation and dephosphorylation of dihydropyridine-sensitive voltage-dependent Ca2+ channel in skeletal muscle membranes by cAMP- and Ca2+-dependent processes. *Proceedings of the National Academy of Sciences of the United States of America.* Jun 1986;83(11):3733-3737.

115. Nastainczyk W, Rohrkasten A, Sieber M, et al. Phosphorylation of the purified receptor for calcium channel blockers by cAMP kinase and protein kinase C. *European journal of biochemistry / FEBS.* Nov 16 1987;169(1):137-142.

116. O'Callahan CM, Hosey MM. Multiple phosphorylation sites in the 165-kilodalton peptide associated with dihydropyridine-sensitive calcium channels. *Biochemistry.* Aug 9 1988;27(16):6071-6077.

117. Takimoto K, Li D, Nerbonne JM, Levitan ES. Distribution, splicing and glucocorticoid-induced expression of cardiac alpha 1C and alpha 1D voltage-gated Ca2+ channel mRNAs. *Journal of molecular and cellular cardiology.* Nov 1997;29(11):3035-3042.

118. Singer D, Biel M, Lotan I, Flockerzi V, Hofmann F, Dascal N. The roles of the subunits in the function of the calcium channel. *Science.* Sep 27 1991;253(5027):1553-1557.

119. Bangalore R, Mehrke G, Gingrich K, Hofmann F, Kass RS. Influence of L-type Ca channel alpha 2/delta-subunit on ionic and gating current in transiently transfected HEK 293 cells. *The American journal of physiology.* May 1996;270(5 Pt 2):H1521-1528.

120. Gurnett CA, Felix R, Campbell KP. Extracellular interaction of the voltage-dependent Ca2+ channel alpha2delta and alpha1 subunits. *The Journal of biological chemistry.* Jul 18 1997;272(29):18508-18512.

121. Yang L, Katchman A, Morrow JP, Doshi D, Marx SO. Cardiac L-type calcium channel (Cav1.2) associates with gamma subunits. *FASEB journal : official publication of the Federation of American Societies for Experimental Biology.* Mar 2011;25(3):928-936.

122. Hullin R, Singer-Lahat D, Freichel M, et al. Calcium channel beta subunit heterogeneity: functional expression of cloned cDNA from heart, aorta and brain. *The EMBO journal.* Mar 1992;11(3):885-890.

123. Perez-Reyes E, Castellano A, Kim HS, et al. Cloning and expression of a cardiac/brain beta subunit of the L-type calcium channel. *The Journal of biological chemistry.* Jan 25 1992;267(3):1792-1797.

124. Castellano A, Wei X, Birnbaumer L, Perez-Reyes E. Cloning and expression of a neuronal calcium channel beta subunit. *The Journal of biological chemistry.* Jun 15 1993;268(17):12359-12366.

125. Pragnell M, Sakamoto J, Jay SD, Campbell KP. Cloning and tissue-specific expression of the brain calcium channel beta-subunit. *FEBS letters.* Oct 21 1991;291(2):253-258.

126. Pragnell M, De Waard M, Mori Y, Tanabe T, Snutch TP, Campbell KP. Calcium channel beta-subunit binds to a conserved motif in the I-II cytoplasmic linker of the alpha 1-subunit. *Nature.* Mar 3 1994;368(6466):67-70.

127. De Waard M, Pragnell M, Campbell KP. Ca2+ channel regulation by a conserved beta subunit domain. *Neuron.* Aug 1994;13(2):495-503.
128. Neely A, Wei X, Olcese R, Birnbaumer L, Stefani E. Potentiation by the beta subunit of the ratio of the ionic current to the charge movement in the cardiac calcium channel. *Science.* Oct 22 1993;262(5133):575-578.
129. Mitterdorfer J, Froschmayr M, Grabner M, Striessnig J, Glossmann H. Calcium channels: the beta-subunit increases the affinity of dihydropyridine and Ca2+ binding sites of the alpha 1-subunit. *FEBS letters.* Sep 26 1994;352(2):141-145.
130. Bichet D, Cornet V, Geib S, et al. The I-II loop of the Ca2+ channel alpha1 subunit contains an endoplasmic reticulum retention signal antagonized by the beta subunit. *Neuron.* Jan 2000;25(1):177-190.
131. Gao T, Chien AJ, Hosey MM. Complexes of the alpha1C and beta subunits generate the necessary signal for membrane targeting of class C L-type calcium channels. *The Journal of biological chemistry.* Jan 22 1999;274(4):2137-2144.
132. Shaw RM, Fay AJ, Puthenveedu MA, von Zastrow M, Jan YN, Jan LY. Microtubule plus-end-tracking proteins target gap junctions directly from the cell interior to adherens junctions. *Cell.* Feb 9 2007;128(3):547-560.
133. Chu PJ, Rivera JF, Arnold DB. A role for Kif17 in transport of Kv4.2. *The Journal of biological chemistry.* Jan 6 2006;281(1):365-373.
134. Nejsum LN, Nelson WJ. A molecular mechanism directly linking E-cadherin adhesion to initiation of epithelial cell surface polarity. *The Journal of cell biology.* Jul 16 2007;178(2):323-335.
135. Ren G, Vajjhala P, Lee JS, Winsor B, Munn AL. The BAR domain proteins: molding membranes in fission, fusion, and phagy. *Microbiology and molecular biology reviews : MMBR.* Mar 2006;70(1):37-120.
136. Lee E, Marcucci M, Daniell L, et al. Amphiphysin 2 (Bin1) and T-tubule biogenesis in muscle. *Science.* Aug 16 2002;297(5584):1193-1196.
137. Nuss HB, Houser SR. T-type Ca2+ current is expressed in hypertrophied adult feline left ventricular myocytes. *Circulation research.* Oct 1993;73(4):777-782.
138. Martinez ML, Heredia MP, Delgado C. Expression of T-type Ca(2+) channels in ventricular cells from hypertrophied rat hearts. *Journal of molecular and cellular cardiology.* Sep 1999;31(9):1617-1625.
139. Fruen BR, Bardy JM, Byrem TM, Strasburg GM, Louis CF. Differential Ca(2+) sensitivity of skeletal and cardiac muscle ryanodine receptors in the presence of calmodulin. *Am J Physiol Cell Physiol.* Sep 2000;279(3):C724-733.
140. Marx SO, Reiken S, Hisamatsu Y, et al. PKA phosphorylation dissociates FKBP12.6 from the calcium release channel (ryanodine receptor): defective regulation in failing hearts. *Cell.* May 12 2000;101(4):365-376.
141. Franzini-Armstrong C, Protasi F, Ramesh V. Shape, size, and distribution of Ca(2+) release units and couplons in skeletal and cardiac muscles. *Biophysical journal.* Sep 1999;77(3):1528-1539.

142. Cheng H, Lederer WJ, Cannell MB. Calcium sparks: elementary events underlying excitation-contraction coupling in heart muscle. *Science.* Oct 29 1993;262(5134):740-744.
143. Wier WG, Balke CW. Ca(2+) release mechanisms, Ca(2+) sparks, and local control of excitation-contraction coupling in normal heart muscle. *Circulation research.* Oct 29 1999;85(9):770-776.
144. Bridge JH, Ershler PR, Cannell MB. Properties of Ca2+ sparks evoked by action potentials in mouse ventricular myocytes. *The Journal of physiology.* Jul 15 1999;518 (Pt 2):469-478.
145. Brandt N. Identification of two populations of cardiac microsomes with nitrendipine receptors: correlation of the distribution of dihydropyridine receptors with organelle specific markers. *Arch Biochem Biophys.* Oct 1985;242(1):306-319.
146. Bodi I, Mikala G, Koch SE, Akhter SA, Schwartz A. The L-type calcium channel in the heart: the beat goes on. *J Clin Invest.* Dec 2005;115(12):3306-3317.
147. Haase H, Kresse A, Hohaus A, et al. Expression of calcium channel subunits in the normal and diseased human myocardium. *J Mol Med.* Feb 1996;74(2):99-104.
148. Cerrone M, Napolitano C, Priori SG. Catecholaminergic polymorphic ventricular tachycardia: A paradigm to understand mechanisms of arrhythmias associated to impaired Ca(2+) regulation. *Heart rhythm : the official journal of the Heart Rhythm Society.* Nov 2009;6(11):1652-1659.
149. O'Rourke B, Kass DA, Tomaselli GF, Kaab S, Tunin R, Marban E. Mechanisms of altered excitation-contraction coupling in canine tachycardia-induced heart failure, I: experimental studies. *Circulation research.* Mar 19 1999;84(5):562-570.
150. Harzheim D, Movassagh M, Foo RS, et al. Increased InsP3Rs in the junctional sarcoplasmic reticulum augment Ca2+ transients and arrhythmias associated with cardiac hypertrophy. *Proceedings of the National Academy of Sciences of the United States of America.* Jul 7 2009;106(27):11406-11411.
151. Cohn JN, Ferrari R, Sharpe N. Cardiac remodeling--concepts and clinical implications: a consensus paper from an international forum on cardiac remodeling. Behalf of an International Forum on Cardiac Remodeling. *Journal of the American College of Cardiology.* Mar 1 2000;35(3):569-582.
152. Dorn GW, 2nd, Robbins J, Sugden PH. Phenotyping hypertrophy: eschew obfuscation. *Circulation research.* Jun 13 2003;92(11):1171-1175.
153. Opie LH, Commerford PJ, Gersh BJ, Pfeffer MA. Controversies in ventricular remodelling. *Lancet.* Jan 28 2006;367(9507):356-367.
154. Benjamin EJ, Chen PS, Bild DE, et al. Prevention of atrial fibrillation: report from a national heart, lung, and blood institute workshop. *Circulation.* Feb 3 2009;119(4):606-618.
155. Hart RG. Atrial fibrillation and stroke prevention. *N Engl J Med.* Sep 11 2003;349(11):1015-1016.

156. Go AS, Hylek EM, Phillips KA, et al. Prevalence of diagnosed atrial fibrillation in adults: national implications for rhythm management and stroke prevention: the AnTicoagulation and Risk Factors in Atrial Fibrillation (ATRIA) Study. *JAMA.* May 9 2001;285(18):2370-2375.

157. Fuster V, Ryden LE, Cannom DS, et al. 2011 ACCF/AHA/HRS focused updates incorporated into the ACC/AHA/ESC 2006 Guidelines for the management of patients with atrial fibrillation: a report of the American College of Cardiology Foundation/American Heart Association Task Force on Practice Guidelines developed in partnership with the European Society of Cardiology and in collaboration with the European Heart Rhythm Association and the Heart Rhythm Society. *Journal of the American College of Cardiology.* Mar 15 2011;57(11):e101-198.

158. Friberg J, Buch P, Scharling H, Gadsbphioll N, Jensen GB. Rising rates of hospital admissions for atrial fibrillation. *Epidemiology.* Nov 2003;14(6):666-672.

159. Jais P, Shah DC, Haissaguerre M, Hocini M, Peng JT, Clementy J. Catheter ablation for atrial fibrillation. *Annual review of medicine.* 2000;51:431-441.

160. Wijffels MCEF, Kirchhof CJHJ, Dorland R, Allessie MA. Atrial Fibrillation Begets Atrial Fibrillation : A Study in Awake Chronically Instrumented Goats. *Circulation.* October 1, 1995 1995;92(7):1954-1968.

161. Nattel S, Burstein B, Dobrev D. Atrial remodeling and atrial fibrillation: mechanisms and implications. *Circ Arrhythm Electrophysiol.* Apr 2008;1(1):62-73.

162. Fareh S, Villemaire C, Nattel S. Importance of refractoriness heterogeneity in the enhanced vulnerability to atrial fibrillation induction caused by tachycardia-induced atrial electrical remodeling. *Circulation.* Nov 17 1998;98(20):2202-2209.

163. Gaspo R, Bosch RF, Talajic M, Nattel S. Functional Mechanisms Underlying Tachycardia-Induced Sustained Atrial Fibrillation in a Chronic Dog Model. *Circulation.* December 2, 1997 1997;96(11):4027-4035.

164. Morillo CA, Klein GJ, Jones DL, Guiraudon CM. Chronic rapid atrial pacing. Structural, functional, and electrophysiological characteristics of a new model of sustained atrial fibrillation. *Circulation.* Mar 1 1995;91(5):1588-1595.

165. Vest JA, Wehrens XH, Reiken SR, et al. Defective cardiac ryanodine receptor regulation during atrial fibrillation. *Circulation.* Apr 26 2005;111(16):2025-2032.

166. Zhou S, Chang CM, Wu TJ, et al. Nonreentrant focal activations in pulmonary veins in canine model of sustained atrial fibrillation. *American journal of physiology. Heart and circulatory physiology.* Sep 2002;283(3):H1244-1252.

167. Yue L, Feng J, Gaspo R, Li G-R, Wang Z, Nattel S. Ionic Remodeling Underlying Action Potential Changes in a Canine Model of Atrial Fibrillation. *Circulation research.* October 19, 1997 1997;81(4):512-525.

168. Bosch RF, Zeng X, Grammer JB, Popovic K, Mewis C, Kuhlkamp V. Ionic mechanisms of electrical remodeling in human atrial fibrillation. *Cardiovascular research.* Oct 1999;44(1):121-131.
169. Dobrev D, Graf E, Wettwer E, et al. Molecular basis of downregulation of G-protein-coupled inward rectifying K(+) current (I(K,ACh) in chronic human atrial fibrillation: decrease in GIRK4 mRNA correlates with reduced I(K,ACh) and muscarinic receptor-mediated shortening of action potentials. *Circulation.* Nov 20 2001;104(21):2551-2557.
170. Dobrev D, Wettwer E, Kortner A, Knaut M, Schuler S, Ravens U. Human inward rectifier potassium channels in chronic and postoperative atrial fibrillation. *Cardiovascular research.* May 2002;54(2):397-404.
171. Gaborit N, Steenman M, Lamirault G, et al. Human atrial ion channel and transporter subunit gene-expression remodeling associated with valvular heart disease and atrial fibrillation. *Circulation.* Jul 26 2005;112(4):471-481.
172. Van Wagoner DR, Pond AL, McCarthy PM, Trimmer JS, Nerbonne JM. Outward K+ current densities and Kv1.5 expression are reduced in chronic human atrial fibrillation. *Circulation research.* Jun 1997;80(6):772-781.
173. Workman AJ, Kane KA, Rankin AC. The contribution of ionic currents to changes in refractoriness of human atrial myocytes associated with chronic atrial fibrillation. *Cardiovascular research.* Nov 2001;52(2):226-235.
174. Cha TJ, Ehrlich JR, Zhang L, Nattel S. Atrial ionic remodeling induced by atrial tachycardia in the presence of congestive heart failure. *Circulation.* Sep 21 2004;110(12):1520-1526.
175. Chen X, Piacentino V, 3rd, Furukawa S, Goldman B, Margulies KB, Houser SR. L-type Ca2+ channel density and regulation are altered in failing human ventricular myocytes and recover after support with mechanical assist devices. *Circulation research.* Sep 20 2002;91(6):517-524.
176. Dun W, Chandra P, Danilo P, Jr., Rosen MR, Boyden PA. Chronic atrial fibrillation does not further decrease outward currents. It increases them. *American journal of physiology. Heart and circulatory physiology.* Oct 2003;285(4):H1378-1384.
177. Courtemanche M, Ramirez RJ, Nattel S. Ionic mechanisms underlying human atrial action potential properties: insights from a mathematical model. *The American journal of physiology.* Jul 1998;275(1 Pt 2):H301-321.
178. Ramirez RJ, Nattel S, Courtemanche M. Mathematical analysis of canine atrial action potentials: rate, regional factors, and electrical remodeling. *American journal of physiology. Heart and circulatory physiology.* Oct 2000;279(4):H1767-1785.
179. Sun H, Chartier D, Leblanc N, Nattel S. Intracellular calcium changes and tachycardia-induced contractile dysfunction in canine atrial myocytes. *Cardiovascular research.* Mar 2001;49(4):751-761.

180. Van Wagoner DR, Pond AL, Lamorgese M, Rossie SS, McCarthy PM, Nerbonne JM. Atrial L-type Ca2+ currents and human atrial fibrillation. *Circulation research.* Sep 3 1999;85(5):428-436.
181. van der Velden HMW, van der Zee L, Wijffels MC, et al. Atrial fibrillation in the goat induces changes in monophasic action potential and mRNA expression of ion channels involved in repolarization. *Journal of cardiovascular electrophysiology.* Nov 2000;11(11):1262-1269.
182. Brundel BJ, Van Gelder IC, Henning RH, et al. Ion channel remodeling is related to intraoperative atrial effective refractory periods in patients with paroxysmal and persistent atrial fibrillation. *Circulation.* Feb 6 2001;103(5):684-690.
183. Brundel BJ, Van Gelder IC, Henning RH, et al. Alterations in potassium channel gene expression in atria of patients with persistent and paroxysmal atrial fibrillation: differential regulation of protein and mRNA levels for K+ channels. *Journal of the American College of Cardiology.* Mar 1 2001;37(3):926-932.
184. Brundel BJ, van Gelder IC, Henning RH, et al. Gene expression of proteins influencing the calcium homeostasis in patients with persistent and paroxysmal atrial fibrillation. *Cardiovascular research.* May 1999;42(2):443-454.
185. Schotten U, Greiser M, Benke D, et al. Atrial fibrillation-induced atrial contractile dysfunction: a tachycardiomyopathy of a different sort. *Cardiovascular research.* Jan 2002;53(1):192-201.
186. Hove-Madsen L, Llach A, Bayes-Genis A, et al. Atrial fibrillation is associated with increased spontaneous calcium release from the sarcoplasmic reticulum in human atrial myocytes. *Circulation.* Sep 14 2004;110(11):1358-1363.
187. Ohkusa T, Ueyama T, Yamada J, et al. Alterations in cardiac sarcoplasmic reticulum Ca2+ regulatory proteins in the atrial tissue of patients with chronic atrial fibrillation. *Journal of the American College of Cardiology.* Jul 1999;34(1):255-263.
188. Uemura N, Ohkusa T, Hamano K, et al. Down-regulation of sarcolipin mRNA expression in chronic atrial fibrillation. *European journal of clinical investigation.* Nov 2004;34(11):723-730.
189. Van Gelder IC, Brundel BJ, Henning RH, et al. Alterations in gene expression of proteins involved in the calcium handling in patients with atrial fibrillation. *Journal of cardiovascular electrophysiology.* Apr 1999;10(4):552-560.
190. Tessier S, Karczewski P, Krause EG, et al. Regulation of the transient outward K(+) current by Ca(2+)/calmodulin-dependent protein kinases II in human atrial myocytes. *Circulation research.* Oct 29 1999;85(9):810-819.
191. Carnes CA, Janssen PM, Ruehr ML, et al. Atrial glutathione content, calcium current, and contractility. *The Journal of biological chemistry.* Sep 21 2007;282(38):28063-28073.

192. Christ T, Boknik P, Wohrl S, et al. L-type Ca2+ current downregulation in chronic human atrial fibrillation is associated with increased activity of protein phosphatases. *Circulation.* Oct 26 2004;110(17):2651-2657.
193. Kannel WB. Incidence and epidemiology of heart failure. *Heart failure reviews.* Jun 2000;5(2):167-173.
194. Kannel WB, Ho K, Thom T. Changing epidemiological features of cardiac failure. *British heart journal.* Aug 1994;72(2 Suppl):S3-9.
195. Mann DL, Bristow MR. Mechanisms and models in heart failure: the biomechanical model and beyond. *Circulation.* May 31 2005;111(21):2837-2849.
196. Drazner MH. The progression of hypertensive heart disease. *Circulation.* Jan 25 2011;123(3):327-334.
197. Hasenfuss G. Animal models of human cardiovascular disease, heart failure and hypertrophy. *Cardiovascular research.* Jul 1998;39(1):60-76.
198. Gaasch WH, Zile MR. Left ventricular diastolic dysfunction and diastolic heart failure. *Annual review of medicine.* 2004;55:373-394.
199. Brower GL, Gardner JD, Forman MF, et al. The relationship between myocardial extracellular matrix remodeling and ventricular function. *European journal of cardio-thoracic surgery : official journal of the European Association for Cardio-thoracic Surgery.* Oct 2006;30(4):604-610.
200. Berk BC, Fujiwara K, Lehoux S. ECM remodeling in hypertensive heart disease. *J Clin Invest.* Mar 2007;117(3):568-575.
201. Rossi MA. Pathologic fibrosis and connective tissue matrix in left ventricular hypertrophy due to chronic arterial hypertension in humans. *Journal of hypertension.* Jul 1998;16(7):1031-1041.
202. Song LS, Sobie EA, McCulle S, Lederer WJ, Balke CW, Cheng H. Orphaned ryanodine receptors in the failing heart. *Proceedings of the National Academy of Sciences of the United States of America.* Mar 14 2006;103(11):4305-4310.
203. Louch WE, Mork HK, Sexton J, et al. T-tubule disorganization and reduced synchrony of Ca2+ release in murine cardiomyocytes following myocardial infarction. *The Journal of physiology.* Jul 15 2006;574(Pt 2):519-533.
204. Heinzel FR, Bito V, Biesmans L, et al. Remodeling of T-tubules and reduced synchrony of Ca2+ release in myocytes from chronically ischemic myocardium. *Circulation research.* Feb 15 2008;102(3):338-346.
205. Lyon AR, MacLeod KT, Zhang Y, et al. Loss of T-tubules and other changes to surface topography in ventricular myocytes from failing human and rat heart. *Proceedings of the National Academy of Sciences of the United States of America.* Apr 21 2009;106(16):6854-6859.
206. Katzmarzyk PT, Mason C. Prevalence of class I, II and III obesity in Canada. *CMAJ : Canadian Medical Association journal = journal de l'Association medicale canadienne.* Jan 17 2006;174(2):156-157.
207. Hensrud DD, Klein S. Extreme obesity: a new medical crisis in the United States. *Mayo Clinic proceedings.* Oct 2006;81(10 Suppl):S5-10.

208. Van Gaal LF, Mertens IL, De Block CE. Mechanisms linking obesity with cardiovascular disease. *Nature.* Dec 14 2006;444(7121):875-880.
209. Douketis JD, Sharma AM. Obesity and cardiovascular disease: pathogenic mechanisms and potential benefits of weight reduction. *Seminars in vascular medicine.* Feb 2005;5(1):25-33.
210. Despres JP. Intra-abdominal obesity: an untreated risk factor for Type 2 diabetes and cardiovascular disease. *Journal of endocrinological investigation.* 2006;29(3 Suppl):77-82.
211. Wilhelmsen L, Rosengren A, Eriksson H, Lappas G. Heart failure in the general population of men--morbidity, risk factors and prognosis. *Journal of internal medicine.* Mar 2001;249(3):253-261.
212. Chen YT, Vaccarino V, Williams CS, Butler J, Berkman LF, Krumholz HM. Risk factors for heart failure in the elderly: a prospective community-based study. *The American journal of medicine.* Jun 1999;106(6):605-612.
213. Alpert MA, Lambert CR, Panayiotou H, et al. Relation of duration of morbid obesity to left ventricular mass, systolic function, and diastolic filling, and effect of weight loss. *The American journal of cardiology.* Dec 1 1995;76(16):1194-1197.
214. Kenchaiah S, Evans JC, Levy D, et al. Obesity and the risk of heart failure. *N Engl J Med.* Aug 1 2002;347(5):305-313.
215. Mazumder PK, O'Neill BT, Roberts MW, et al. Impaired cardiac efficiency and increased fatty acid oxidation in insulin-resistant ob/ob mouse hearts. *Diabetes.* Sep 2004;53(9):2366-2374.
216. Finck BN, Lehman JJ, Leone TC, et al. The cardiac phenotype induced by PPARalpha overexpression mimics that caused by diabetes mellitus. *J Clin Invest.* Jan 2002;109(1):121-130.
217. Finck BN, Han X, Courtois M, et al. A critical role for PPARalpha-mediated lipotoxicity in the pathogenesis of diabetic cardiomyopathy: modulation by dietary fat content. *Proceedings of the National Academy of Sciences of the United States of America.* Feb 4 2003;100(3):1226-1231.
218. Haemmerle G, Lass A, Zimmermann R, et al. Defective lipolysis and altered energy metabolism in mice lacking adipose triglyceride lipase. *Science.* May 5 2006;312(5774):734-737.
219. Cheng L, Ding G, Qin Q, et al. Cardiomyocyte-restricted peroxisome proliferator-activated receptor-delta deletion perturbs myocardial fatty acid oxidation and leads to cardiomyopathy. *Nature medicine.* Nov 2004;10(11):1245-1250.
220. de Vries JE, Vork MM, Roemen TH, et al. Saturated but not mono-unsaturated fatty acids induce apoptotic cell death in neonatal rat ventricular myocytes. *Journal of lipid research.* Jul 1997;38(7):1384-1394.
221. Okere IC, Chandler MP, McElfresh TA, et al. Differential effects of saturated and unsaturated fatty acid diets on cardiomyocyte apoptosis, adipose distribution, and serum leptin. *American journal of physiology. Heart and circulatory physiology.* Jul 2006;291(1):H38-44.

222. Miller TA, LeBrasseur NK, Cote GM, et al. Oleate prevents palmitate-induced cytotoxic stress in cardiac myocytes. *Biochemical and biophysical research communications.* Oct 14 2005;336(1):309-315.
223. Listenberger LL, Han X, Lewis SE, et al. Triglyceride accumulation protects against fatty acid-induced lipotoxicity. *Proceedings of the National Academy of Sciences of the United States of America.* Mar 18 2003;100(6):3077-3082.
224. Wong CY, O'Moore-Sullivan T, Leano R, Byrne N, Beller E, Marwick TH. Alterations of left ventricular myocardial characteristics associated with obesity. *Circulation.* Nov 9 2004;110(19):3081-3087.
225. Peterson LR, Waggoner AD, Schechtman KB, et al. Alterations in left ventricular structure and function in young healthy obese women: assessment by echocardiography and tissue Doppler imaging. *Journal of the American College of Cardiology.* Apr 21 2004;43(8):1399-1404.
226. Morricone L, Malavazos AE, Coman C, Donati C, Hassan T, Caviezel F. Echocardiographic abnormalities in normotensive obese patients: relationship with visceral fat. *Obesity research.* Jun 2002;10(6):489-498.
227. Mensah GA, Treiber FA, Kapuku GK, Davis H, Barnes VA, Strong WB. Patterns of body fat deposition in youth and their relation to left ventricular markers of adverse cardiovascular prognosis. *The American journal of cardiology.* Sep 1 1999;84(5):583-588.
228. Iacobellis G. True uncomplicated obesity is not related to increased left ventricular mass and systolic dysfunction. *Journal of the American College of Cardiology.* Dec 7 2004;44(11):2257; author reply 2258.
229. Avelar E, Cloward TV, Walker JM, et al. Left ventricular hypertrophy in severe obesity: interactions among blood pressure, nocturnal hypoxemia, and body mass. *Hypertension.* Jan 2007;49(1):34-39.
230. Alexander JK. The cardiomyopathy of obesity. *Progress in cardiovascular diseases.* Mar-Apr 1985;27(5):325-334.
231. Iacobellis G, Leonetti F. Epicardial adipose tissue and insulin resistance in obese subjects. *J Clin Endocrinol Metab.* Nov 2005;90(11):6300-6302.
232. Iacobellis G, Ribaudo MC, Leto G, et al. Influence of excess fat on cardiac morphology and function: study in uncomplicated obesity. *Obesity research.* Aug 2002;10(8):767-773.
233. Peterson LR, Herrero P, Schechtman KB, et al. Effect of obesity and insulin resistance on myocardial substrate metabolism and efficiency in young women. *Circulation.* May 11 2004;109(18):2191-2196.
234. Rabkin SW. Epicardial fat: properties, function and relationship to obesity. *Obes Rev.* May 2007;8(3):253-261.
235. Sacks HS, Fain JN. Human epicardial adipose tissue: a review. *Am Heart J.* Jun 2007;153(6):907-917.
236. Silaghi A, Piercecchi-Marti MD, Grino M, et al. Epicardial adipose tissue extent: relationship with age, body fat distribution, and coronaropathy. *Obesity.* Nov 2008;16(11):2424-2430.

237. Shin SY, Yong HS, Lim HE, et al. Total and interatrial epicardial adipose tissues are independently associated with left atrial remodeling in patients with atrial fibrillation. *Journal of cardiovascular electrophysiology.* Jun 2011;22(6):647-655.
238. Iacobellis G, Corradi D, Sharma AM. Epicardial adipose tissue: anatomic, biomolecular and clinical relationships with the heart. *Nat Clin Pract Cardiovasc Med.* Oct 2005;2(10):536-543.
239. Al Chekakie MO, Welles CC, Metoyer R, et al. Pericardial Fat Is Independently Associated With Human Atrial Fibrillation. *Journal of the American College of Cardiology.* August 31, 2010 2010;56(10):784-788.
240. Batal O, Schoenhagen P, Shao M, et al. Left atrial epicardial adiposity and atrial fibrillation. *Circ Arrhythm Electrophysiol.* Jun 1 2010;3(3):230-236.
241. Hany S. Abed MB, B. Pharmacy, Christopher X. Wong, Anthony G. Brooks, BS, Paymen Molaee, FRACP, Adam J. Nelson, Benjamin K. Dundon, FRACP, Leong P. Darryl, MBBS, Walter P. Abhayaratna, MBBS, PhD, Gary A. Wittert, MBBS, PhD, et al. Periatrial Fat Volume Is Predictive Of Atrial Fibrillation Severity. *Heart rhythm : the official journal of the Heart Rhythm Society.* 2010;Vol. 7(No. 5):S327.
242. Hsuan-Ming Tsao M, Wei-Chih Hu, PhD, Mei-Han Wu, MD and Shih-Ann Chen, MD., I-Lan, Taiwan, Chun-Li. Abundance and Distribution of Epicardial Adipose Tissue Surrounding the Left Atrium in Patients with Atrial Fibrillation. *Heart rhythm : the official journal of the Heart Rhythm Society.* 2010;Vol. 7(No. 5):S327.
243. Thanassoulis G, Massaro JM, O'Donnell CJ, et al. Pericardial fat is associated with prevalent atrial fibrillation: the Framingham Heart Study. *Circ Arrhythm Electrophysiol.* Aug 2010;3(4):345-350.
244. Wang TJ, Parise H, Levy D, et al. Obesity and the risk of new-onset atrial fibrillation. *JAMA.* Nov 24 2004;292(20):2471-2477.
245. Tedrow UB, Conen D, Ridker PM, et al. The long- and short-term impact of elevated body mass index on the risk of new atrial fibrillation the WHS (women's health study). *Journal of the American College of Cardiology.* May 25 2010;55(21):2319-2327.
246. Dublin S, French B, Glazer NL, et al. Risk of new-onset atrial fibrillation in relation to body mass index. *Archives of internal medicine.* Nov 27 2006;166(21):2322-2328.
247. Tsang TS, Barnes ME, Miyasaka Y, et al. Obesity as a risk factor for the progression of paroxysmal to permanent atrial fibrillation: a longitudinal cohort study of 21 years. *Eur Heart J.* Sep 2008;29(18):2227-2233.
248. Pantanowitz L. Fat infiltration in the heart. *Heart.* Mar 2001;85(3):253.
249. Maan A, Mansour M, Ruskin JN, Heist EK. Role of Epicardial Fat in Atrial Fibrillation Pathophysiology and Clincial Implications. *The Journal of Innovations in Cardiac Rhythm Management.* 2013 2013;4:1077-1082.
250. Gong D, Yang R, Munir KM, Horenstein RB, Shuldiner AR. New progress in adipocytokine research. *Current Opinion in Endocrinology, Diabetes and Obesity.* 2003;10(2):115-121.

251. Karmazyn M, Purdham DM, Rajapurohitam V, Zeidan A. Signalling mechanisms underlying the metabolic and other effects of adipokines on the heart. *Cardiovascular research.* Jul 15 2008;79(2):279-286.
252. Damron DS, Van Wagoner DR, Moravec CS, Bond M. Arachidonic acid and endothelin potentiate Ca2+ transients in rat cardiac myocytes via inhibition of distinct K+ channels. *The Journal of biological chemistry.* Dec 25 1993;268(36):27335-27344.
253. Kang JX, Xiao YF, Leaf A. Free, long-chain, polyunsaturated fatty acids reduce membrane electrical excitability in neonatal rat cardiac myocytes. *Proceedings of the National Academy of Sciences of the United States of America.* Apr 25 1995;92(9):3997-4001.
254. Leaf A. The electrophysiological basis for the antiarrhythmic actions of polyunsaturated fatty acids. *European Heart Journal Supplements.* 2001;3(suppl D):D98.
255. Boland L, Drzewiecki M. Polyunsaturated Fatty Acid Modulation of Voltage-Gated Ion Channels. *Cell biochemistry and biophysics.* 2008;52(2):59-84.
256. Haim TE, Wang W, Flagg TP, et al. Palmitate attenuates myocardial contractility through augmentation of repolarizing Kv currents. *Journal of molecular and cellular cardiology.* Feb 2010;48(2):395-405.
257. Barber MC, Ward RJ, Richards SE, et al. Ovine adipose tissue monounsaturated fat content is correlated to depot-specific expression of the stearoyl-CoA desaturase gene. *J Anim Sci.* Jan 2000;78(1):62-68.
258. Veiga-Lopez AB, C. Padmanabhan, V. Developmental Programming: Prenatal Testosterone and Postnatal Obesity Induce Free Fatty Acid Imbalance in Sheep. *Endocrinology.* 2011.
259. Nye ER, Buchanan H. Short-term effect of nicotinic acid on plasma level and turnover of free fatty acids in sheep and man. *Journal of lipid research.* Mar 1969;10(2):193-196.
260. Kim JY, Park JY, Kim OY, et al. Metabolic profiling of plasma in overweight/obese and lean men using ultra performance liquid chromatography and Q-TOF mass spectrometry (UPLC-Q-TOF MS). *J Proteome Res.* Sep 3 2010;9(9):4368-4375.
261. Kankaanpaa M, Lehto HR, Parkka JP, et al. Myocardial triglyceride content and epicardial fat mass in human obesity: relationship to left ventricular function and serum free fatty acid levels. *J Clin Endocrinol Metab.* Nov 2006;91(11):4689-4695.
262. Dibb KM, Clarke JD, Eisner DA, Richards MA, Trafford AW. A functional role for transverse (t-) tubules in the atria. *Journal of molecular and cellular cardiology.* May 2013;58:84-91.
263. Louch WE, Sejersted OM, Swift F. There goes the neighborhood: pathological alterations in T-tubule morphology and consequences for cardiomyocyte Ca2+ handling. *J Biomed Biotechnol.* 2010;2010:503906.

264. Anumonwo JM, Tallini YN, Vetter FJ, Jalife J. Action potential characteristics and arrhythmogenic properties of the cardiac conduction system of the murine heart. *Circulation research.* Aug 17 2001;89(4):329-335.
265. Wolf CM, Berul CI. Inherited conduction system abnormalities--one group of diseases, many genes. *Journal of cardiovascular electrophysiology.* Apr 2006;17(4):446-455.
266. Nerbonne JM. Studying cardiac arrhythmias in the mouse--a reasonable model for probing mechanisms? *Trends in cardiovascular medicine.* Apr 2004;14(3):83-93.
267. Nerbonne JM, Nichols CG, Schwarz TL, Escande D. Genetic manipulation of cardiac K(+) channel function in mice: what have we learned, and where do we go from here? *Circulation research.* Nov 23 2001;89(11):944-956.
268. Herron TJ, Milstein ML, Anumonwo J, Priori SG, Jalife J. Purkinje cell calcium dysregulation is the cellular mechanism that underlies catecholaminergic polymorphic ventricular tachycardia. *Heart rhythm : the official journal of the Heart Rhythm Society.* Aug 2010;7(8):1122-1128.
269. Kang G, Giovannone SF, Liu N, et al. Purkinje cells from RyR2 mutant mice are highly arrhythmogenic but responsive to targeted therapy. *Circulation research.* Aug 20 2010;107(4):512-519.
270. Li L, Niederer SA, Idigo W, et al. A mathematical model of the murine ventricular myocyte: a data-driven biophysically based approach applied to mice overexpressing the canine NCX isoform. *American journal of physiology. Heart and circulatory physiology.* Oct 2010;299(4):H1045-1063.
271. Miquerol L, Meysen S, Mangoni M, et al. Architectural and functional asymmetry of the His-Purkinje system of the murine heart. *Cardiovascular research.* Jul 1 2004;63(1):77-86.
272. Dhamoon AS, Pandit SV, Sarmast F, et al. Unique Kir2.x Properties Determine Regional and Species Differences in the Cardiac Inward Rectifier K+ Current. *Circulation research.* May 28, 2004 2004;94(10):1332-1339.
273. Vaidyanathan R, Taffet SM, Vikstrom KL, Anumonwo JM. Regulation of cardiac inward rectifier potassium current (IK1) by synapse associated protein-97. *The Journal of biological chemistry.* Jun 8 2010.
274. Cribbs LL, Martin BL, Schroder EA, Keller BB, Delisle BP, Satin J. Identification of the t-type calcium channel (Ca(v)3.1d) in developing mouse heart. *Circulation research.* Mar 2 2001;88(4):403-407.
275. Markandeya YS, Fahey JM, Pluteanu F, Cribbs LL, Balijepalli RC. Caveolin-3 Regulates Protein Kinase A Modulation of the CaV3.2 ({alpha}1H) T-type Ca2+ Channels. *J Biol Chem.* Jan 28 2011;286(4):2433-2444.
276. Viragh S, Stoeckel ME, Porte A. Light and electron microscopic structure of the cardiac Purkinje fibers--review. *Physiol Bohemoslov.* 1987;36(3):233-242.

277. Schram G, Pourrier M, Melnyk P, Nattel S. Differential distribution of cardiac ion channel expression as a basis for regional specialization in electrical function. *Circulation research.* May 17 2002;90(9):939-950.
278. Dumaine R, Cordeiro JM. Comparison of K+ currents in cardiac Purkinje cells isolated from rabbit and dog. *Journal of molecular and cellular cardiology.* Feb 2007;42(2):378-389.
279. Dun W, Boyden PA. The Purkinje cell; 2008 style. *Journal of molecular and cellular cardiology.* Nov 2008;45(5):617-624.
280. Verkerk AO, Veldkamp MW, Abbate F, et al. Two types of action potential configuration in single cardiac Purkinje cells of sheep. *The American journal of physiology.* Oct 1999;277(4 Pt 2):H1299-1310.
281. Vassalle M. The vicissitudes of the pacemaker current I (Kdd) of cardiac purkinje fibers. *J Biomed Sci.* Nov 2007;14(6):699-716.
282. Lakatta EG, Maltsev VA, Bogdanov KY, Stern MD, Vinogradova TM. Cyclic variation of intracellular calcium: a critical factor for cardiac pacemaker cell dominance. *Circulation research.* Feb 21 2003;92(3):e45-50.
283. Shi W, Wymore R, Yu H, et al. Distribution and prevalence of hyperpolarization-activated cation channel (HCN) mRNA expression in cardiac tissues. *Circulation research.* Jul 9 1999;85(1):e1-6.
284. Cordeiro JM, Spitzer KW, Giles WR. Repolarizing K+ currents in rabbit heart Purkinje cells. *The Journal of physiology.* May 1 1998;508 (Pt 3):811-823.
285. Han W, Chartier D, Li D, Nattel S. Ionic remodeling of cardiac Purkinje cells by congestive heart failure. *Circulation.* Oct 23 2001;104(17):2095-2100.
286. Han W, Zhang L, Schram G, Nattel S. Properties of potassium currents in Purkinje cells of failing human hearts. *American journal of physiology. Heart and circulatory physiology.* Dec 2002;283(6):H2495-2503.
287. Gaborit N, Le Bouter S, Szuts V, et al. Regional and tissue specific transcript signatures of ion channel genes in the non-diseased human heart. *The Journal of physiology.* Jul 15 2007;582(Pt 2):675-693.
288. Allessie M, Ausma J, Schotten U. Electrical, contractile and structural remodeling during atrial fibrillation. *Cardiovascular research.* May 2002;54(2):230-246.
289. Lomax AE, Kondo CS, Giles WR. Comparison of time- and voltage-dependent K+ currents in myocytes from left and right atria of adult mice. *American journal of physiology. Heart and circulatory physiology.* Nov 2003;285(5):H1837-1848.
290. Babij P, Askew GR, Nieuwenhuijsen B, et al. Inhibition of cardiac delayed rectifier K+ current by overexpression of the long-QT syndrome HERG G628S mutation in transgenic mice. *Circulation research.* Sep 21 1998;83(6):668-678.

291. Jaleel N, Nakayama H, Chen X, et al. Ca2+ influx through T- and L-type Ca2+ channels have different effects on myocyte contractility and induce unique cardiac phenotypes. *Circulation research.* Nov 7 2008;103(10):1109-1119.
292. Vassalle M, Bocchi L, Du F. A slowly inactivating sodium current (INa2) in the plateau range in canine cardiac Purkinje single cells. *Exp Physiol.* Jan 2007;92(1):161-173.
293. Dhamoon AS, Pandit SV, Sarmast F, et al. Unique Kir2.x properties determine regional and species differences in the cardiac inward rectifier K+ current. *Circulation research.* May 28 2004;94(10):1332-1339.
294. Sun H, Kerfant BG, Zhao D, et al. Insulin-like growth factor-1 and PTEN deletion enhance cardiac L-type Ca2+ currents via increased PI3Kalpha/PKB signaling. *Circulation research.* Jun 9 2006;98(11):1390-1397.
295. Graner M, Siren R, Nyman K, et al. Cardiac steatosis associates with visceral obesity in nondiabetic obese men. *J Clin Endocrinol Metab.* Mar 2013;98(3):1189-1197.
296. Ricci E, Smallwood S, Chouabe C, et al. Electrophysiological characterization of left ventricular myocytes from obese Sprague-Dawley rat. *Obesity.* May 2006;14(5):778-786.
297. Lin YK, Chen YC, Chen JH, Chen SA, Chen YJ. Adipocytes modulate the electrophysiology of atrial myocytes: implications in obesity-induced atrial fibrillation. *Basic Res Cardiol.* Sep 2012;107(5):293.
298. Abed HS, Samuel CS, Lau DH, et al. Obesity results in progressive atrial structural and electrical remodeling: implications for atrial fibrillation. *Heart rhythm : the official journal of the Heart Rhythm Society.* Jan 2013;10(1):90-100.
299. Xiao YF, Gomez AM, Morgan JP, Lederer W, Leaf A. Suppression of voltage-gated L-type Ca2+ currents by polyunsaturated fatty acids in adult and neonatal rat ventricular myocytes. *Proceedings of the National Academy of Sciences.* 1997;94(8):4182.
300. Pedrotty DM, Klinger RY, Kirkton RD, Bursac N. Cardiac fibroblast paracrine factors alter impulse conduction and ion channel expression of neonatal rat cardiomyocytes. *Cardiovascular research.* Sep 1 2009;83(4):688-697.
301. Patel SP, Campbell DL. Transient outward potassium current, 'Ito', phenotypes in the mammalian left ventricle: underlying molecular, cellular and biophysical mechanisms. *The Journal of physiology.* Nov 15 2005;569(Pt 1):7-39.
302. Birnbaum SG, Varga AW, Yuan LL, Anderson AE, Sweatt JD, Schrader LA. Structure and function of Kv4-family transient potassium channels. *Physiological reviews.* Jul 2004;84(3):803-833.
303. Grandi E, Pandit SV, Voigt N, et al. Human atrial action potential and Ca2+ model: sinus rhythm and chronic atrial fibrillation. *Circulation research.* Oct 14 2011;109(9):1055-1066.

304. Musa H, Kaur K, O'Connell R, et al. Inhibition of platelet-derived growth factor-AB signaling prevents electromechanical remodeling of adult atrial myocytes that contact myofibroblasts. *Heart rhythm : the official journal of the Heart Rhythm Society.* Mar 14 2013.
305. Lu L, Zhang Q, Timofeyev V, et al. Molecular coupling of a Ca2+-activated K+ channel to L-type Ca2+ channels via alpha-actinin2. *Circulation research.* Jan 5 2007;100(1):112-120.
306. Catterall WA. Structure and regulation of voltage-gated Ca2+ channels. *Annu Rev Cell Dev Biol.* 2000;16:521-555.
307. Campbell DL, Stamler JS, Strauss HC. Redox modulation of L-type calcium channels in ferret ventricular myocytes. Dual mechanism regulation by nitric oxide and S-nitrosothiols. *The Journal of general physiology.* Oct 1996;108(4):277-293.
308. Lenaerts I, Bito V, Heinzel FR, et al. Ultrastructural and functional remodeling of the coupling between Ca2+ influx and sarcoplasmic reticulum Ca2+ release in right atrial myocytes from experimental persistent atrial fibrillation. *Circulation research.* Oct 23 2009;105(9):876-885.
309. Iacobellis G, Pond CM, Sharma AM. Different "weight" of cardiac and general adiposity in predicting left ventricle morphology. *Obesity.* Oct 2006;14(10):1679-1684.
310. Katz AM, Messineo FC. Lipids and membrane function: implications in arrhythmias. *Hosp Pract (Off Ed).* Jul 1981;16(7):49-59.
311. Kemi OJ, Hoydal MA, Macquaide N, et al. The effect of exercise training on transverse tubules in normal, remodeled, and reverse remodeled hearts. *J Cell Physiol.* Sep 2011;226(9):2235-2243.
312. Riquelme CA, Magida JA, Harrison BC, et al. Fatty acids identified in the Burmese python promote beneficial cardiac growth. *Science.* Oct 28 2011;334(6055):528-531.
313. Marshall C, Hitman GA, Cassell PG, Turner MD. Effect of glucolipotoxicity and rosiglitazone upon insulin secretion. *Biochemical and biophysical research communications.* May 11 2007;356(3):756-762.
314. Padmanabhan V, Veiga-Lopez A, Abbott DH, Recabarren SE, Herkimer C. Developmental programming: impact of prenatal testosterone excess and postnatal weight gain on insulin sensitivity index and transfer of traits to offspring of overweight females. *Endocrinology.* Feb 2010;151(2):595-605.
315. Bloor ID, Sebert SP, Saroha V, et al. Sex Differences in Metabolic and Adipose Tissue Responses to Juvenile-Onset Obesity in Sheep. *Endocrinology.* Jul 24 2013.
316. Bjorntorp P, Karlsson M, Pertoft H, Pettersson P, Sjostrom L, Smith U. Isolation and characterization of cells from rat adipose tissue developing into adipocytes. *Journal of lipid research.* Mar 1978;19(3):316-324.
317. Wright M, Sacher F, Haissaguerre M. Catheter ablation for patients with ventricular fibrillation. *Current opinion in cardiology.* Jan 2009;24(1):56-60.

318. Kus T, Sasyniuk BI. Electrophysiological actions of disopyramide phosphate on canine ventricular muscle and purkinje fibers. *Circulation research.* Dec 1975;37(6):844-854.
319. Davis LD, Temte JV. Electrophysiological actions of lidocaine on canine ventricular muscle and Purkinje fibers. *Circulation research.* May 1969;24(5):639-655.
320. Kasanuki H, Ohnishi S, Ohtuka M, et al. Idiopathic ventricular fibrillation induced with vagal activity in patients without obvious heart disease. *Circulation.* May 6 1997;95(9):2277-2285.
321. Morady F, DiCarlo LA, Jr., Baerman JM, de Buitleir M. Comparison of coupling intervals that induce clinical and nonclinical forms of ventricular tachycardia during programmed stimulation. *The American journal of cardiology.* Jun 1 1986;57(15):1269-1273.
322. Belhassen B, Shapira I, Sheps D, Laniado S. Programmed ventricular stimulation using up to two extrastimuli and repetition of double extrastimulation for induction of ventricular tachycardia: a new highly sensitive and specific protocol. *The American journal of cardiology.* Mar 1 1990;65(9):615-622.
323. Janse MJ, Kleber AG, Capucci A, Coronel R, Wilms-Schopman F. Electrophysiological basis for arrhythmias caused by acute ischemia. Role of the subendocardium. *Journal of molecular and cellular cardiology.* Apr 1986;18(4):339-355.
324. Cha YM, Uchida T, Wolf PL, et al. Effects of chemical subendocardial ablation on activation rate gradient during ventricular fibrillation. *The American journal of physiology.* Dec 1995;269(6 Pt 2):H1998-2009.
325. Berenfeld O, Jalife J. Purkinje-muscle reentry as a mechanism of polymorphic ventricular arrhythmias in a 3-dimensional model of the ventricles. *Circulation research.* Jun 1 1998;82(10):1063-1077.
326. Sommer JR, Johnson EA. Cardiac muscle. A comparative study of Purkinje fibers and ventricular fibers. *The Journal of cell biology.* Mar 1968;36(3):497-526.
327. Stuyvers BD, Dun W, Matkovich S, Sorrentino V, Boyden PA, ter Keurs HE. Ca2+ sparks and waves in canine purkinje cells: a triple layered system of Ca2+ activation. *Circulation research.* Jul 8 2005;97(1):35-43.
328. Boyden PA, Hirose M, Dun W. Cardiac Purkinje cells. *Heart rhythm : the official journal of the Heart Rhythm Society.* Jan 2010;7(1):127-135.
329. Kaufmann SG, Westenbroek RE, Maass AH, et al. Distribution and function of sodium channel subtypes in human atrial myocardium. *Journal of molecular and cellular cardiology.* Aug 2013;61:133-141.
330. Gavillet B, Rougier JS, Domenighetti AA, et al. Cardiac sodium channel Nav1.5 is regulated by a multiprotein complex composed of syntrophins and dystrophin. *Circulation research.* Aug 18 2006;99(4):407-414.
331. Li S, Zhang HY, Hu CC, et al. Assessment of diet-induced obese rats as an obesity model by comparative functional genomics. *Obesity.* Apr 2008;16(4):811-818.

332. Martinez-Palomo A, Alanis J, Benitez D. Transitional cardiac cells of the conductive system of the dog heart. Distinguishing morphological and electrophysiological features. *The Journal of cell biology.* Oct 1970;47(1):1-17.
333. Behradfar E, Nygren A, Vigmond EJ. The Role of Purkinje-Myocardial Coupling during Ventricular Arrhythmia: A Modeling Study. *PloS one.* 2014;9(2):e88000.
334. Cheng LF, Wang F, Lopatin AN. Metabolic stress in isolated mouse ventricular myocytes leads to remodeling of t tubules. *American journal of physiology. Heart and circulatory physiology.* Nov 2011;301(5):H1984-1995.
335. Lemieux H, Bulteau AL, Friguet B, Tardif JC, Blier PU. Dietary fatty acids and oxidative stress in the heart mitochondria. *Mitochondrion.* Jan 2011;11(1):97-103.
336. Suzuki T. Ultrastructural changes of heart muscle in cyanide poisoning. *The Tohoku journal of experimental medicine.* Jul 1968;95(3):271-287.
337. Emken EA. Metabolism of dietary stearic acid relative to other fatty acids in human subjects. *The American journal of clinical nutrition.* Dec 1994;60(6 Suppl):1023S-1028S.
338. Tillman TS, Cascio M. Effects of membrane lipids on ion channel structure and function. *Cell biochemistry and biophysics.* 2003;38(2):161-190.
339. Matsufuji T, Ikeda M, Naito A, et al. Arylpiperazines as fatty acid transport protein 1 (FATP1) inhibitors with improved potency and pharmacokinetic properties. *Bioorganic & medicinal chemistry letters.* May 1 2013;23(9):2560-2565.
340. Sabbah HN, Chandler MP, Mishima T, et al. Ranolazine, a partial fatty acid oxidation (pFOX) inhibitor, improves left ventricular function in dogs with chronic heart failure. *Journal of cardiac failure.* Dec 2002;8(6):416-422.
341. Sabbah HH, Stanley WC. Partial fatty acid oxidation inhibitors: a potentially new class of drugs for heart failure. *European journal of heart failure.* Jan 2002;4(1):3-6.
342. Montaigne D, Marechal X, Lefebvre P, et al. Mitochondrial dysfunction as an arrhythmogenic substrate: a translational proof-of-concept study in patients with metabolic syndrome in whom post-operative atrial fibrillation develops. *Journal of the American College of Cardiology.* Oct 15 2013;62(16):1466-1473.
343. Kostin S, Scholz D, Shimada T, et al. The internal and external protein scaffold of the T-tubular system in cardiomyocytes. *Cell and tissue research.* Dec 1998;294(3):449-460.
344. Pouvreau S, Berthier C, Blaineau S, Amsellem J, Coronado R, Strube C. Membrane cholesterol modulates dihydropyridine receptor function in mice fetal skeletal muscle cells. *The Journal of physiology.* Mar 1 2004;555(Pt 2):365-381.

345. Viswanathan PC, Shaw RM, Rudy Y. Effects of IKr and IKs heterogeneity on action potential duration and its rate dependence: a simulation study. *Circulation.* May 11 1999;99(18):2466-2474.
346. Colatsky TJ. Voltage clamp measurements of sodium channel properties in rabbit cardiac Purkinje fibres. *The Journal of physiology.* Aug 1980;305:215-234.
347. Puglisi JL, Bers DM. LabHEART: an interactive computer model of rabbit ventricular myocyte ion channels and Ca transport. *Am J Physiol Cell Physiol.* Dec 2001;281(6):C2049-2060.
348. Stewart P, Aslanidi OV, Noble D, Noble PJ, Boyett MR, Zhang H. Mathematical models of the electrical action potential of Purkinje fibre cells. *Philos Transact A Math Phys Eng Sci.* Jun 13 2009;367(1896):2225-2255.
349. Bondarenko VE, Szigeti GP, Bett GC, Kim SJ, Rasmusson RL. Computer model of action potential of mouse ventricular myocytes. *American journal of physiology. Heart and circulatory physiology.* Sep 2004;287(3):H1378-1403.
350. Hou L, Deo M, Furspan P, et al. A major role for HERG in determining frequency of reentry in neonatal rat ventricular myocyte monolayer. *Circulation research.* Dec 10 2010;107(12):1503-1511.
351. Korhonen T, Hanninen SL, Tavi P. Model of excitation-contraction coupling of rat neonatal ventricular myocytes. *Biophysical journal.* Feb 2009;96(3):1189-1209.
352. Dawson SP, Keizer J, Pearson JE. Fire-diffuse-fire model of dynamics of intracellular calcium waves. *Proceedings of the National Academy of Sciences of the United States of America.* May 25 1999;96(11):6060-6063.